MHD SIMULATION IN THE SOLAR CORONA TO OBTAIN CONDITIONS FOR THE ACCELERATION OF COSMIC RAYS DURING SOLAR FLARES

A. I. Podgorny[1], I. M. Podgorny[2], A.V. Borisenko[1]

[1]Lebedev Physical Institute RAS, podgorny@lebedev.ru
[2]Institute of Astronomy RAS

Solar cosmic rays (SCR) are the streams of accelerated charged particles, primarily protons with energies up to 20 GeV, which are produced by some solar flares. Solar cosmic rays are generated during the rapid release of energy during solar flares. Therefore, in order to understand the physical mechanism of SCR generation (in particular, in order to later be able to predict the appearance of SCRs based on understanding the physical mechanism of their generation), it is necessary to study simultaneously the physical mechanism of a solar flare and the physical mechanism of charged particle acceleration during an explosive flare process.

The study of SCRs can expand our understanding of the cosmic ray generation mechanism in the general case, since galactic cosmic rays can be generated during superflares on stars that are of the same nature as solar flares. The energy of superflares on class G dwarf stars can reach 10^{36} erg (compared to the solar flare energy of 10^{32} erg), and the energy of cosmic rays generated by them can reach 10^{15} eV.

During a solar flare, a few tens of minutes release ~ 10^{32} erg of magnetic energy, which is converted into thermal energy of a plasma heated to ~ 10^{7} ^{o}K, the kinetic energy of coronal plasma emissions, the energy of accelerated charged particles (protons - up to 20 GeV) and radiation energy in a wide the range produced by accelerated and thermal particles — radio emission, optical radiation, ultraviolet radiation, x-rays (soft thermal 1–20 keV, and hard beam 20–200 and above keV), γ-radiation.

SOLAR FLARE OCCURS IN THE SOLAR CORONA ON HEIGHTS 15 - 70 THOUSANDS KILOMETERS, WHICH IS 1/40 – 1/10 OF SOLAR RADIUS.

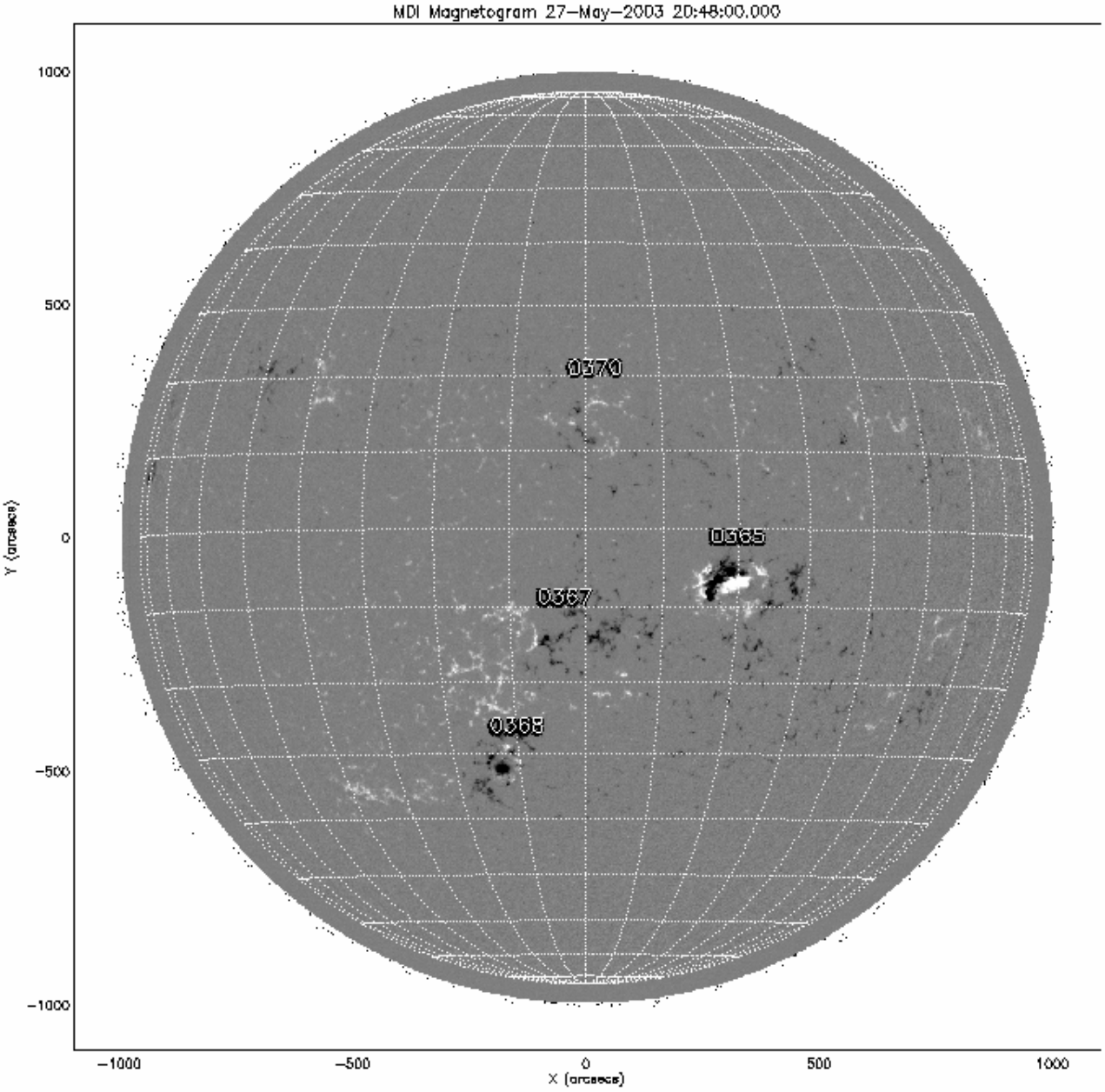

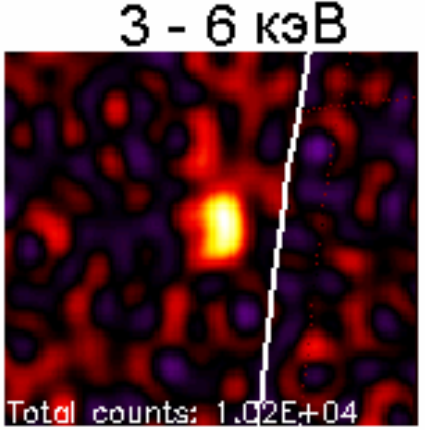

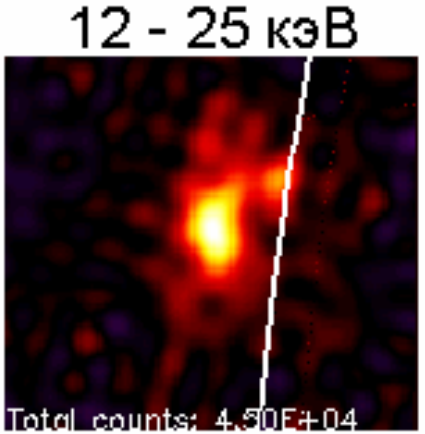

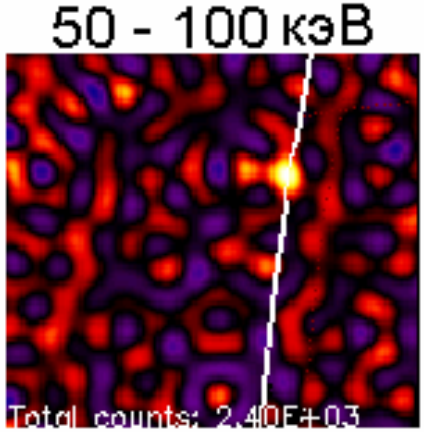

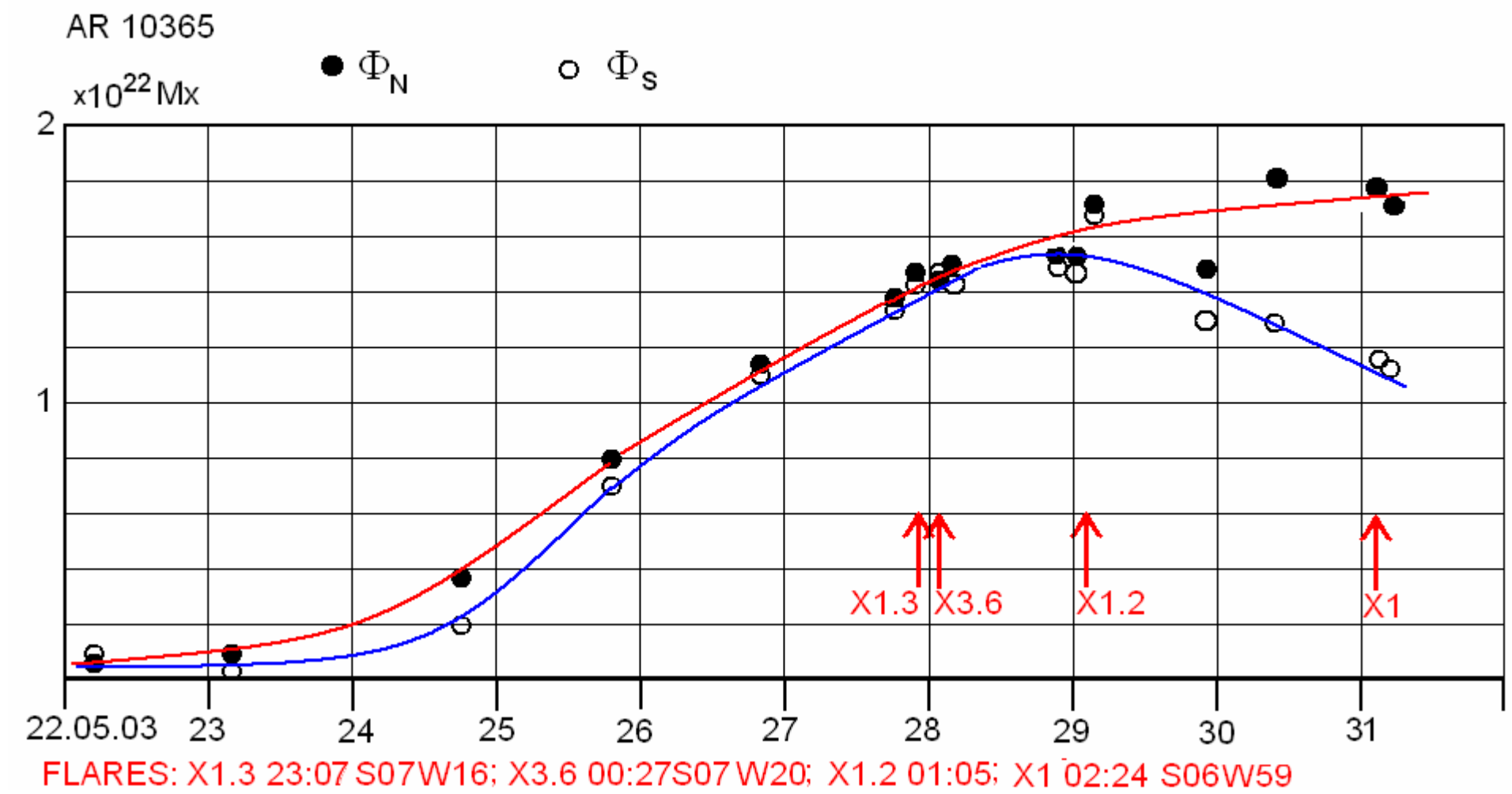
AR 10365
x10^22 Mx
Φ_N
Φ_S
2
1
X1.3
X3.6
X1.2
X1
22.05.03
23
24
25
26
27
28
29
30
31
FLARES: X1.3 23:07 S07W16; X3.6 00:27 S07W20; X1.2 01:05; X1 02:24 S06W59

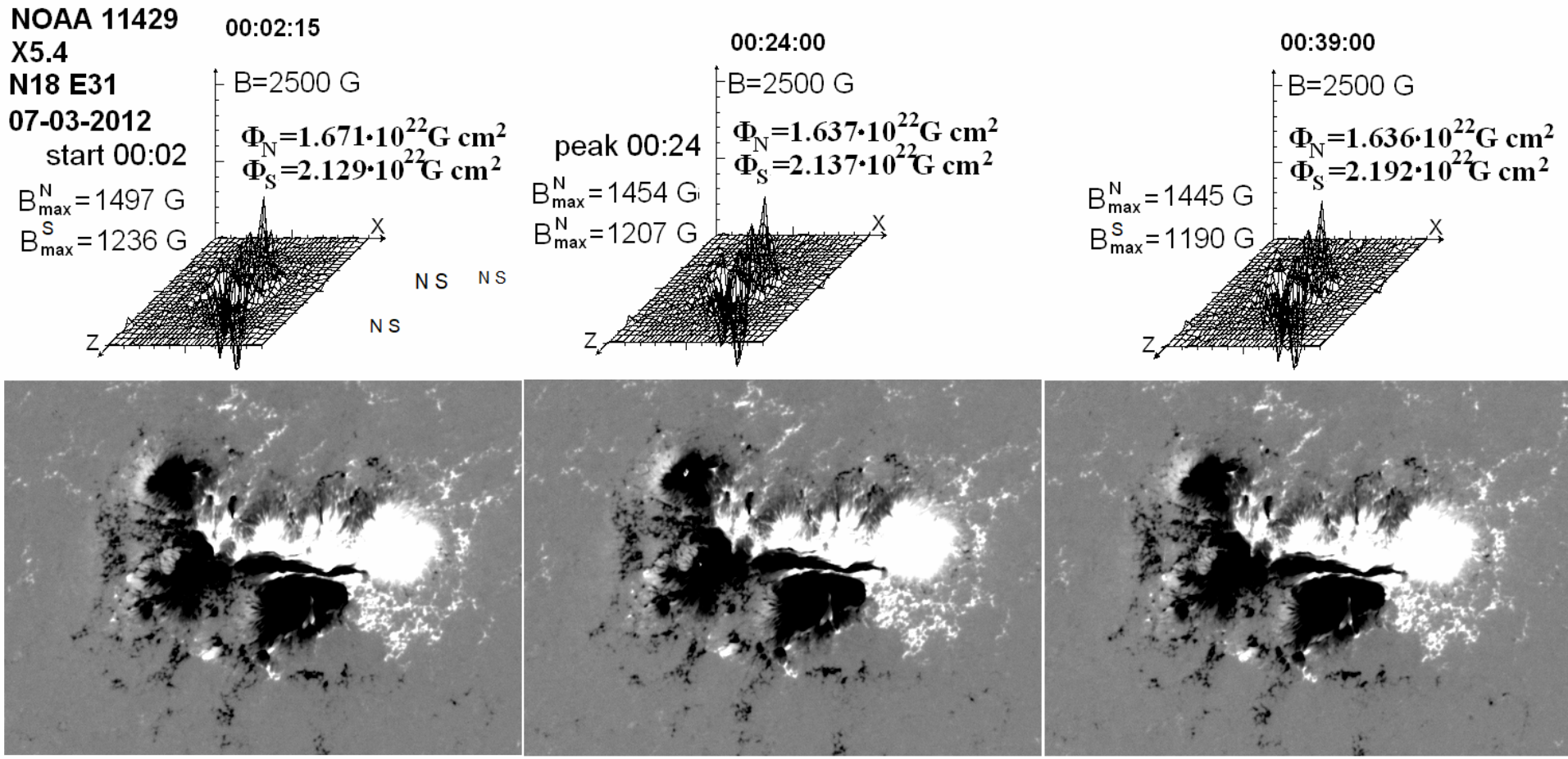

Podgorny, Podgorny, Meshalkina. Astron. Rep. 59, 795, 2015

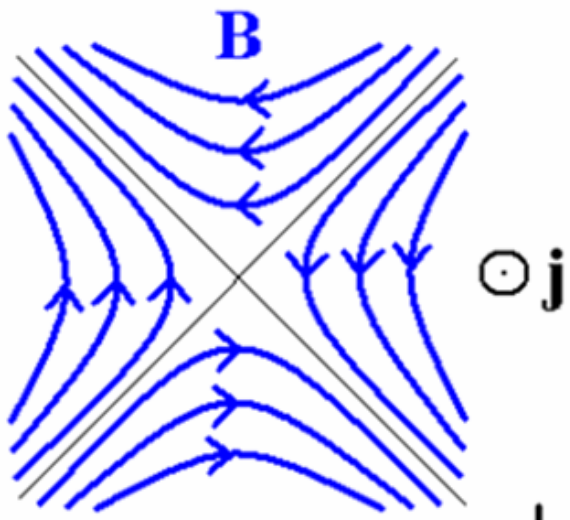

S. I. Syrovatskii 1966
A. Bratenahl, W. Hirsh 1966

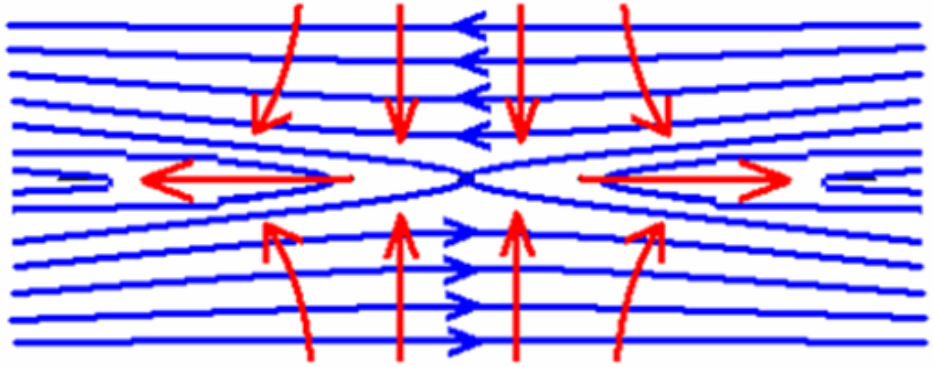

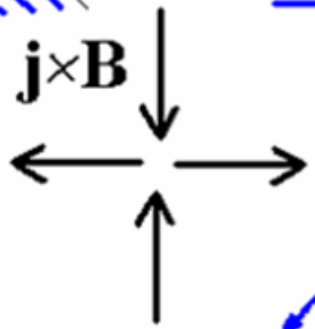

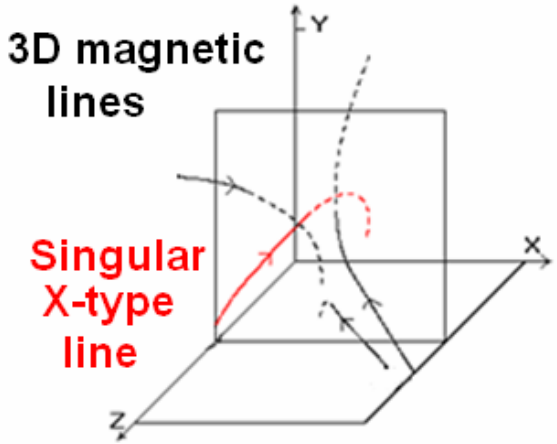

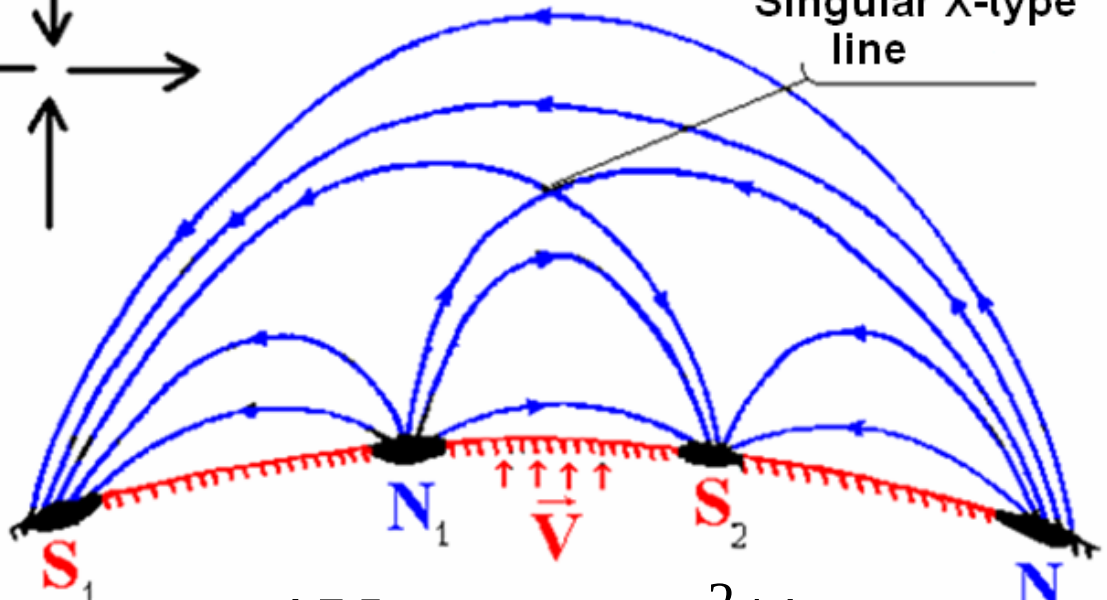

$$a=\nu_m / V_{in}\ ;\ \ \nu_m = c^2/4\pi\sigma$$

After the quasi-steady evolution the current sheet transfers into an unstable state. As a result, explosive instability develops, which cause the flare energy release.

CURRENT SHEET INSTABILITY

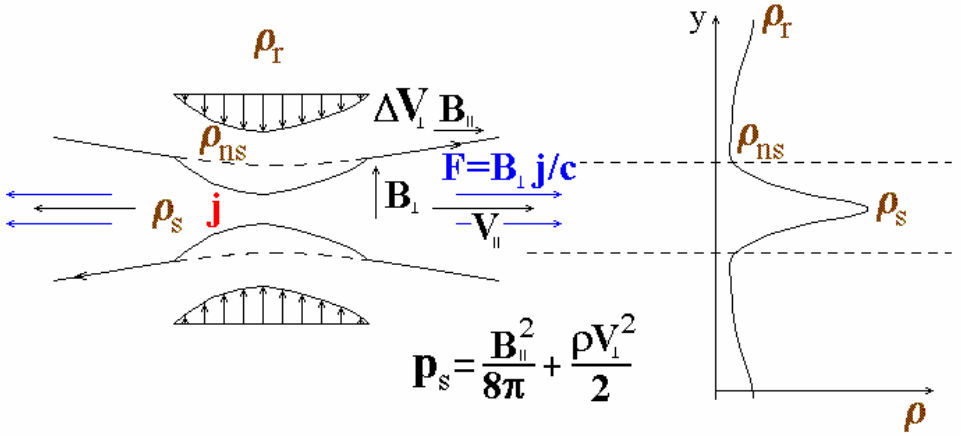

$$\rho_s \frac{dD_V}{dt} = -D_V A \rho_s + D_B \frac{B_s}{4\pi a} + V_{in1} K_I \frac{B_s h}{4\pi \nu_m} + \rho_1 \left(\frac{T_s}{b_1^2} - A^2 \right)$$

$$\rho_{ns} \frac{dV_{in1}}{dt} = V_{in1} K_V \frac{\rho_{ns} V_{in0}}{a} - \rho_1 K_p \frac{T_s}{a} - D_B \frac{B_s}{4\pi}$$

$$\frac{d\rho_1}{dt} = -\rho_1 A - D_V \rho_s + V_{in1} \frac{\rho_{ns}}{a}$$

$$\frac{dD_B}{dt} = -2 D_V h - D_B \left(A + \frac{\nu_m}{b_1^2} + \frac{\nu_m}{a^2} \right) + V_{in1} \frac{B_s}{b_1^2} K_B$$

$$A = \frac{\partial V_x}{\partial x} = \frac{V_{out}}{b} = \sqrt{\frac{1}{ab} \frac{B_x B_n}{4\pi \rho_s}}, \quad \frac{\partial V_{y1}}{\partial x} = D_V, \quad \frac{\partial B_{y1}}{\partial y} = D_B, \quad h = \frac{\partial B_{y0}}{\partial z} = \frac{B_n}{b}$$

CONDITION OF CURRENT SHEET INSTABILITY $\gamma_{max} > 0$
HAVE A FORM:

$$\varepsilon_v^2 \mathrm{Re}_m \sqrt{\frac{\rho_r}{\rho_s} \frac{\rho_{ns}}{\rho_r} \frac{1}{K_B}} < \frac{1}{2} \qquad (K_B \lesssim 1)$$

Implementation of Igor Maksimovich Podgorny plans continues.

Electrodynamic model of solar flare.

Igor M. Podgorny using results of measurements on the satellite Intercosmos-Bulgaria-1300

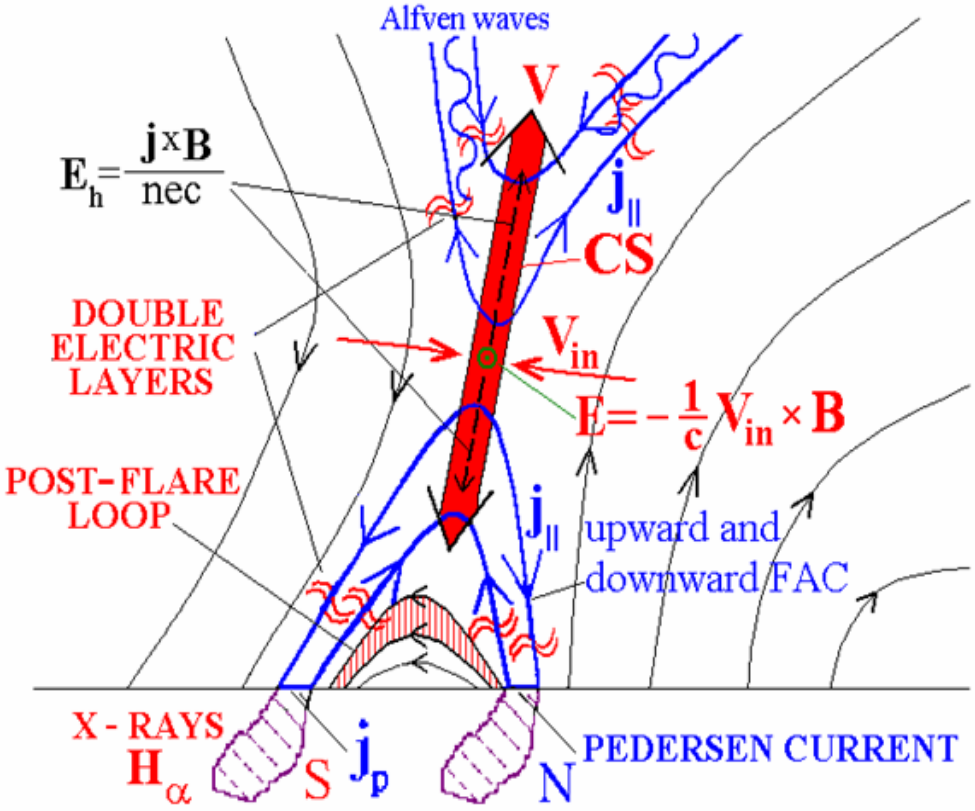

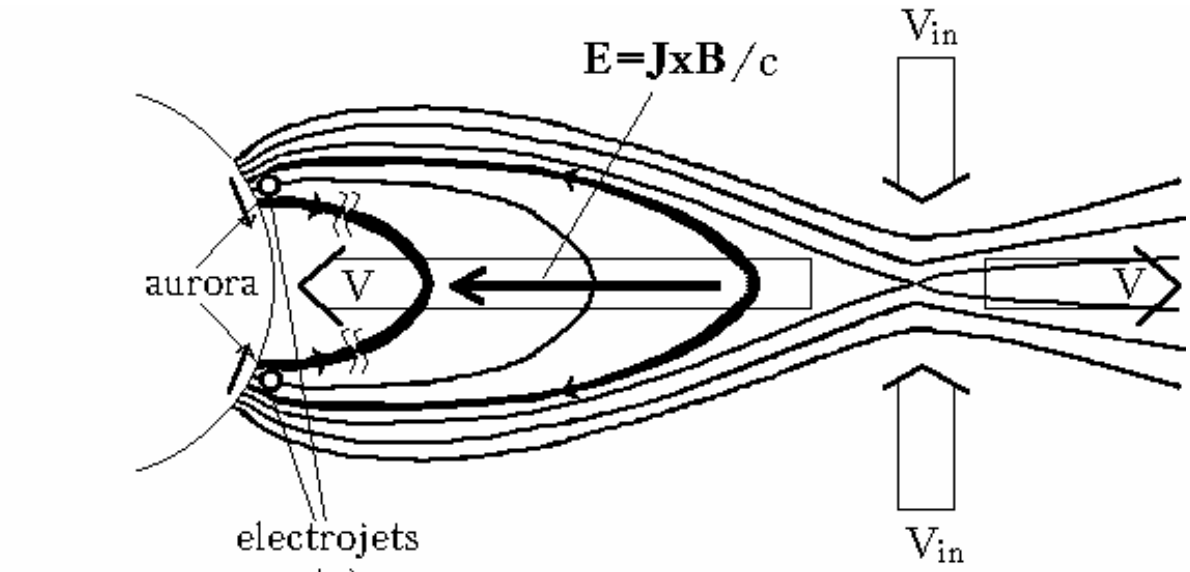

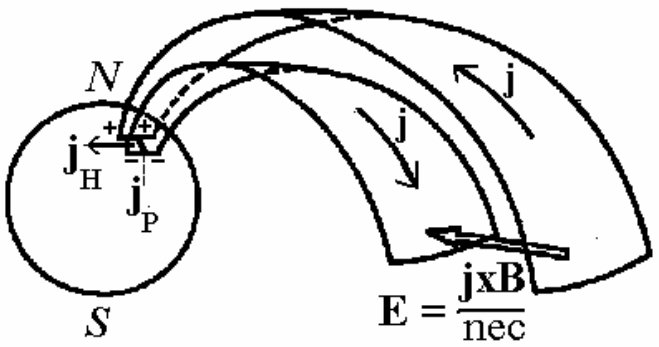

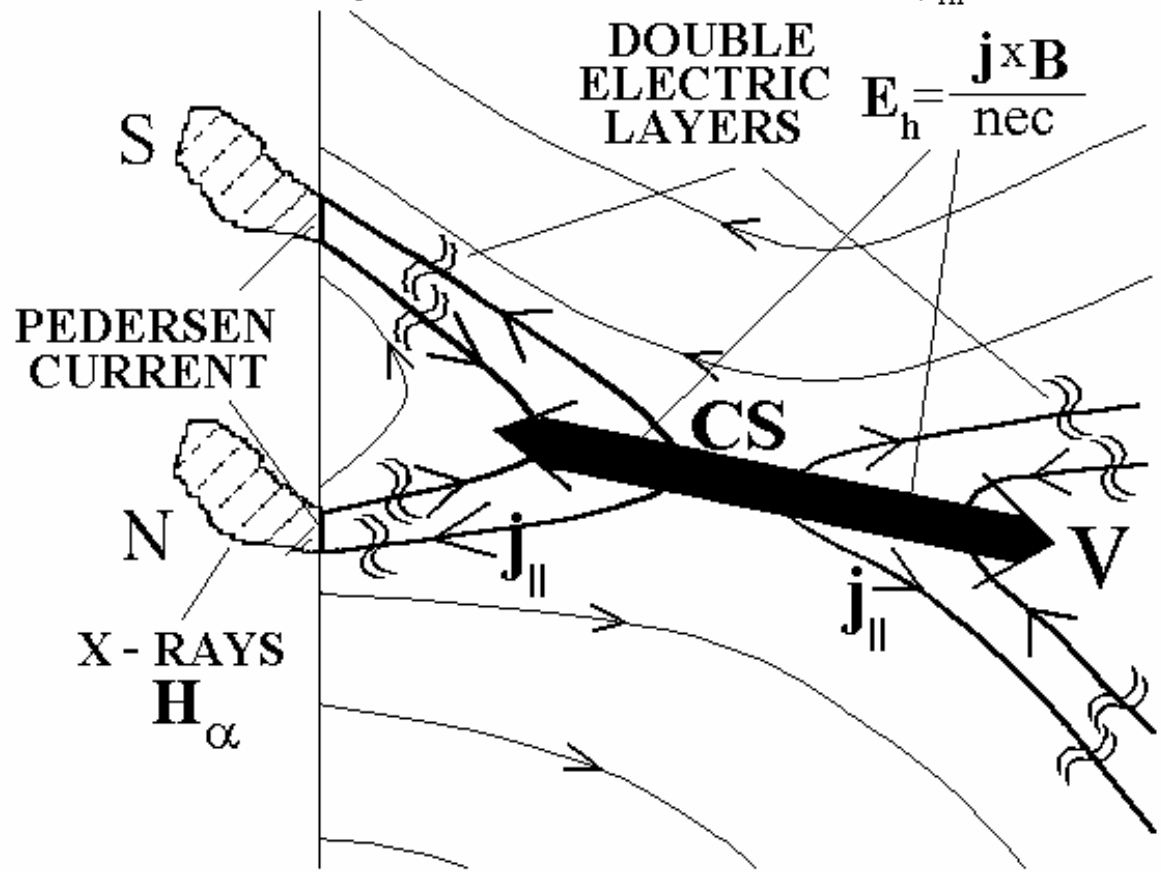

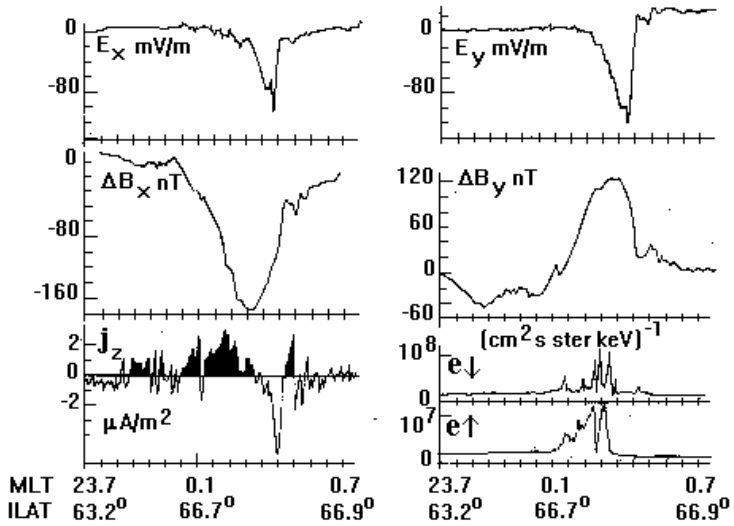

Basing on measurements made on the Soviet-Bulgarian spacecraft Intercosmos Bulgaria-1300, Igor Maksimovich Podgorny proposed an electrodynamic model of substorm.

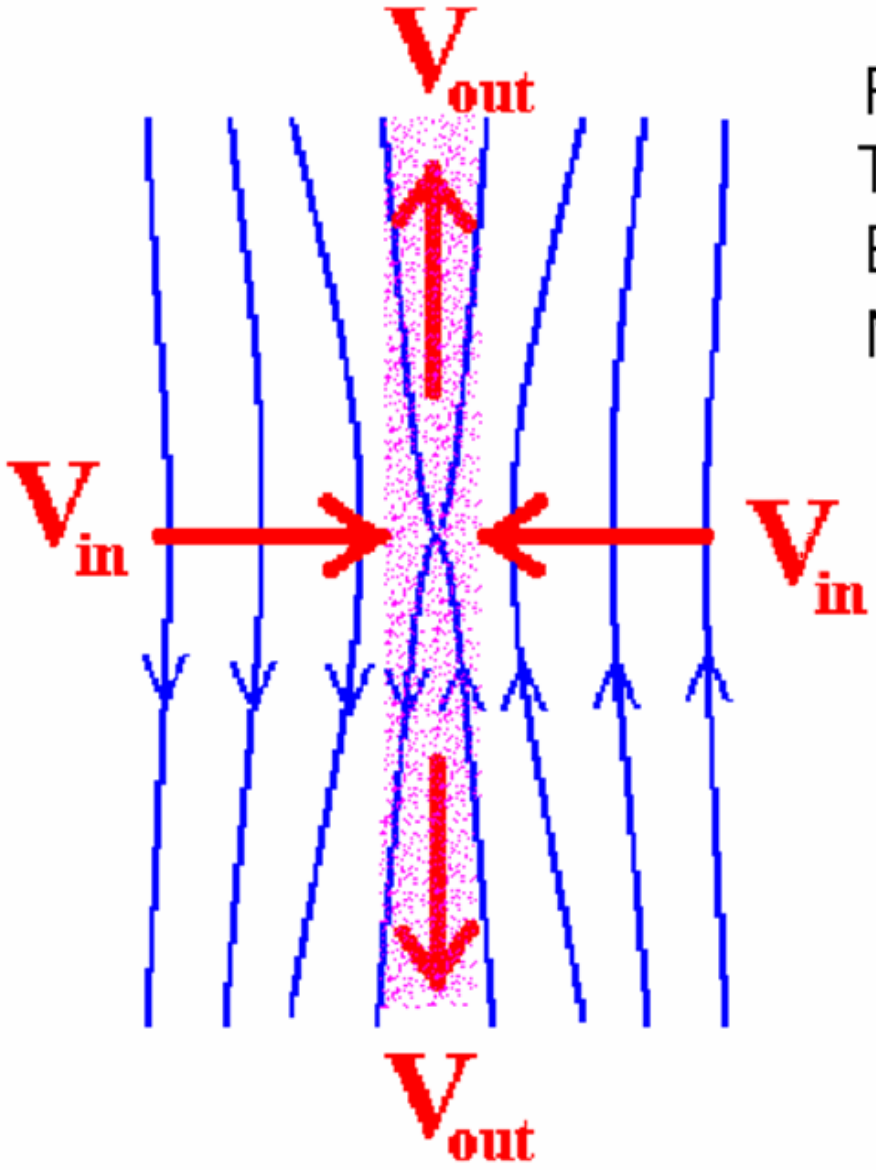

From RHESSI: $(ME)=5\cdot10^{49}\,cm^{-3}$.
$T=3.1$ keV $n=10^{11}\,cm^{-3}$.
$B^2/8\pi = nkT \rightarrow B = 110\,G$.
$M = Nm_p \sim 10^{15}\,g$ --- CME.

At $V_{in} = 2\times10^{7}$ cm/s and $L=10^{9}$ cm.

$E = V \times B/c$. $E=20$ V/cm.

$W=2\times10^{10}$ eV.

The compression of the gas discharge by its own magnetic field at the currents of 200 kA leads to generation of the Lorentz electric field, directed along the axis of discharge. The energy of accelerated particles ~300 KeV at an applied potential difference of ~15 KV.

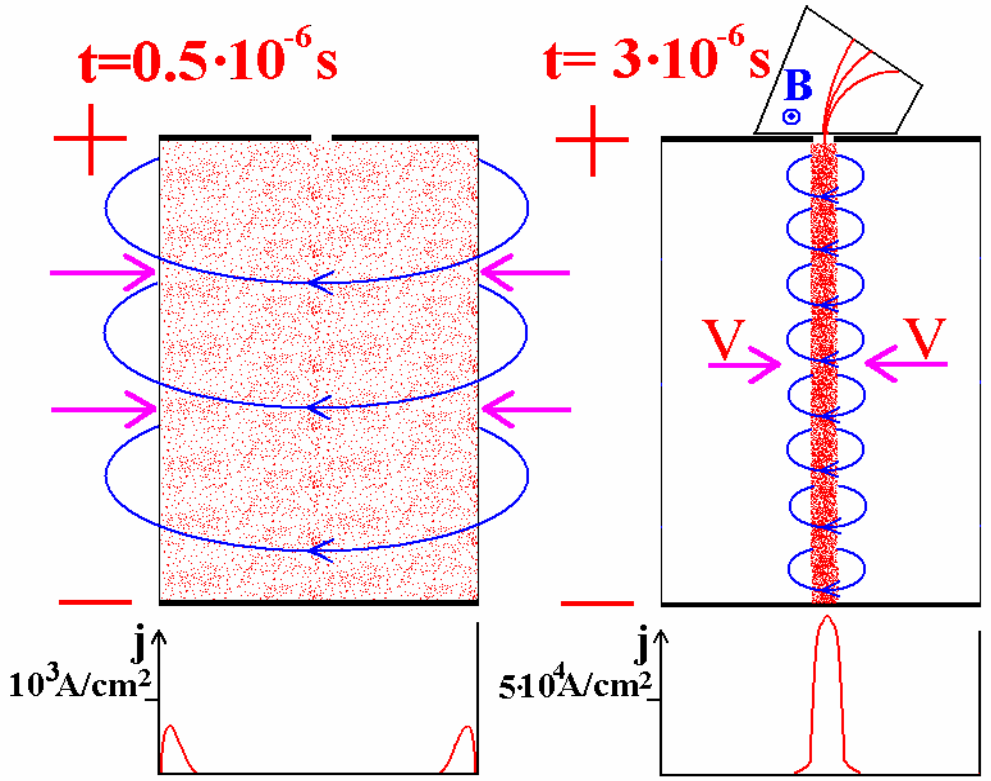

$\varphi = 15$ kV

$dI/dt = 10^{11}$ A/s

$I_{max} = 200$ kA

W>300keV

$\mathbf{E} = -\mathbf{V} \times \mathbf{B}/c$

$V \sim 10^7$ cm/s

$B_{max} \sim 4 \cdot 10^4$ G

$E \sim 4 \cdot 10^3$ V/cm

Lab. № 2. 1954.
Atomnaja energija
№ 3. 1956.
Artsimovich et. al. P. 84.
Lukjanov, Podgorny. P. 93.

НИЯФ МГУ 1957.
Podgorny, Kovalsky,
Palchikov.
DAN SSSR. 123, 825 (1958).

1957.
Severny } Electric discharge
Toneman } in solar corona.

С. Н. Вернов

Lab. № 2. 1954. Atomnaja. energija №3. 1956. Artsimovich et. al. P.84. Lukjanov, Podgorny. P. 93.

НИИЯФ МГУ 1957. Podgorny, Kovalsky, Palchikov. DAN USSR. 123 825 (1958)

Cosmic ray generation mechanism by Igor Maksimovich Podgorny

The mechanism of I. M. Podgorny accelerates charged particles by an induction electric field equal to the field VxB / c near the main current that creates the field B. The mechanism accelerates charged particles in the pinch and in the current sheet (the resulting physical process of magnetic field dissipation in a thin current sheet formed in an X-type magnetic field configuration is sometimes called the reconnection process, but this name is not necessary). At the point of acceleration, the magnetic field is early to zero or is directed parallel to the electric field. Acceleration of charged particles by an electric field in the current sheet leads to the generation of solar cosmic rays during solar flares and to the generation of galactic cosmic rays during powerful flares on stars.

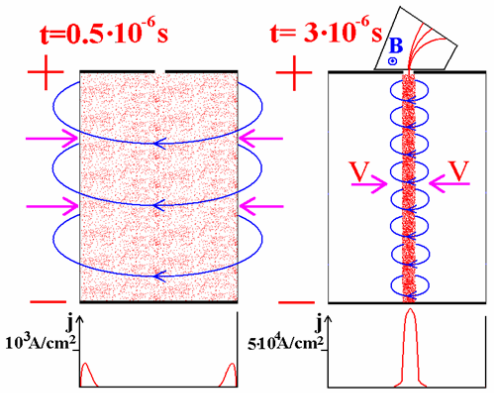

φ =15 kV
dI/dt = 10^{11} A/s
I_{max} =200 kA
W>300keV
E=-V×B/c
V~10^7cm/s
B_{max}~4·10^4G
E ~4·10^3 V/cm

Lab. № 2. 1954.
Atomnaja energija
№ 3. 1956.
Artsimovich et. al. P. 84.
Lukjanov, Podgorny. P. 93.

НИЯФ МГУ 1957.
Podgorny, Kovalsky, Palchikov.
DAN SSSR. 123, 825 (1958).

1957.
Severny } Electric discharge
Toneman } in solar corona.

С. Н. Вернов

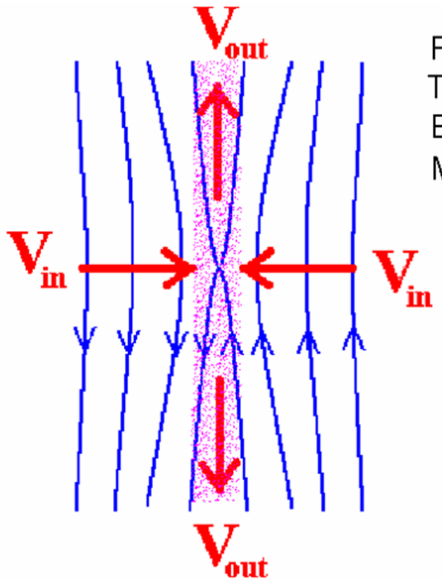

From RHESSI: (ME)=5·10^{49} cm^{-3}.
T=3.1 keV n=10^{11} cm^{-3}.
$B^2/8\pi = nkT \rightarrow B = 110G$.
$M = Nm_p \sim 10^{15}$ g --- CME.

At $V_{in} = 2 \times 10^7$ cm/s and $L = 10^9$ cm.
E= V×B/c. E=20 V/cm.

$W = 2 \times 10^{10}$ eV.

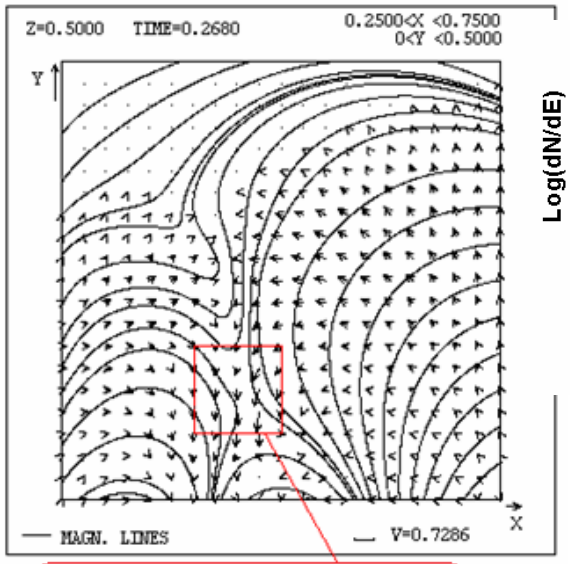

Область, в которой проводится расчет ускоренных частиц

The area in which the calculation of accelerated particles is carried out.

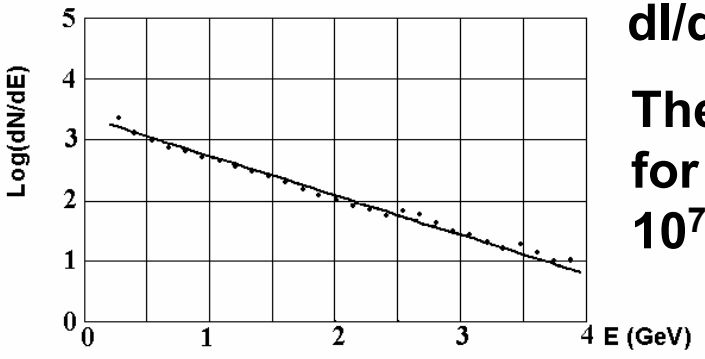

$dI/dE \sim \exp(-E/E_0)$ E_0=0.6 GeV

The rate of reconnection for E_0 ~ 0.6 GeV is order of 10^7 cm/s.

$$E=V_{in}\ B/c$$

Подгорный, Балабин, Вашенюк, Подгорный Астр. Журн. Т. 87, С. 704 (2010)

Podgorny, Balabin, Podgorny, Vashenyuk Journ. Atm. Solar-Ter. Phys. V. 72. P. 988 (2010)

It is necessary, by performing MHD simulations in the corona above the active region, to more accurately determine the electric and magnetic fields at the site of the flare energy release and the surrounding space in order to study the mechanism of cosmic ray acceleration and the possibility of their exit from a strong magnetic field above the active region by calculating the trajectories of charged particles in the obtained fields.

Since there is no information about plasma inhomogeneities, and, consequently, the diffusion coefficient in the equation for the propagation of accelerated particles is unknown, the prognozis for the appearance of cosmic rays in interplanetary space that can cause cosmonaut exposure is supposed to be based on the arrival times obtained by I. M. Podgorny (JASTP 2018. V. 180. P. 9.) by analyzing observational data.

Now it is necessary to find conditions for study cosmic ray acceleration by calculating the trajectories of charged particles in the electric and magnetic fields.

For this purpose MHD simulation is performed in the corona above the real active region.

The results of recent studies lead to the conclusion that in order to study the mechanism of a solar flare, the calculation should begin several days before the appearance of flares, when the magnetic energy for the flare has not yet accumulated in the corona.

Podgorny A.I., Podgorny I.M., Borisenko A.V. 2022. Open Astronomy. 31: 27–37. https://doi.org/10.1515/astro-2022-0006

Borisenko A.V., Podgorny I.M., Podgorny A.I. 2022. Open Astronomy. 31: 58–66. https://doi.org/10.1515/astro-2022-0008

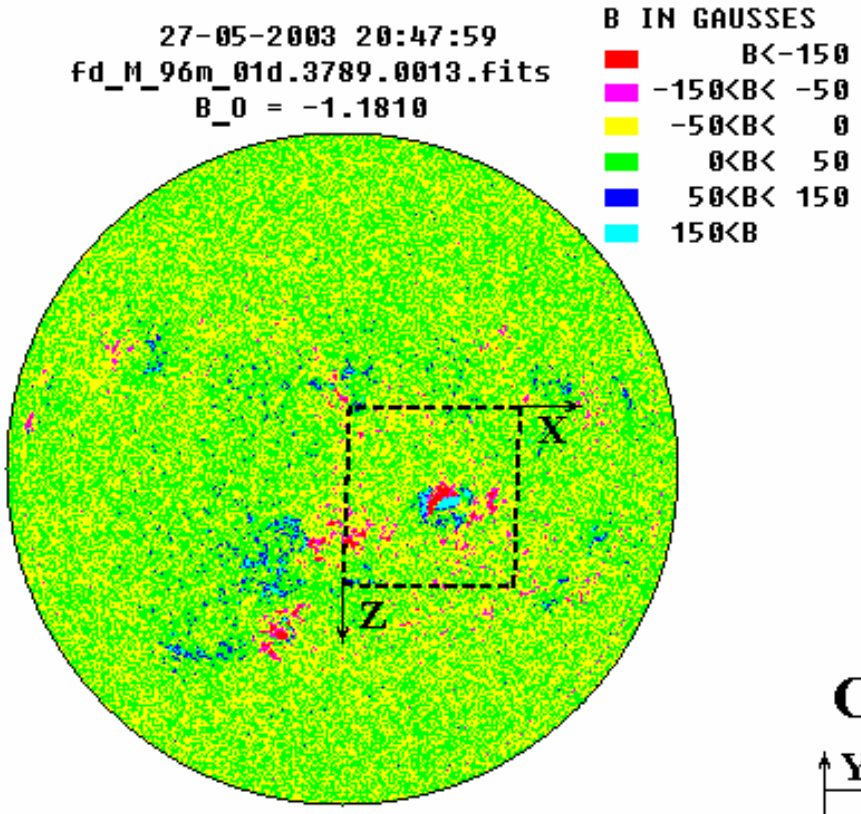

--- REGION IN PICTURE PLANE

COMPUTATIONAL DOMAIN IN CORONA ABOVE ACTIVE REGION

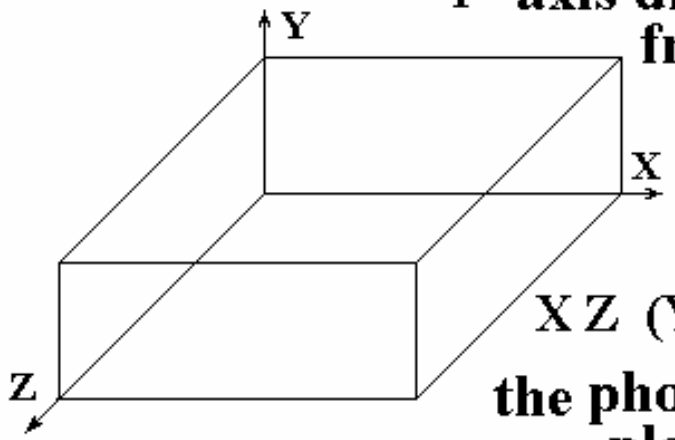

Y- axis directed from the Sun

X Z (Y=0) - is the photosphere plane

Cross-section Z=const

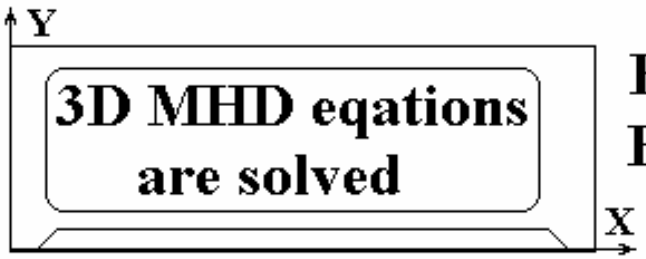

Photospheric boundary:

$B_{||}$ from calculated potential field for observed $B_{line\text{-}of\text{-}site}$

$B_{\perp}$ from $divB = 0$; $\rho = const$; $\partial V/\partial n = 0$; $\partial T/\partial n = 0$

Nonphotospheric boundary:

$B_{\perp}$ from $divB = 0$

$B_{||}$ from $\partial j/\partial n = 0$

$\partial \rho/\partial n = 0$

$\partial V/\partial n = 0$

$\partial T/\partial n = 0$

($V = 0$

$T = const$

$B_{||} = const$)

The numerical 3D simulation in corona above active region. The system of MHD equations for compressible plasma with dissipative terms and anisotropy of thermal conductivity is solved. The numerical instability is stabilized by introducing an artificial viscosity.

$$\frac{\partial \mathbf{B}}{\partial t} = \mathrm{rot}(\mathbf{V}\times\mathbf{B}) - \frac{1}{\mathrm{Re}_m}\mathrm{rot}\left(\frac{\sigma_0}{\sigma}\mathrm{rot}\mathbf{B}\right) + \mathrm{rot}\left(\nu_{m\_\mathrm{Art}}\mathrm{rot}\mathbf{B}\right) \quad (1)$$

$$\frac{\partial \rho}{\partial t} = -\mathrm{div}(\mathbf{V}\rho) \quad (2)$$

$$\frac{\partial \mathbf{V}}{\partial t} = -(\mathbf{V},\nabla)\mathbf{V} - \frac{\beta_0}{2\rho}\nabla(\rho T) - \frac{1}{\rho}(\mathbf{B}\times\mathrm{rot}\mathbf{B}) + \frac{1}{\mathrm{Re}\rho}\Delta\mathbf{V} + G_g\mathbf{G} + \nu_{\mathrm{Art}}\Delta\mathbf{V} \quad (3)$$

$$\frac{\partial T}{\partial t} = -(\mathbf{V},\nabla)T - (\gamma-1)T\mathrm{div}\mathbf{V} + (\gamma-1)\frac{2\sigma_0}{\mathrm{Re}_m\sigma\beta_0\rho}(\mathrm{rot}\mathbf{B})^2 - (\gamma-1)G_q\rho L'(T) +$$
$$+\frac{\gamma-1}{\rho}\mathrm{div}\left(\mathbf{e}_{\|}\kappa_{dl}(\mathbf{e}_{\|},\nabla T) + \mathbf{e}_{\perp 1}\kappa_{\perp dl}(\mathbf{e}_{\perp 1},\nabla T) + \mathbf{e}_{\perp 2}\kappa_{\perp dl}(\mathbf{e}_{\perp 2},\nabla T)\right) \quad (4)$$

The PERESVET program was developed

A.I. Podgorny Solar Phys. 156,41,1995.

A.I. Podgorny, I.M. Podgorny

Solar Phys. 139, 125, 1992 — Cosmic Research 35, 35, 1997
161, 165, 1995 — 35, 235, 1997
182, 159, 1998 — 36, 492, 1998
207, 323, 2002

Astronomy Reports 42, 116, 1998 — 45, 60, 2001 — 48, 435, 2004
43, 608, 1999 — 46, 65, 2002 — 49, 837, 2005
44, 407, 2000 — 47,696,2003 — 52, 666, 2008

Comput. Mathem. Mathematical Phys 44, 1784, 2004 — 54, 645, 2010

Absolutely implicit upwind finite-difference scheme, conservative with respect to the magnetic flux

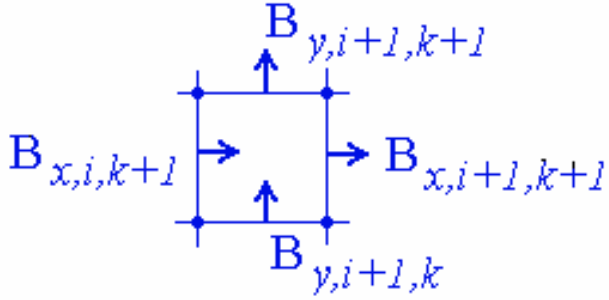

$$\sum \mathbf{B}_n \Delta S = 0$$

Precise conservation of [div B]=0 : equations

$$\partial \mathbf{B} / \partial t = \mathrm{rot}(\mathbf{V} \times \mathbf{B}) + \nu_m \Delta \mathbf{B}$$ **and**

$$\partial \mathbf{B} / \partial t = \mathrm{rot}(\mathbf{V} \times \mathbf{B}) - \nu_m \mathrm{rot}(\mathrm{rot}\mathbf{B})$$ **are equivalent.**

During dissipative relaxation of magnetic field numerical value of current density [rot B] → 0.

For upwind upproximation of $\mathrm{rot}(\mathbf{V} \times \mathbf{B})$ the elements of vector $\mathbf{V} \times \mathbf{B}$ are approximated by:

For $V_{x,i,k} > 0$

$$(V_x B_y)_{i,k} = V_{x,i,k}\, B_{y,i,k}$$

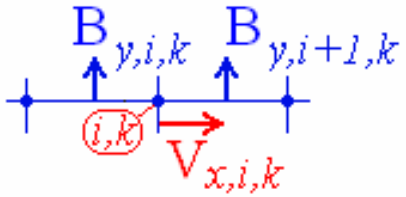

For $V_{x,i,k} < 0$

$$(V_x B_y)_{i,k} = V_{x,i,k}\, B_{y,i+1,k}$$

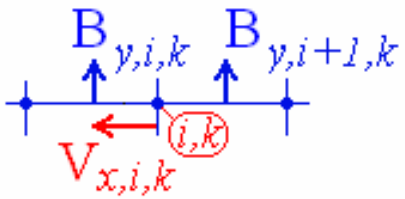

Despite the use of specially developed methods, the calculations are slow. To perform MHD simulation in the real scale of time **there is a need to use parallel computing.**

Parallelization of computations was carried out using CUDA technology on modern graphics cards (GPU). The modern software (Fortran PGI) was used. The methods of optimizing the parallelization of calculations were develop including minimization of data exchange between the memory of GPU and the memory of central processor.

For optimization of the algorithm parallelization calculations it was performed more than 20 modernizations of the code, as the result of which the speed of calculation increase in 7.5 times and became 120 times faster than the calculation speed of a non-parallel program, in which in which the same difference scheme is realized. After the performed optimization, the computation time for one iteration on the used grid of the difference scheme $135 \times 41 \times 135$ was 0.02 sec.

SET OF FLARES MAY 26-29, 2003

AR 10365

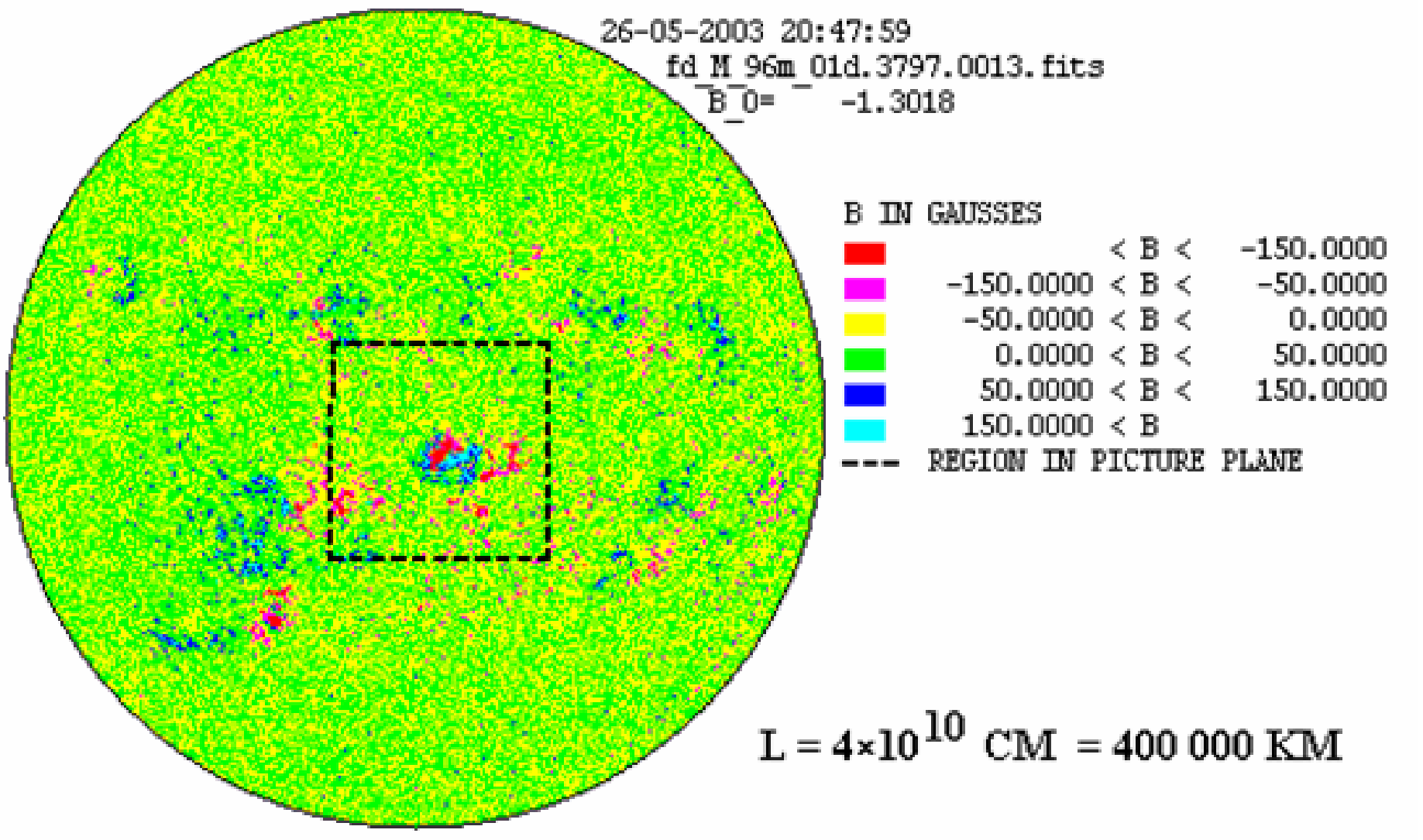

MHD simulation above AR 10365 within 3 days starting from the moment of 24.05.2003 20:48

The parameters are chosen in accordance with the principle of limited simulation (I.M. Podgorny, 1978), according to which much larger or much smaller units, dimensionless parameters remain much larger or smaller than units when simulated without their exact preservation.

Parameters in the region in corona above the chosen active region:

$Re_m = L_0 V_0/\nu_m = 2\times10^{16}$, $Re = 10^4$, $Re_{(B\text{-}MAGNET)} = 10^{20}$,

$\beta = 8\pi p_0/B_0^2 = 0.6\times10^{-5}$

(B_0=300Gs, $n_0 = 10^8$ cm^{-3}, T_0=1.5×10^6 ^{0}K=130 eV = 2×10^{-10} erg)

$Re_m = 10^9$, $Re = 10^7$, $\beta=0.6\times10^{-5}$ –

the set of parameters is now selected. At low viscosities, the perturbation propagating from the photospheric boundary was not suppressed, which contributed to the accumulation of the energy of flare above the AR and the formation of pronounced current sheets in the vicinity of singular lines.

Obtaining a stable solution near the boundary of the domain is one of the main problems of numerical methods.

The calculations showed the appearance of instability at simulation in the real scale of time (since the instability has time to develop over a sufficiently long period of time, despite using the specially developed numerical methods and parallel computations).

Stabilization of the numerical instability near the boundary of computational domain using the artificial viscosity

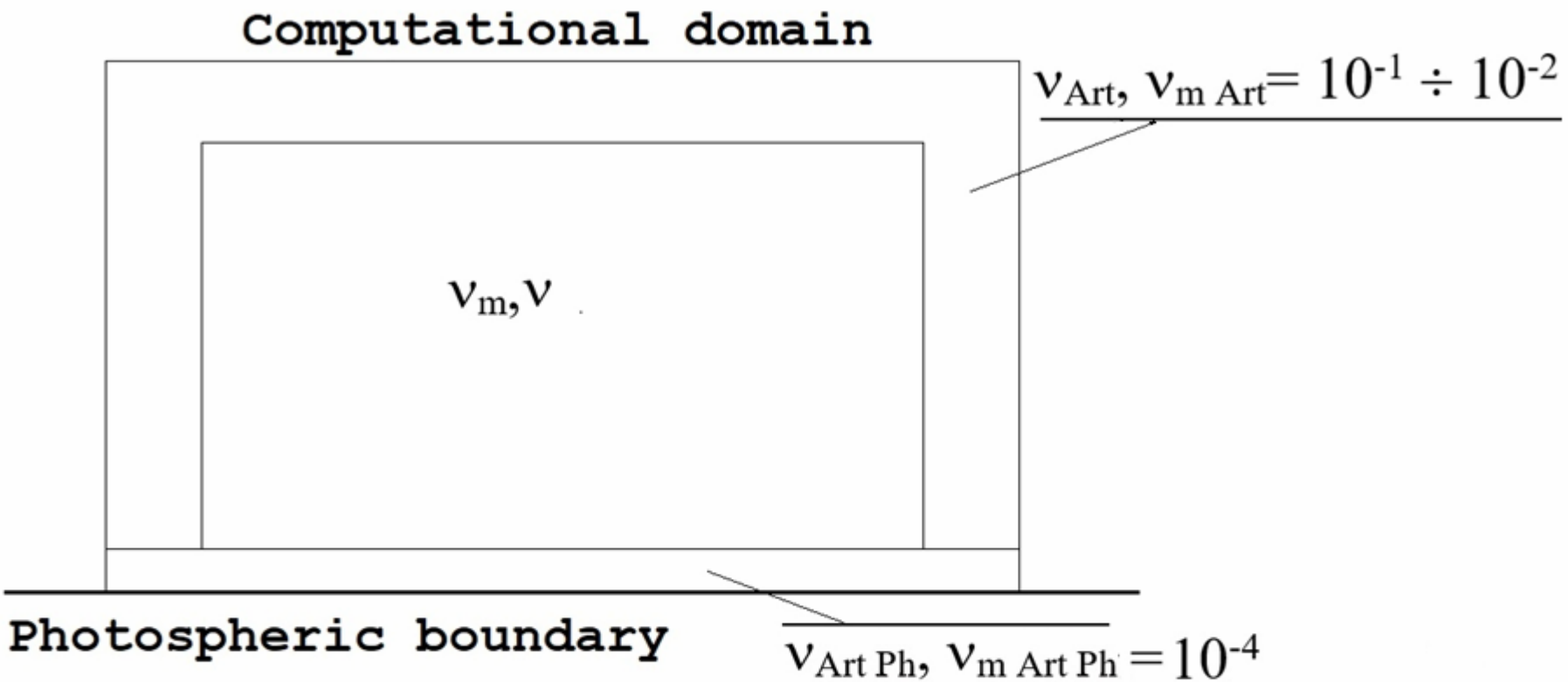

$\nu_m=10^{-9}$ ($Rm=10^9$); $\nu=10^{-7}$ ($Re=10^7$)

(In the solar corona $Rm=10^{16}$, $Re=10^4$, $Re_B=10^{20}$; the grid viscosity $\nu_{grid}=h\,V_{DimLess}$; $h=0.5\times10^{-2}$; $V_{DimLess}=10^{-6} \div 10^{-3}$; $a=\nu_m/V_{in}$)

The problem of instability stabilization near the boundary is partially solved.

When instability appears at the boundary, in addition to applying the proposed methods, smaller time steps and a larger number of iterations are required to stabilize it.

For calculations with low viscosities ($Re_m = 10^9$, $Re = 10^7$), which is of the greatest interest, the problem of instability stabilization near the boundary is partially solved. It was possible to carry out the simulation for a period close to three days, although at the end of this period the calculation was very slow, since it was possible to stabilize the instabilities near the boundary only for very small time steps.

The results obtained make it possible to determine ways to further improve the technique for stabilizing numerical instabilities.

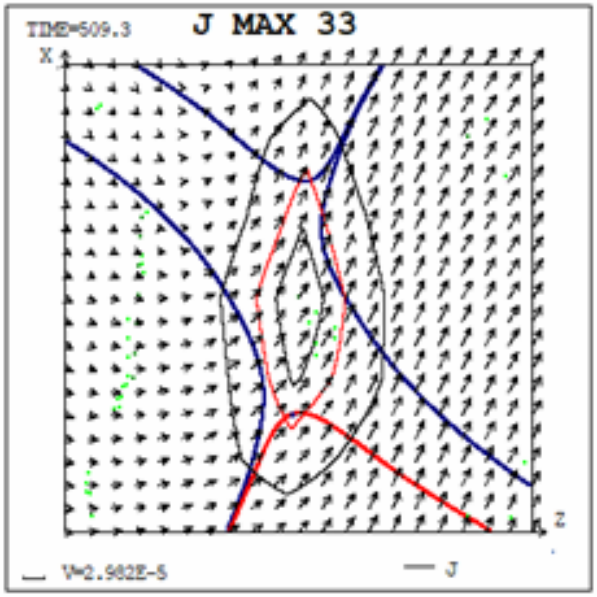
TIME=509.3
J MAX 33
X
Z
V=2.962E-5
J

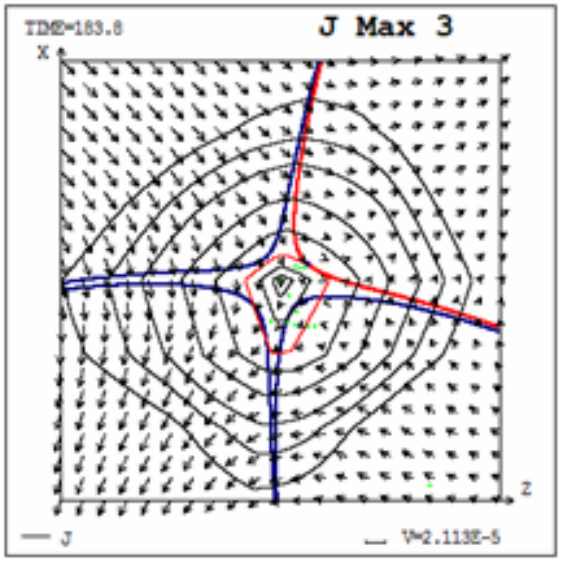
TIME=183.8
J Max 3
X
Z
J
V=2.113E-5

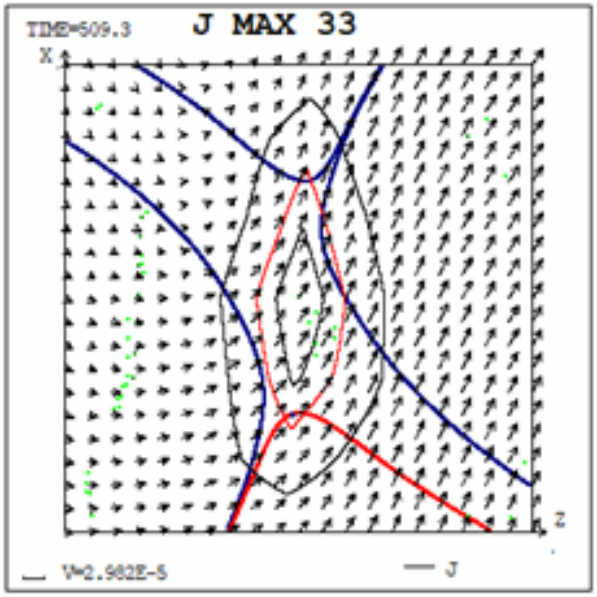
TIME=509.3
J MAX 33
X
Z
V=2.962E-5
J

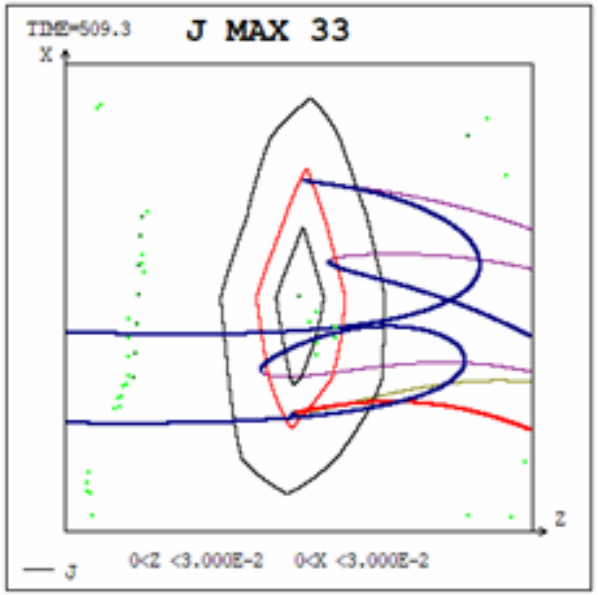
TIME=509.3
J MAX 33
X
Z
J
0<Z <3.000E-2
0<X <3.000E-2

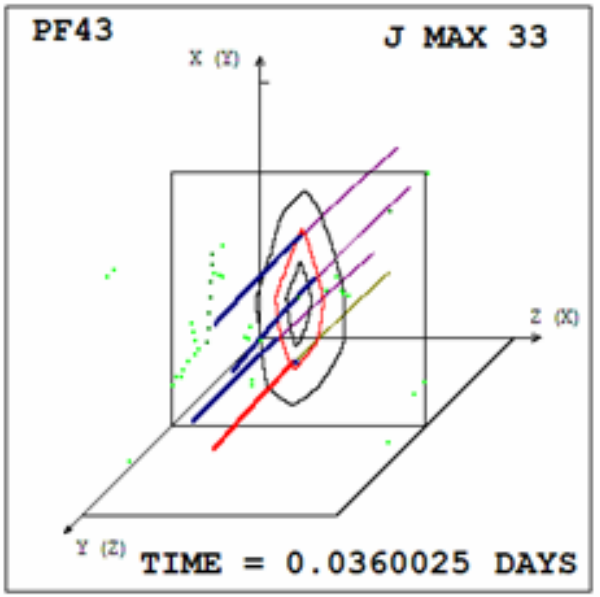
PF43
J MAX 33
X (Y)
Z (X)
Y (Z)
TIME = 0.0360025 DAYS

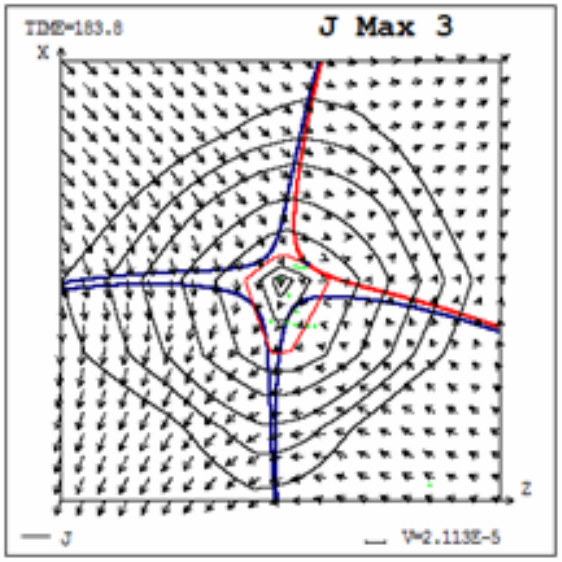
TIME=183.8
J Max 3
X
Z
J
V=2.113E-5

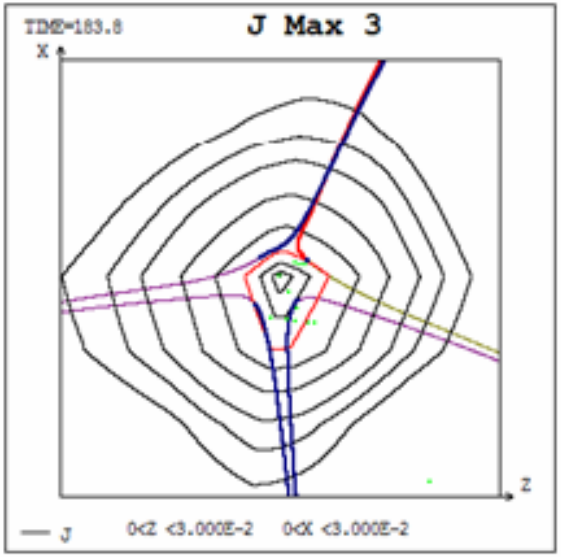
TIME=183.8
J Max 3
X
Z
J
0<Z <3.000E-2
0<X <3.000E-2

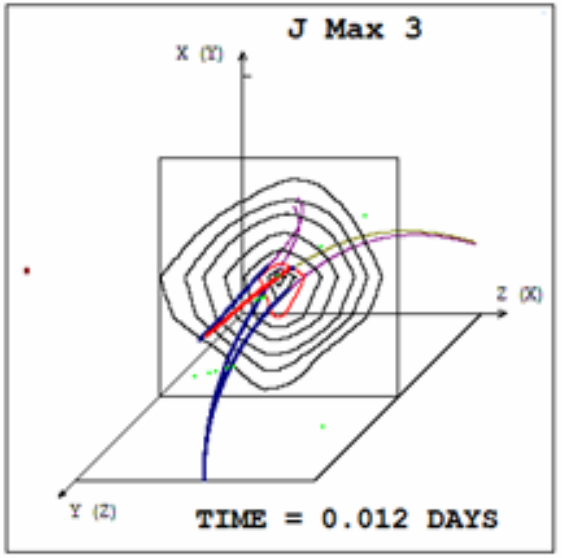
J Max 3
X (Y)
Z (X)
Y (Z)
TIME = 0.012 DAYS

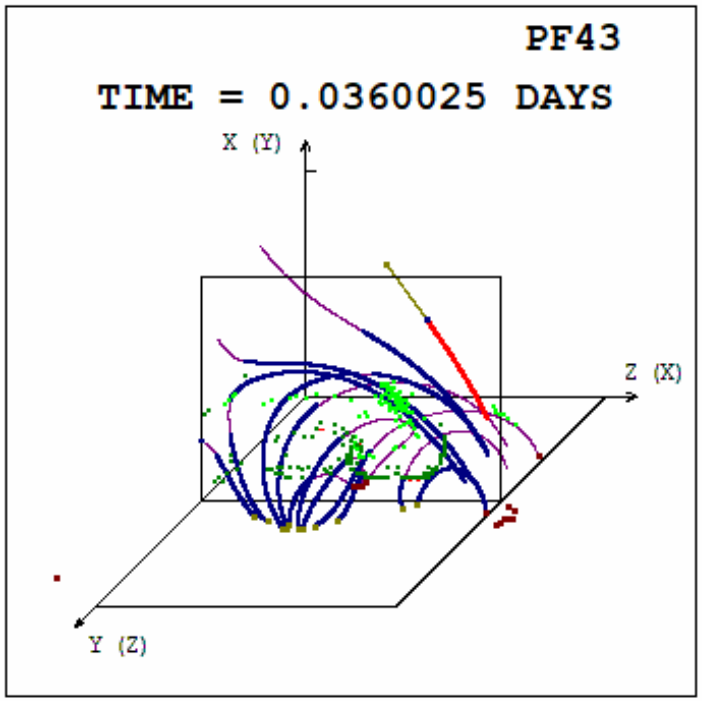
PF43
TIME = 0.0360025 DAYS
X (Y)
Z (X)
Y (Z)

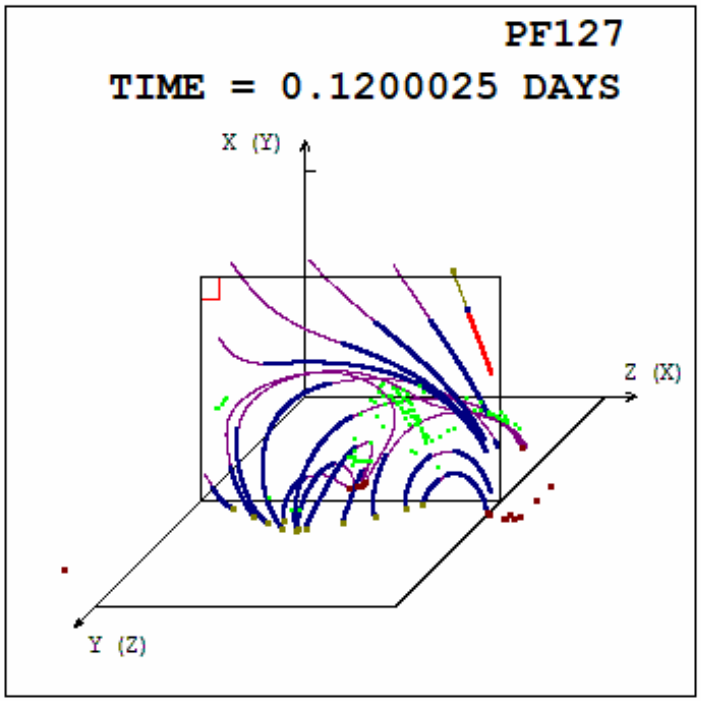
PF127
TIME = 0.1200025 DAYS
X (Y)
Z (X)
Y (Z)

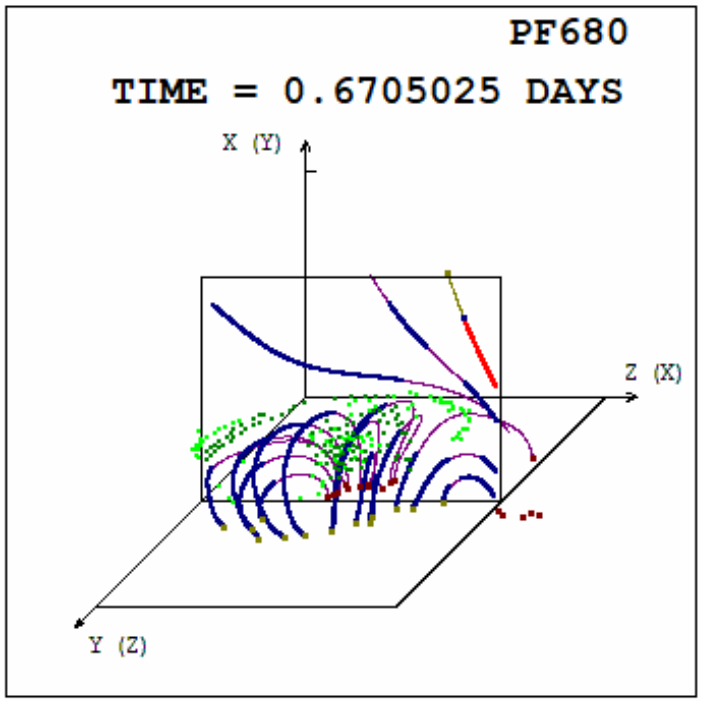
PF680
TIME = 0.6705025 DAYS
X (Y)
Z (X)
Y (Z)

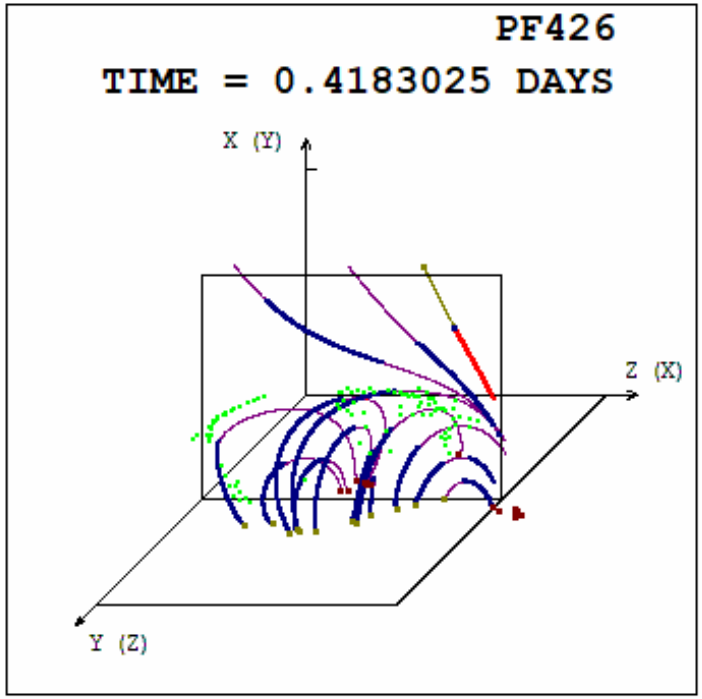
PF426
TIME = 0.4183025 DAYS
X (Y)
Z (X)
Y (Z)

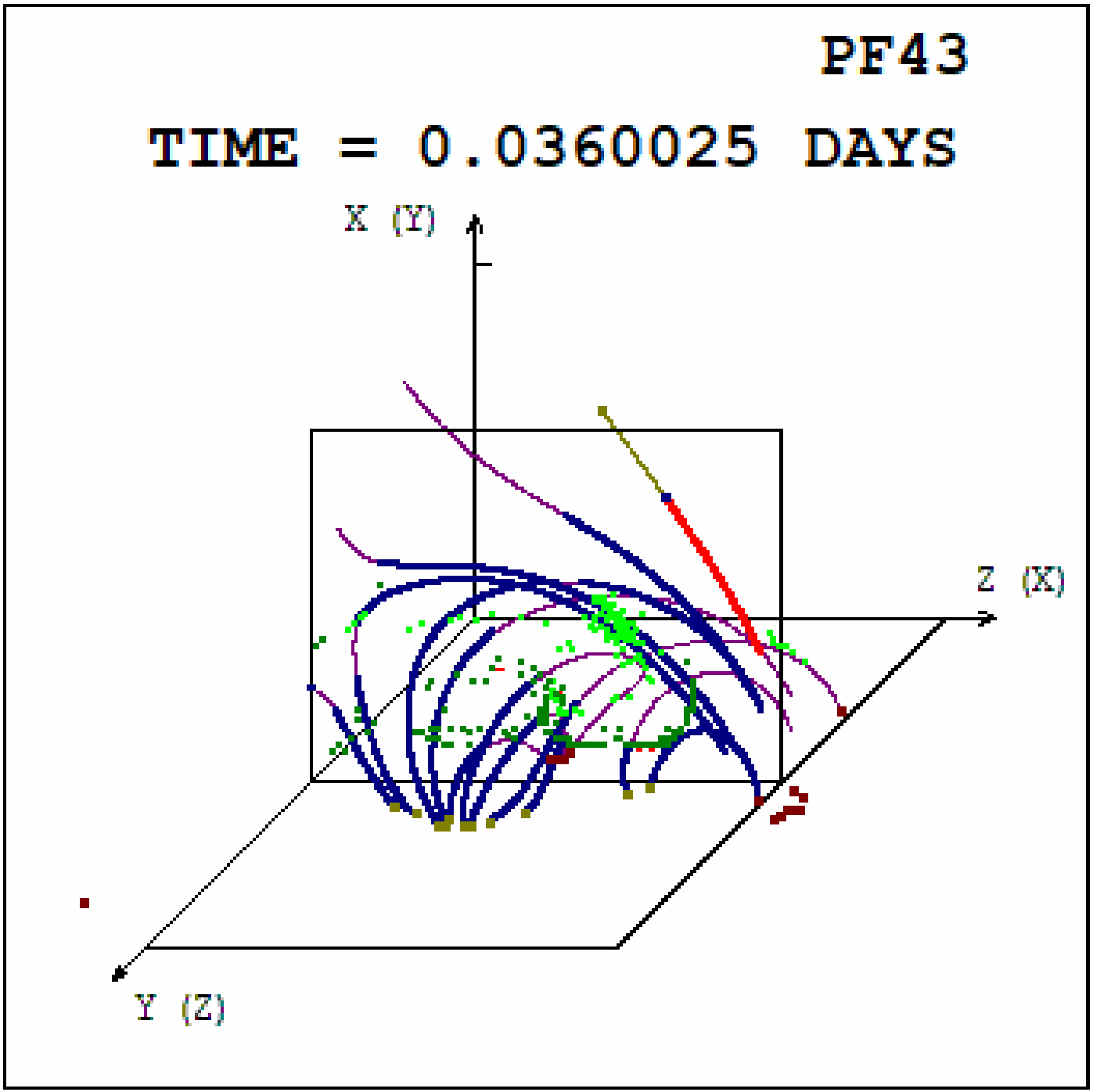
PF43
TIME = 0.0360025 DAYS
X (Y)
Z (X)
Y (Z)

The graphical system for searching of flare positions from the results of MHD simulation to compare with positions of sources of thermal X-ray emission is specially developed.

To search for the position of the current sheet, its property is used, according to which the local maximum of the absolute value of the current density is located in the center of the current sheet. The positions of all local maxima of the current density are sought. In the vicinity of the point of maximum current density, which lie on an X-type singular line, the configuration of the magnetic field is investigated. The analysis of the magnetic field configuration is carried out primarily in the so-called configuration plane, i.e. in the plane perpendicular to the magnetic field vector.

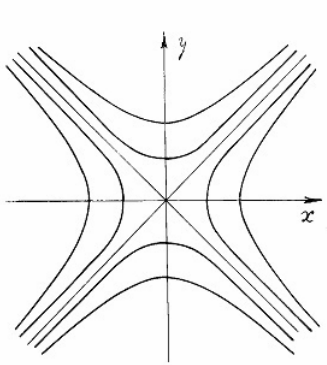

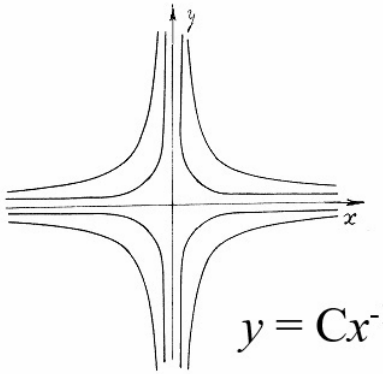

$y = Cx^{-1}$

$$\nabla \mathbf{B} = \begin{pmatrix} \frac{dB_x}{dx} & \frac{dB_x}{dy} & \frac{dB_x}{dz} \\ \frac{dB_y}{dx} & \frac{dB_y}{dy} & \frac{dB_y}{dz} \\ \frac{dB_z}{dx} & \frac{dB_z}{dy} & \frac{dB_y}{dz} \end{pmatrix} \quad \begin{pmatrix} \frac{dB_x}{dx} & \frac{dB_x}{dy} \\ \frac{dB_y}{dx} & \frac{dB_y}{dy} \end{pmatrix} \quad \begin{pmatrix} \lambda_1 & 0 \\ 0 & \lambda_2 \end{pmatrix}$$

$y = Cx^{\alpha}$, $\alpha = \lambda_2/\lambda_1$

$y = Cx^{-1}$

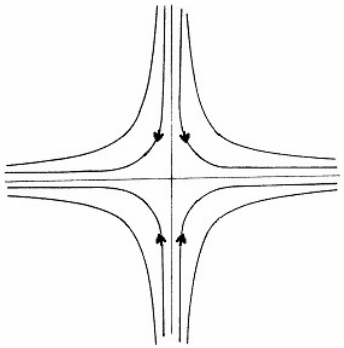

+

$y = Cx$

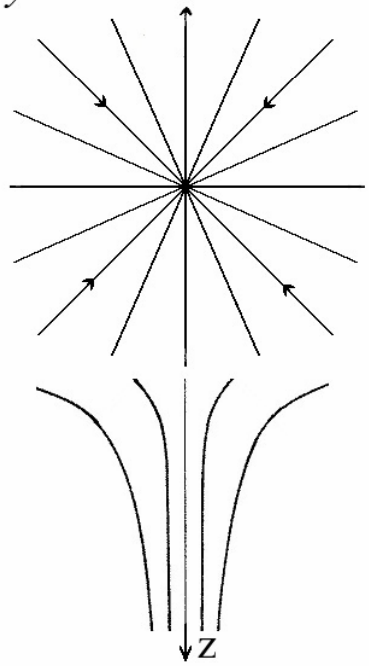

=

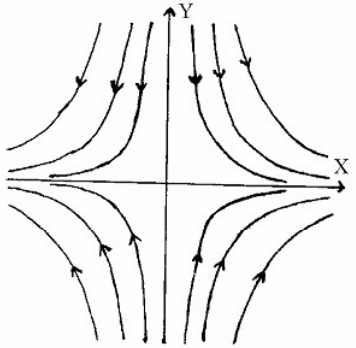

$\alpha < 0$

λ_1 и λ_2 разных знаков

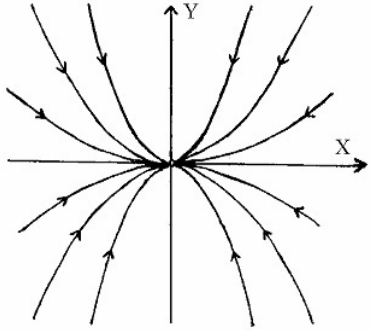

$\alpha > 0$

λ_1 и λ_2 одного знака

$y = Cx^{\alpha}$, $\alpha = \lambda_2/\lambda_1$

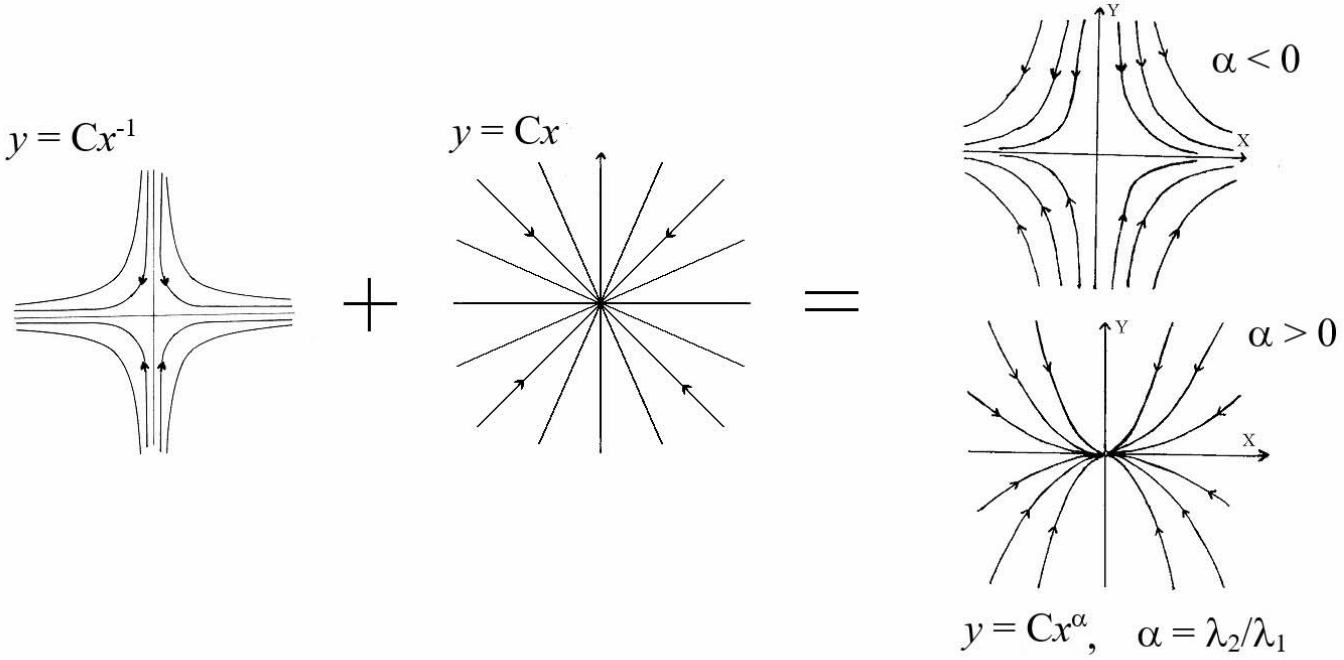
$y = Cx^{-1}$
$y = Cx$
$\alpha < 0$
$\alpha > 0$
Y
X
$y = Cx^{\alpha}, \quad \alpha = \lambda_2/\lambda_1$

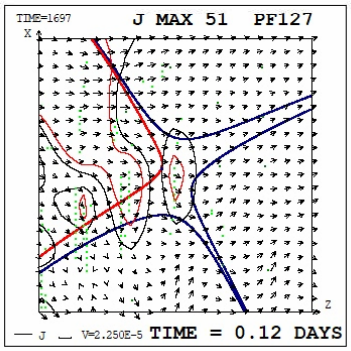
TIME=1697
J MAX 51 PF127
V=2.250E-5
TIME = 0.12 DAYS

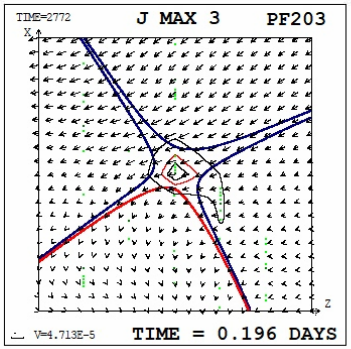
TIME=2772
J MAX 3 PF203
V=4.713E-5
TIME = 0.196 DAYS

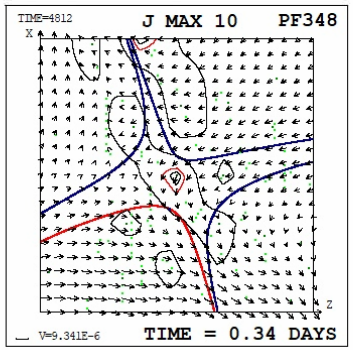
TIME=4812
J MAX 10 PF348
V=9.341E-6
TIME = 0.34 DAYS

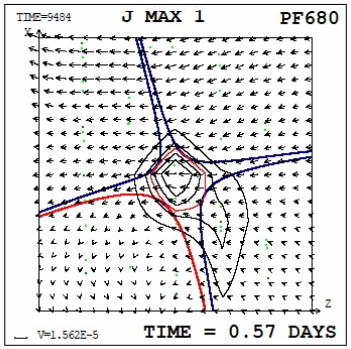
TIME=9484
J MAX 1 PF680
V=1.562E-5
TIME = 0.57 DAYS

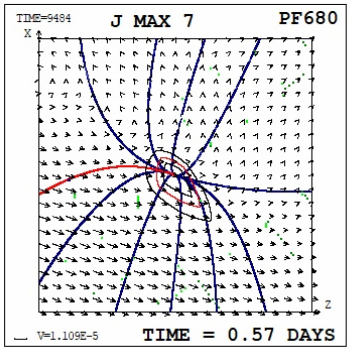
TIME=9484
J MAX 7 PF680
V=1.109E-5
TIME = 0.57 DAYS

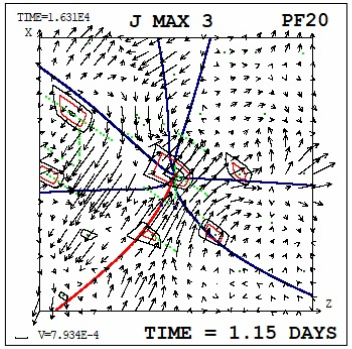
TIME=1.631E4
J MAX 3 PF20
V=7.934E-4
TIME = 1.15 DAYS

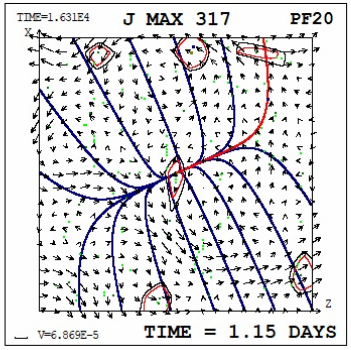
TIME=1.631E4
J MAX 317 PF20
V=6.869E-5
TIME = 1.15 DAYS

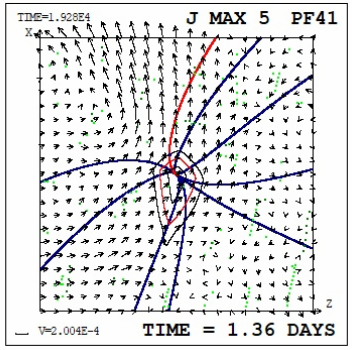
TIME=1.928E4
J MAX 5 PF41
V=2.004E-4
TIME = 1.36 DAYS

$y = Cx^{-1}$

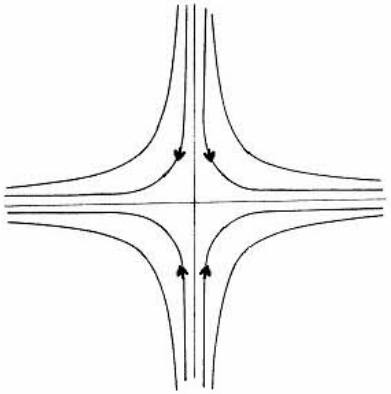

$y = Cx$

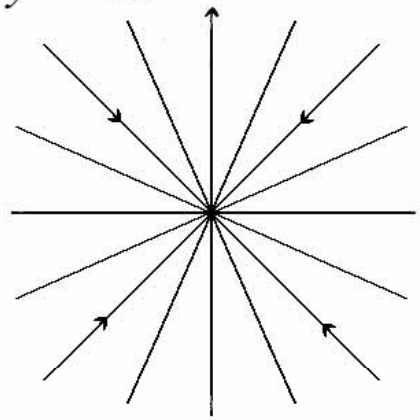

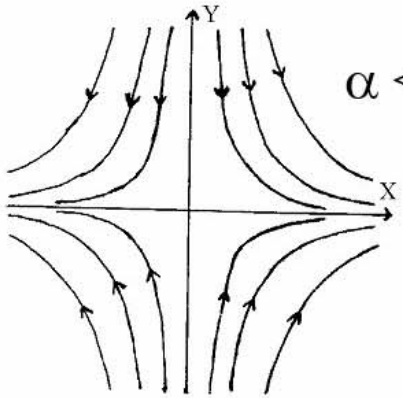

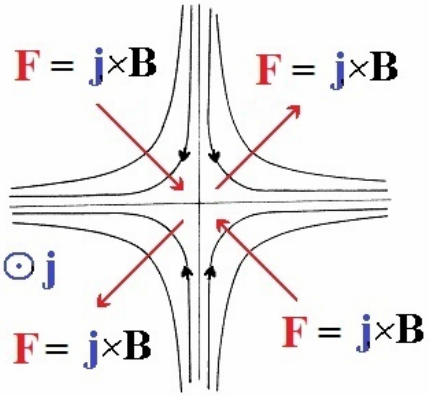

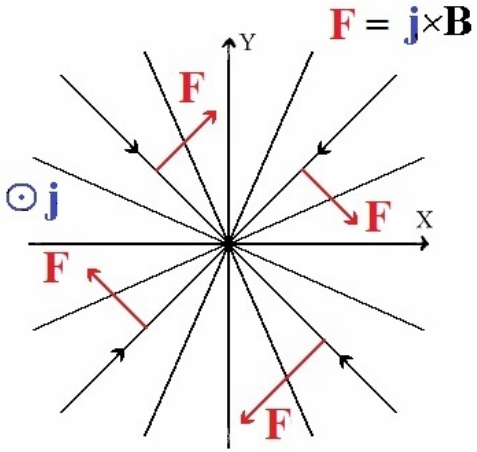

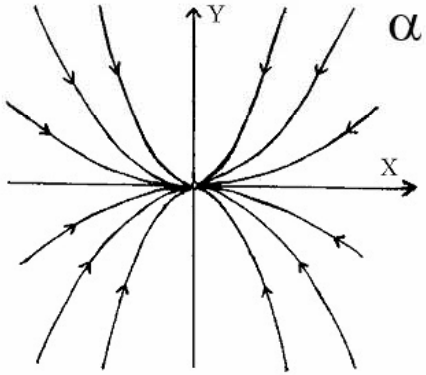

$y = Cx^{\alpha}, \quad \alpha = \lambda_2/\lambda_1$

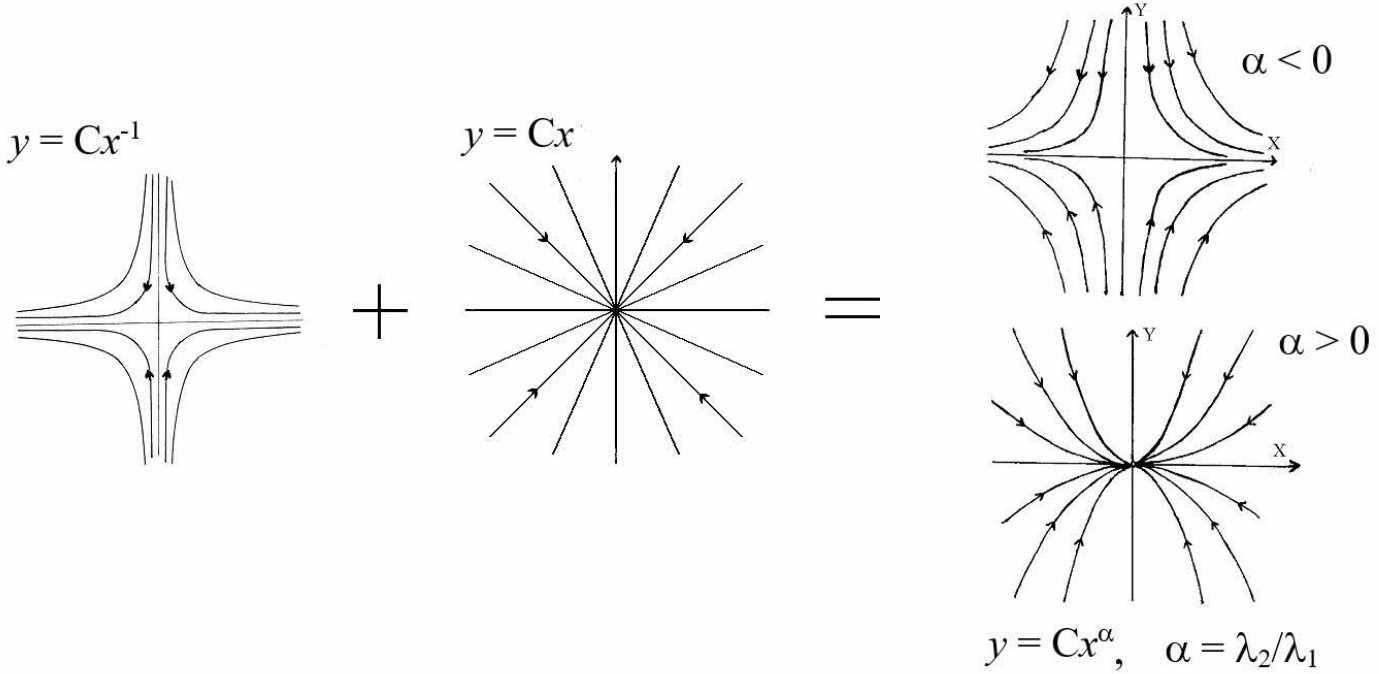
$y = Cx^{-1}$
$y = Cx$
$\alpha < 0$
$\alpha > 0$
X
Y
$y = Cx^{\alpha}, \quad \alpha = \lambda_2/\lambda_1$

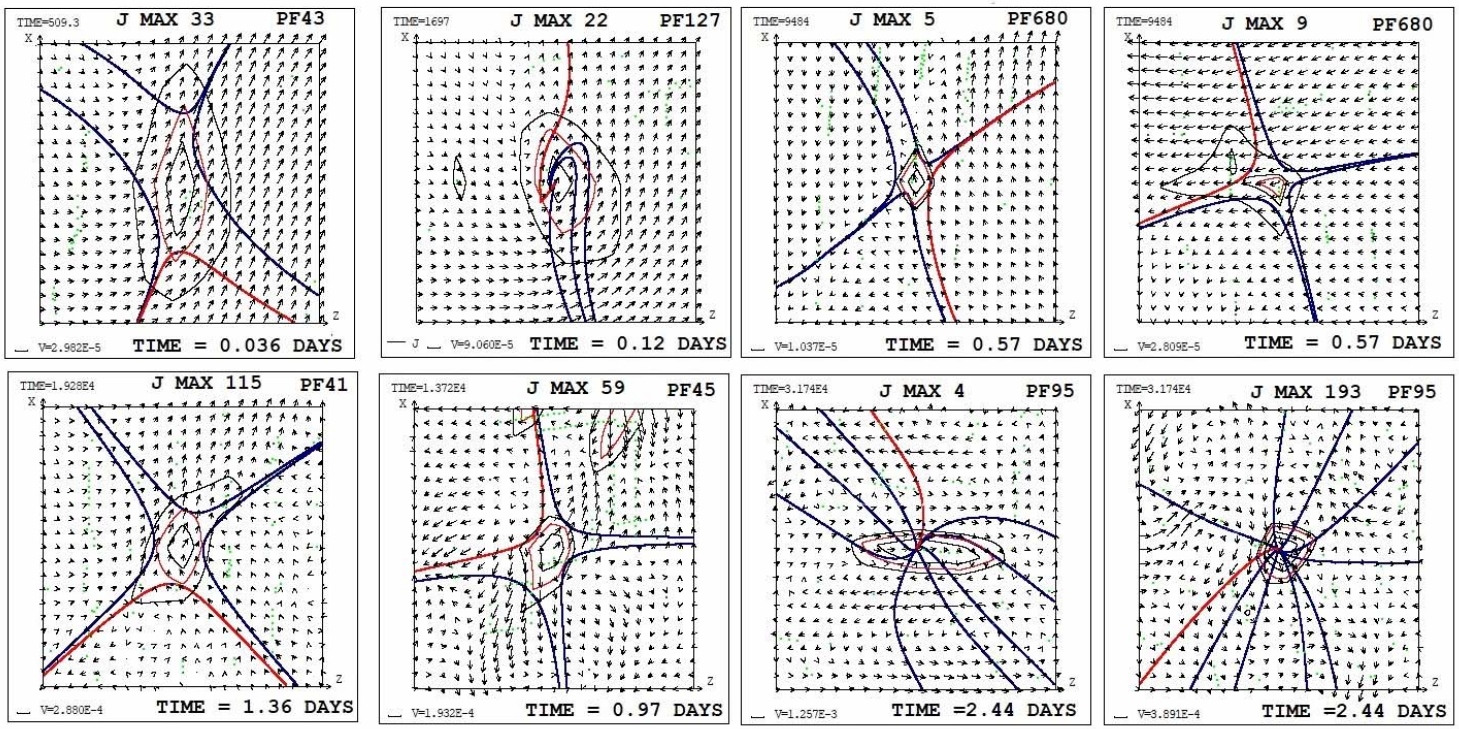
TIME=509.3 J MAX 33 PF43
TIME = 0.036 DAYS
TIME=1697 J MAX 22 PF127
TIME = 0.12 DAYS
TIME=9484 J MAX 5 PF680
TIME = 0.57 DAYS
TIME=9484 J MAX 9 PF680
TIME = 0.57 DAYS
TIME=1.928E4 J MAX 115 PF41
TIME = 1.36 DAYS
TIME=1.372E4 J MAX 59 PF45
TIME = 0.97 DAYS
TIME=3.174E4 J MAX 4 PF95
TIME =2.44 DAYS
TIME=3.174E4 J MAX 193 PF95
TIME =2.44 DAYS

Flare M1.9 26.05.2003 at 05:34 above AR 10365

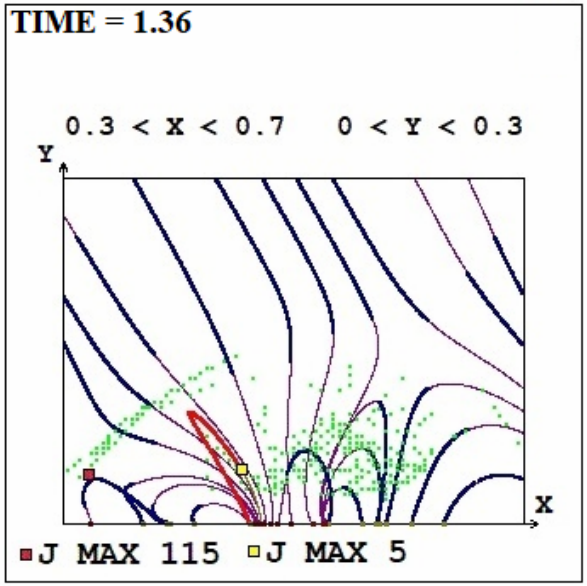

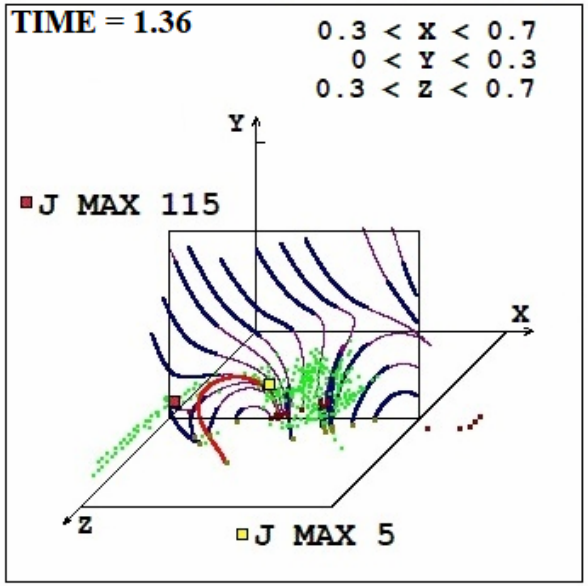

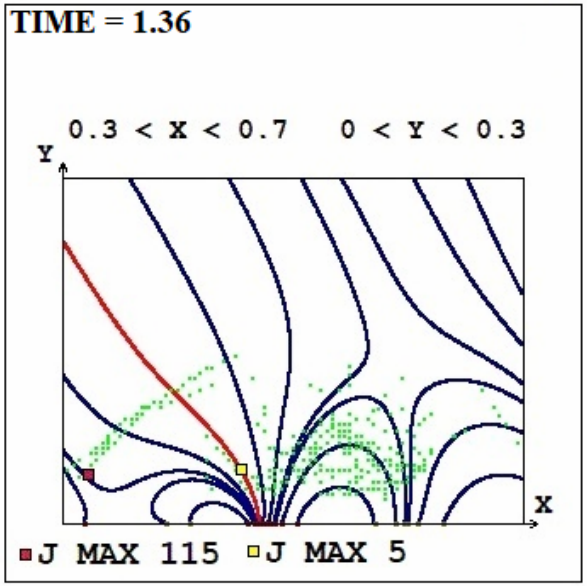

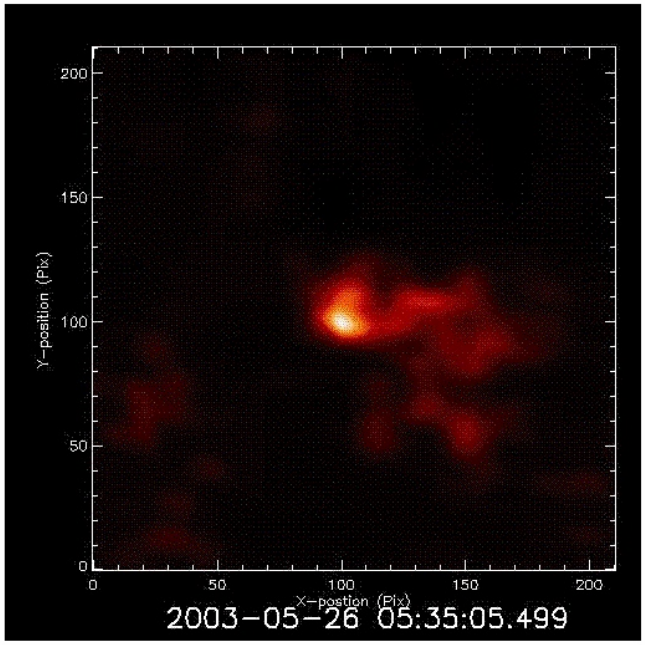

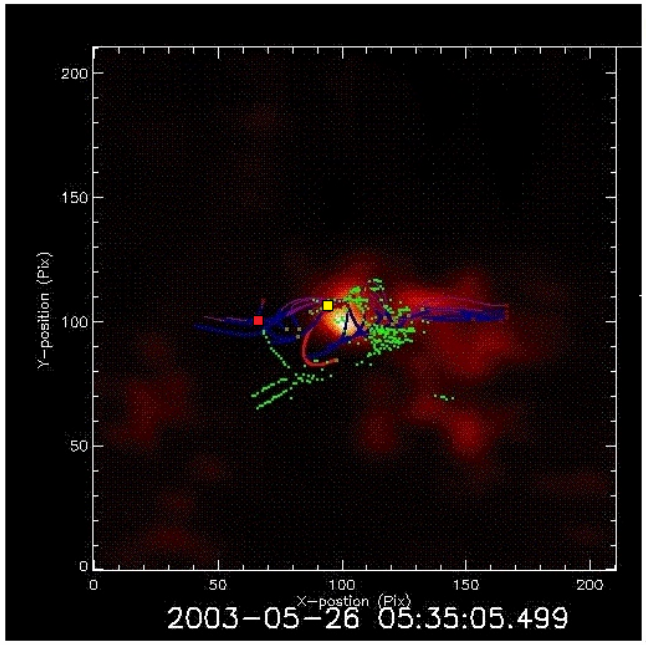

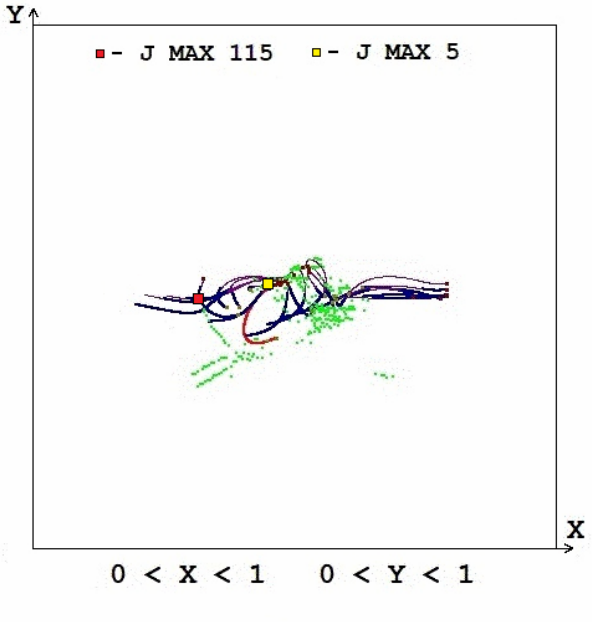

Radio emission at a frequency of 17 Ghz, obtained with the Nobeyama Radioheliograph

Flare M1.9 26.05.2003 at 05:34 above AR 10365

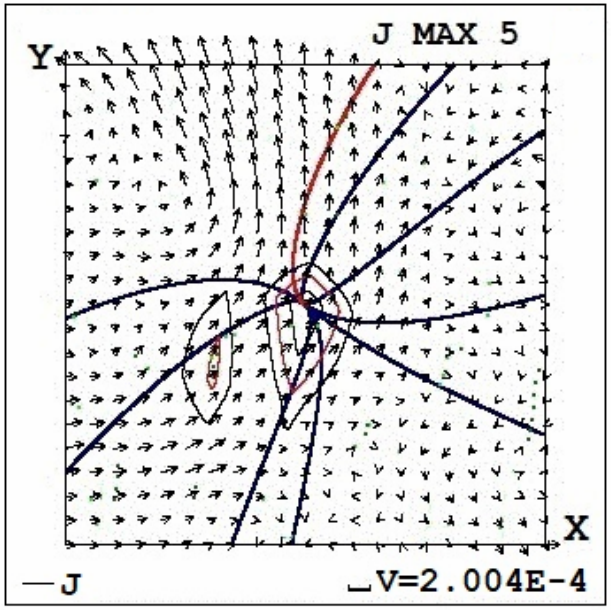

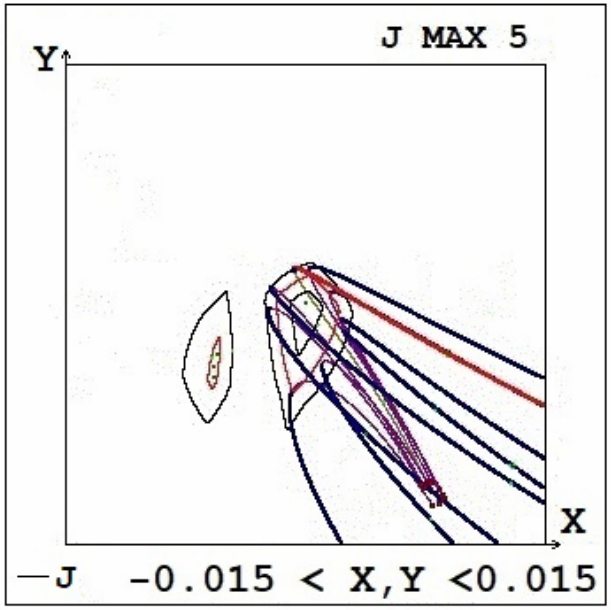

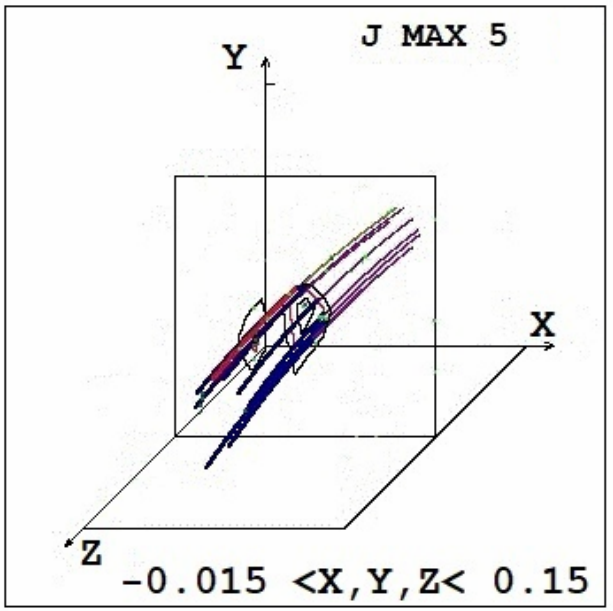

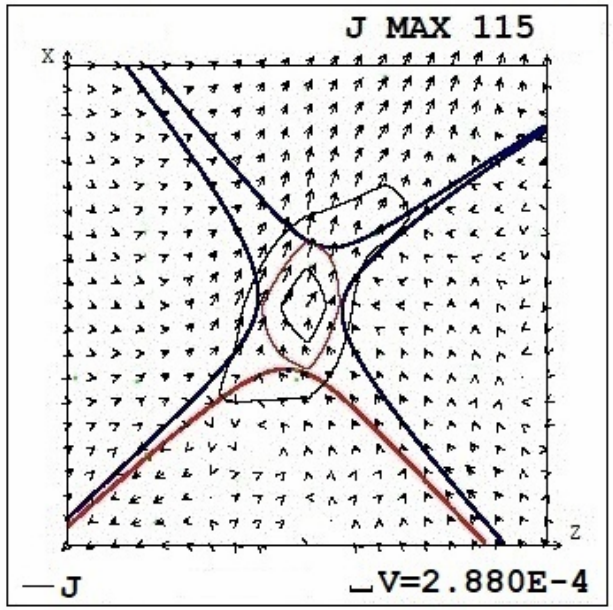

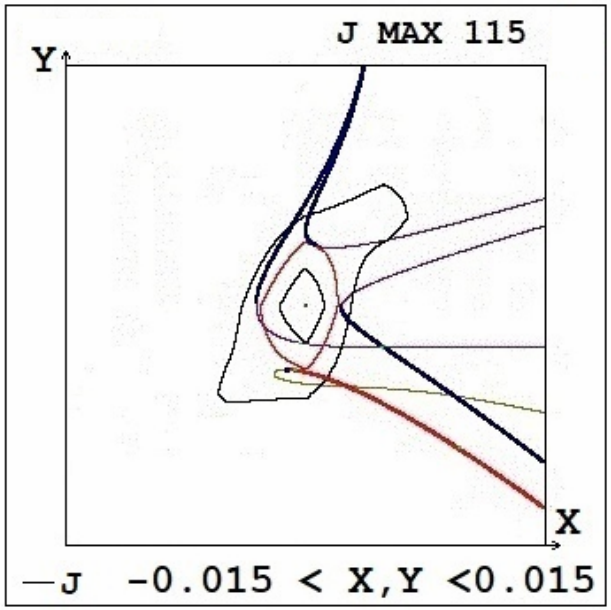

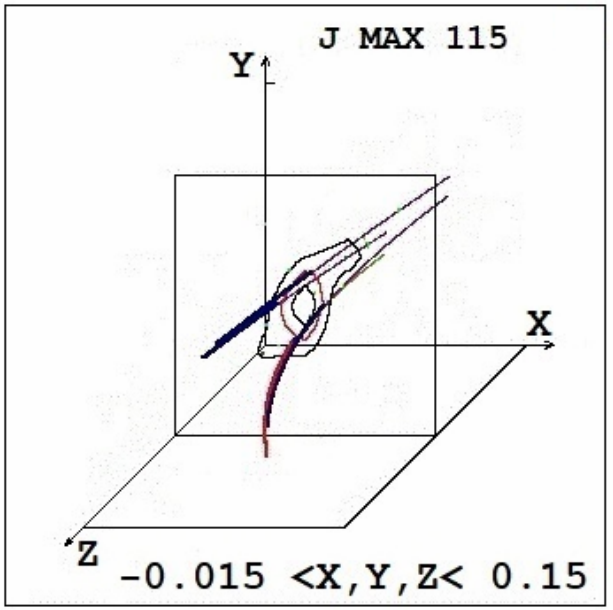

Flare M1.4 27.05.2003 at 02:43 above AR 10365

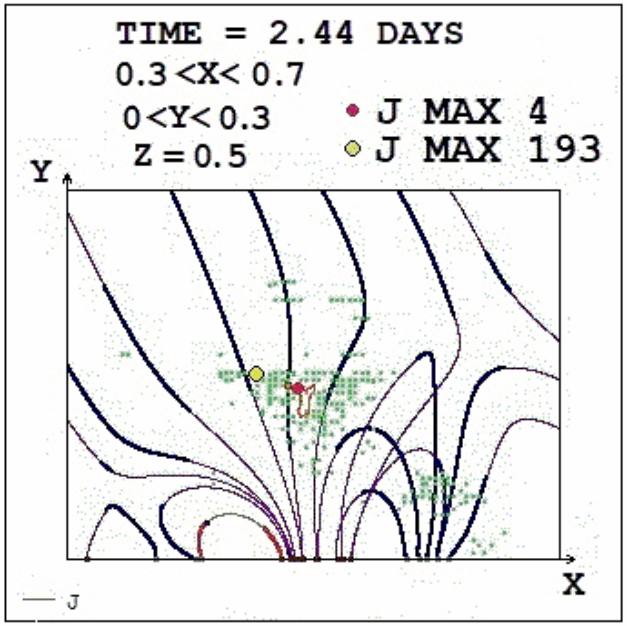

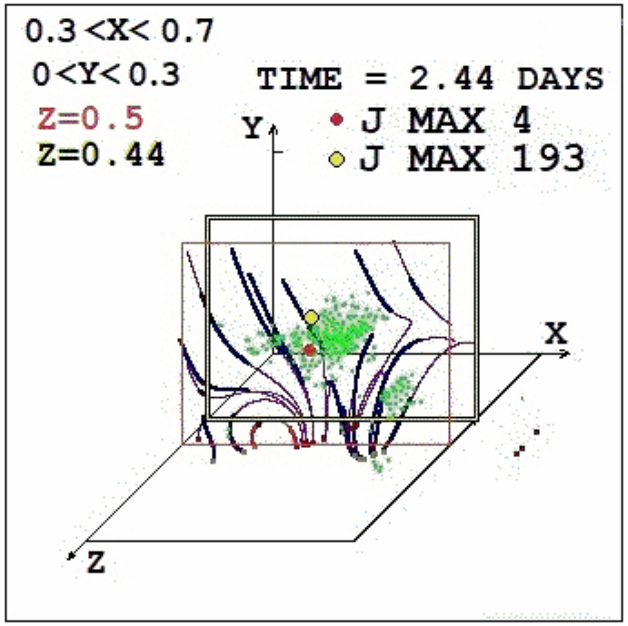

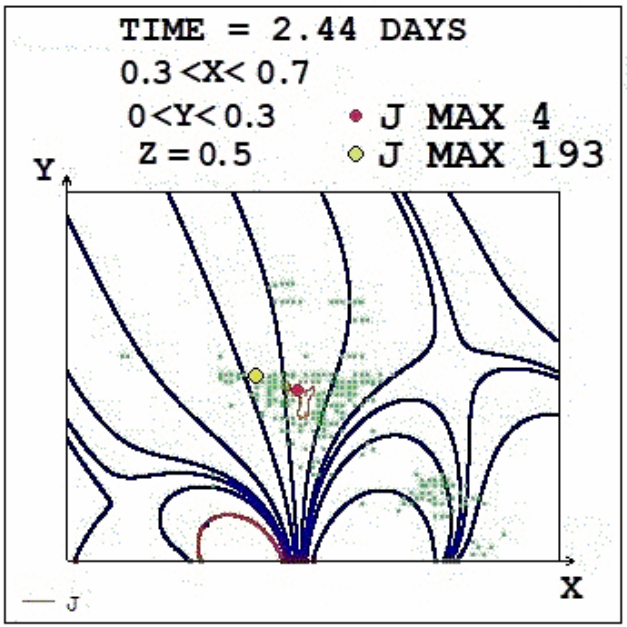

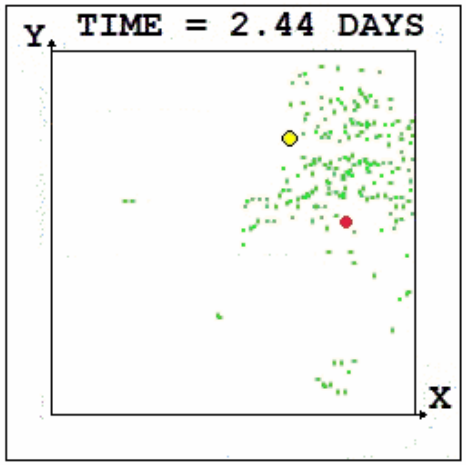

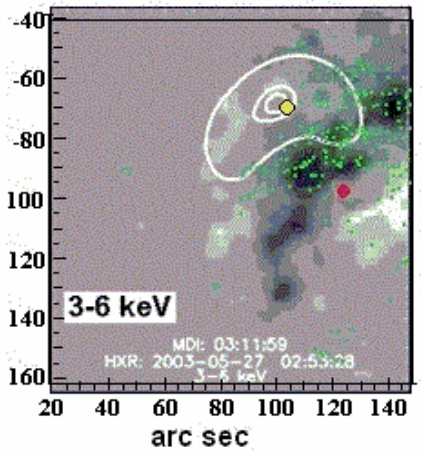

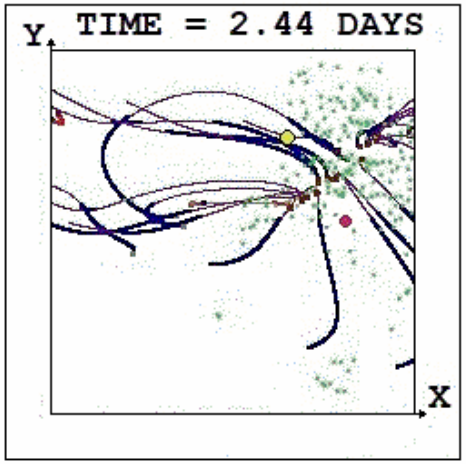

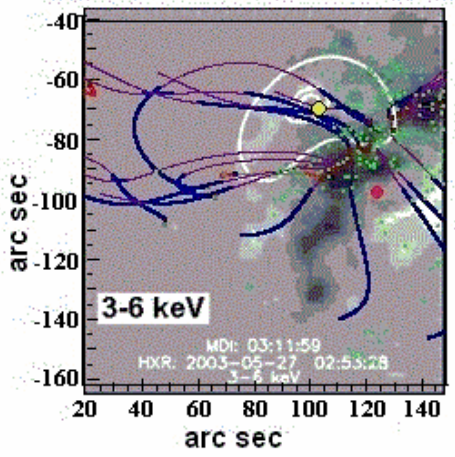

J MAX 4 0<X<1
J MAX 193 0<Z<1

Soft X-ray emission of 3-6 keV, received by the RHESSI Spacecraft (http://rhessidatacenter.ssl.berkeley.edu)

J MAX 4 0<X<1
J MAX 193 0<Z<1

Flare M1.4 27.05.2003 at 02:43 above AR 10365

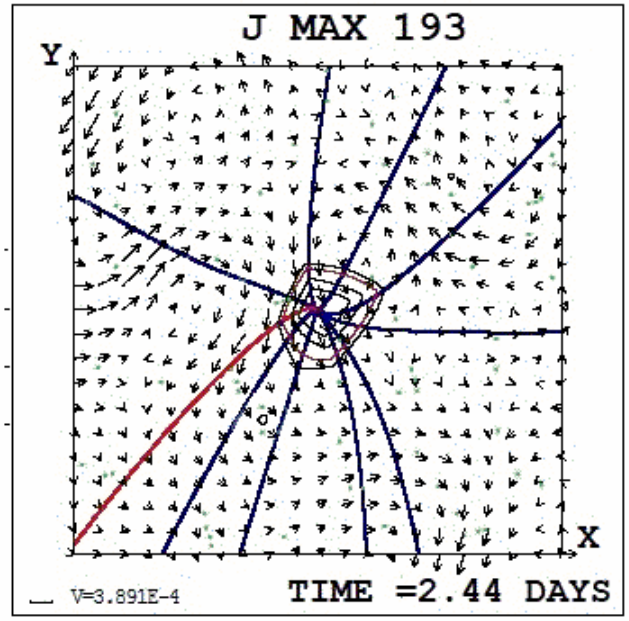

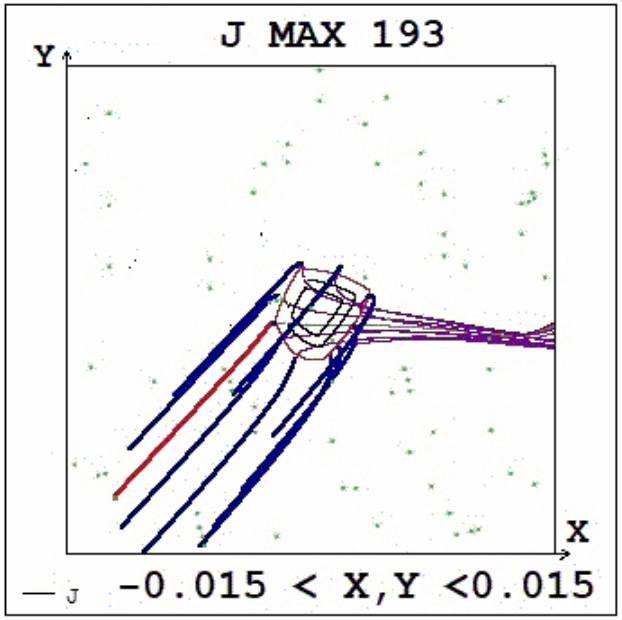

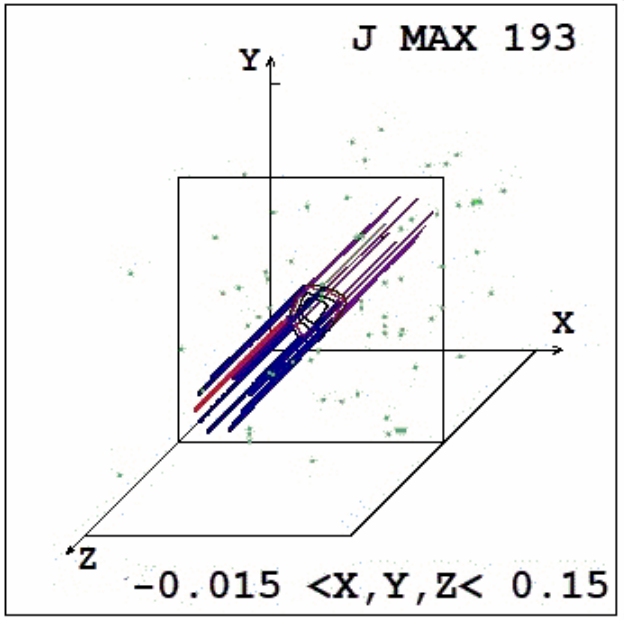

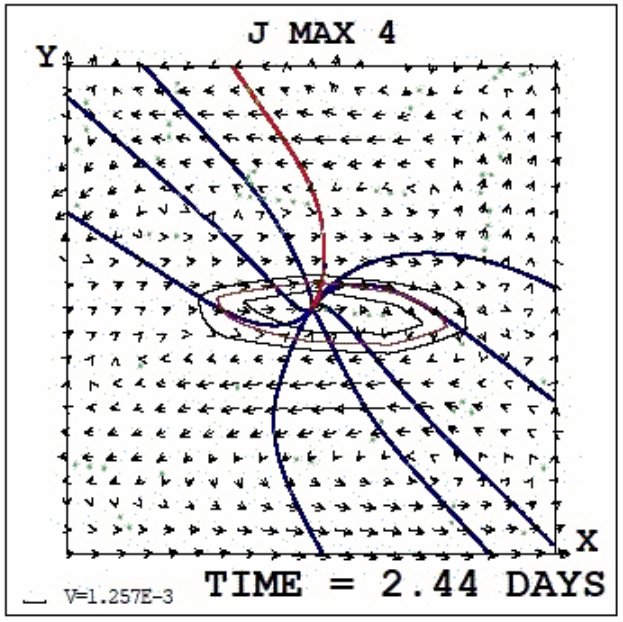

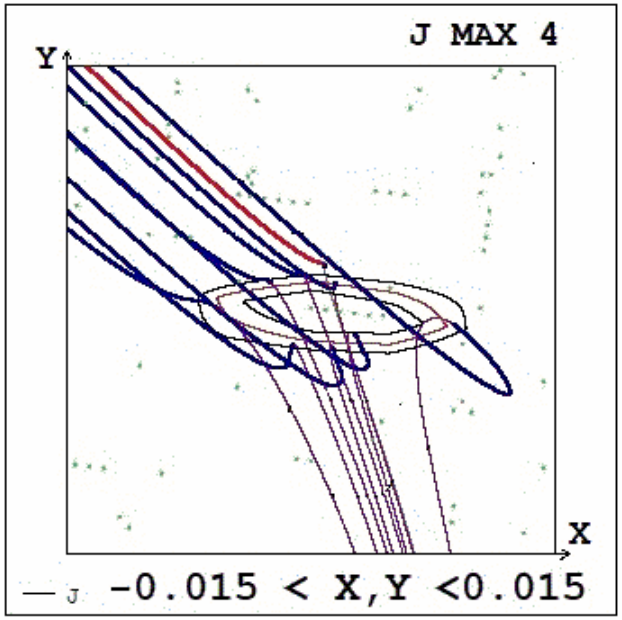

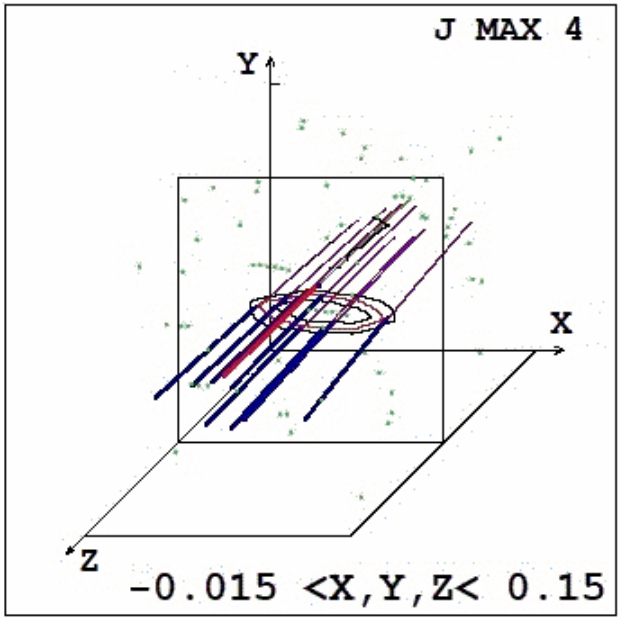

Conclusion

Methods have been developed, without which it is impossible to carry out MHD simulation in order to study the mechanism of a solar flare, and physical results have been obtained that make it possible to better understand the mechanism of a solar flare.

1. The developed technique made it possible to carry out MHD simulation in the solar corona in the real scale of time, the results of which made it possible to better understand the mechanism of a solar flare.

1.1. To reduce the calculation time, an absolutely implicit upwind finite-difference scheme was developed, conservative with respect to the magnetic flux, in order to maximize the time step at which the scheme remains stable.

1.2. The equipment and software were selected that allowed parallelizing computations using CUDA technology on graphics processing units (GPU). A number of optimizations of the parallel computing algorithm were carried out, including minimization of data exchange between the GPU memory and the central processor memory. The computational speed has increased by 120 times, which made it possible to carry out MHD simulations in the real scale of time.

1.3. The calculations showed the appearance of numerical instabilities near the boundary of the computational domain, which have time to develop significantly during the computational time interval, since it becomes rather long in simulations in real scale of time. Methods have been developed to stabilize these instabilities, including the use of artificial viscosity near the boundary. The use of stabilization methods made it possible to carry out the calculation.

2. The mechanism of the release of energy accumulated in the magnetic field of the current sheet makes it possible to explain the accumulation of energy in a stable configuration and then its transition to an unstable state, with a rapid release of energy during a flare.

2.1. The current density maxima appeared, located on singular lines of the X-type magnetic field. In the vicinity of such a line, a current sheet forms.

2.2. The configuration of the magnetic field above the active region 10365 is so complex, that the positions of singular lines and the current sheets can be find only using a specially developed system of search.

2.3. In the vicinity of the singular magnetic field line, a divergent magnetic field can be superimposed on the X-type field. Even if the divergent magnetic field dominates such that the superimposition gives a deformed divergent magnetic field configuration, due to the presence of an X-type configuration, a sufficiently strong current sheet can be formed in such a field.

2.4. The found points of the current density maxima are arranged in groups of several tens of points, which apparently indicates the possibility of the appearance of a large number of closely spaced singular lines.

2.5. Comparison of the calculation results with observations showed the appearance of current density maxima at the flare sites with a field configuration strongly distorted by the superimposed diverging magnetic field. Perhaps for this reason, solar flares above AR 10365 on May 26 and 27, 2003 were not very large.

2.6. Coincidence of position of flare emission with places on the singular lines where current sheets are created **confirms the flare mechanism** based on flare energy accumulation in the magnetic field of current sheet.

The physical and methodological results obtained make it possible to develop a plan for upgrading the methods of MHD simulation in the solar corona, including methods for stabilizing instabilities, which should make it possible to more accurately obtain the flare situation above the active region. In is necessary to study more precisely acceleration of charged particles during the solar flare and to study the possibility of escape accelerated particles from magnetic field above the active region.

Thank you!

Additional slides

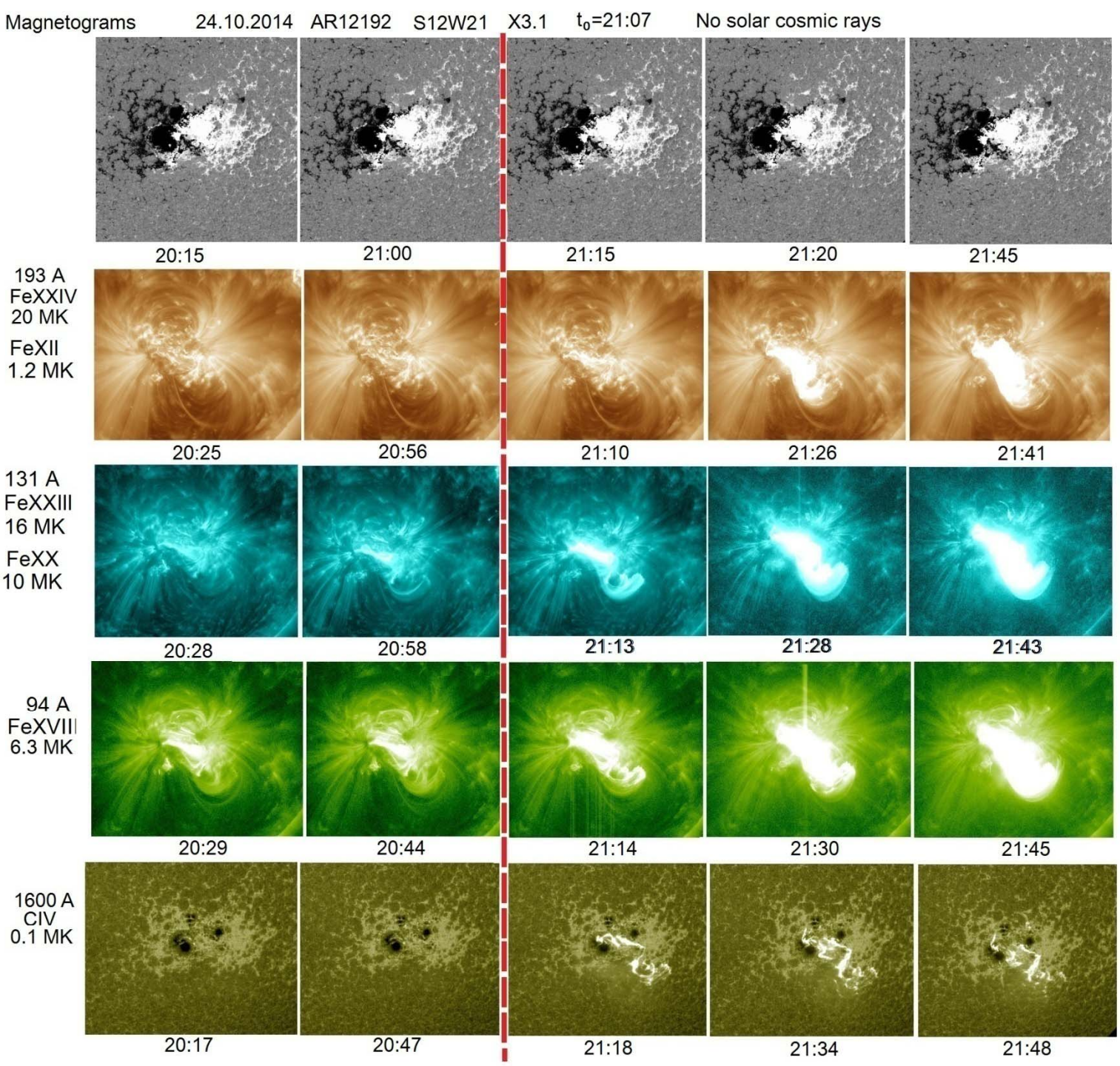
Magnetograms 24.10.2014 AR12192 S12W21 X3.1 t_0=21:07 No solar cosmic rays
20:15
21:00
21:15
21:20
21:45
193 A
FeXXIV
20 MK
FeXII
1.2 MK
20:25
20:56
21:10
21:26
21:41
131 A
FeXXIII
16 MK
FeXX
10 MK
20:28
20:58
21:13
21:28
21:43
94 A
FeXVIII
6.3 MK
20:29
20:44
21:14
21:30
21:45
1600 A
CIV
0.1 MK
20:17
20:47
21:18
21:34
21:48

Dumbovic M. Utilizing galactic cosmic rays to understand the Sun-to-Earth evolution of CMEs. VarSITI Symposium. София, Болгария. июнь, 2019

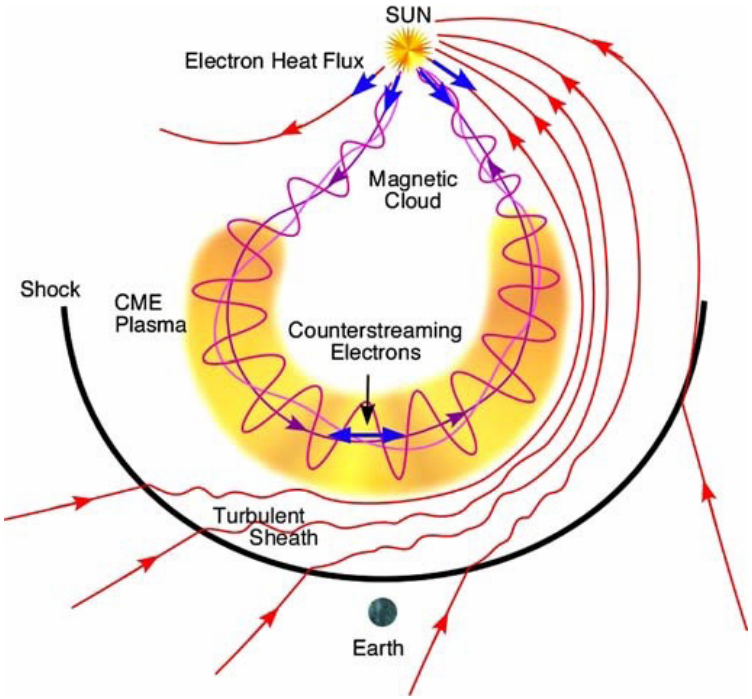

From the report of Mateja Dumbovik: According to measurements on satellites, the magnetic field of 70% CME does not have a twisted structure.
(ropes does not appear)

Из доклада Матеи Думбовик: По измерениям на спутниках магнитное поле в 70% выбросов не имеет скрученной структуры.
(Жгут не появляется)

Examples of alternative models of the solar flare

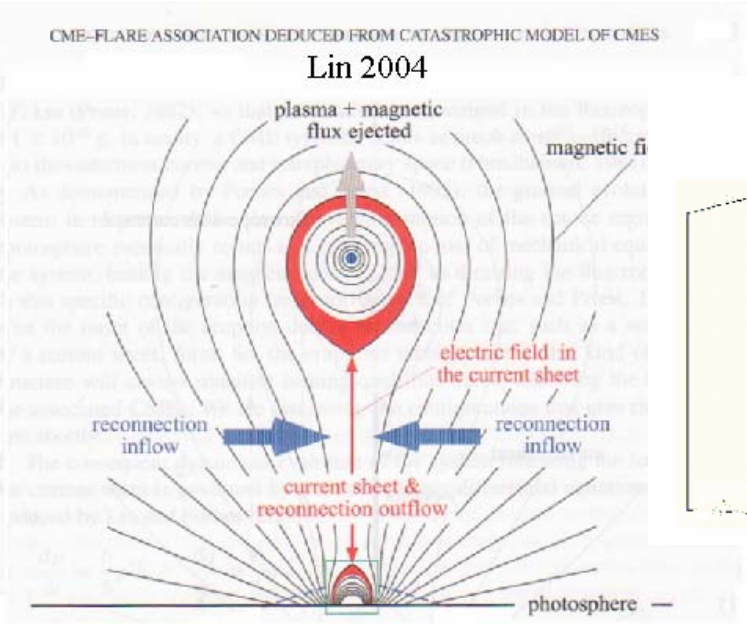

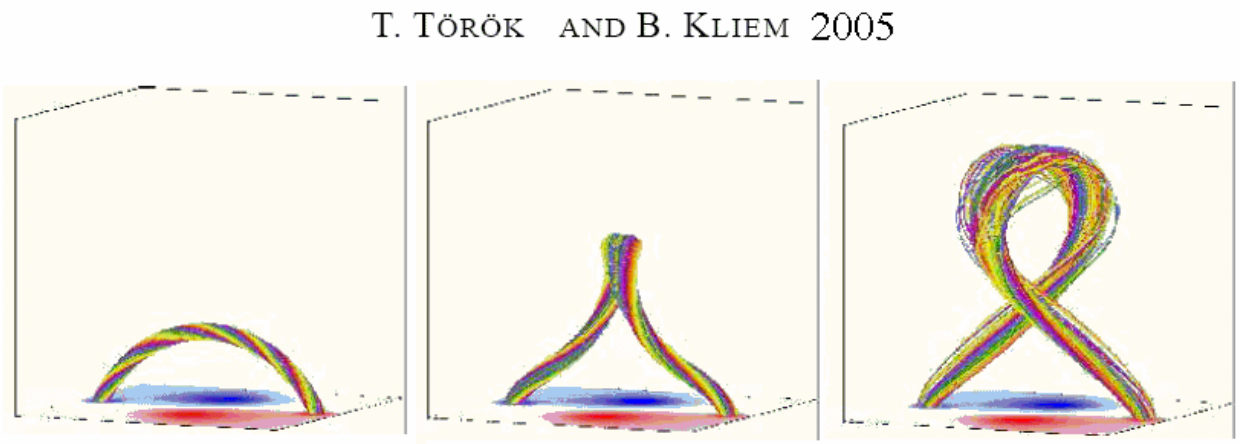

It is unclear how the rope can appear due to real disturbances on the photosphere.

In any case to verify the validity of these models it is necessary to perform presented here MHD simulations for real active region.

Calculation of magnetic field in **force-free** approximation (rot**B**=α**B**).

SAVCHEVA, VAN BALLEGOOIJEN, DELUCA, APJ 744:78, 2012

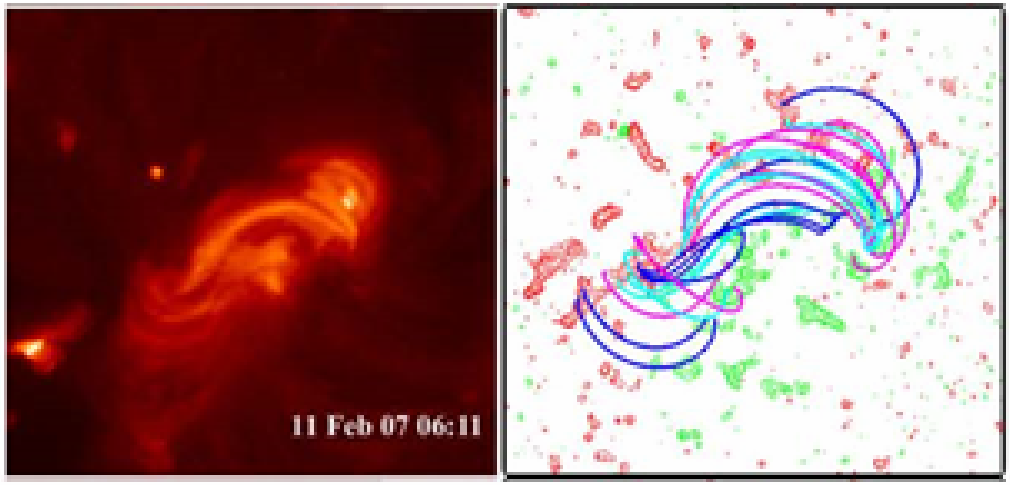

Savcheva et al. ApJ, 750:15, 2012

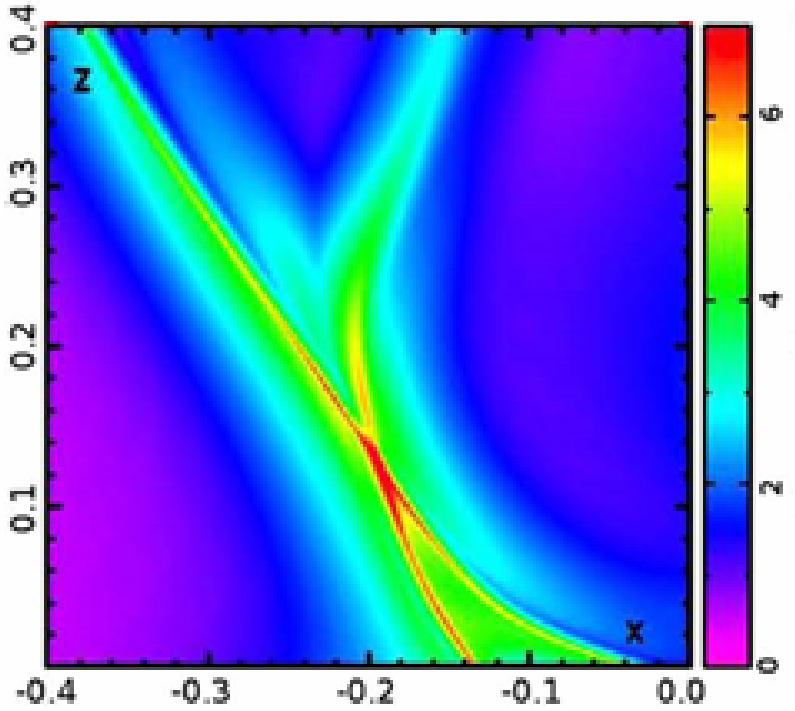

Jiang, C., Wu, S.T., Yurchyshyn, V., Wang, H., Feng, X., Hu, Q. 2016

2014 October 24 21:00 UT
AR 12192 X3.1

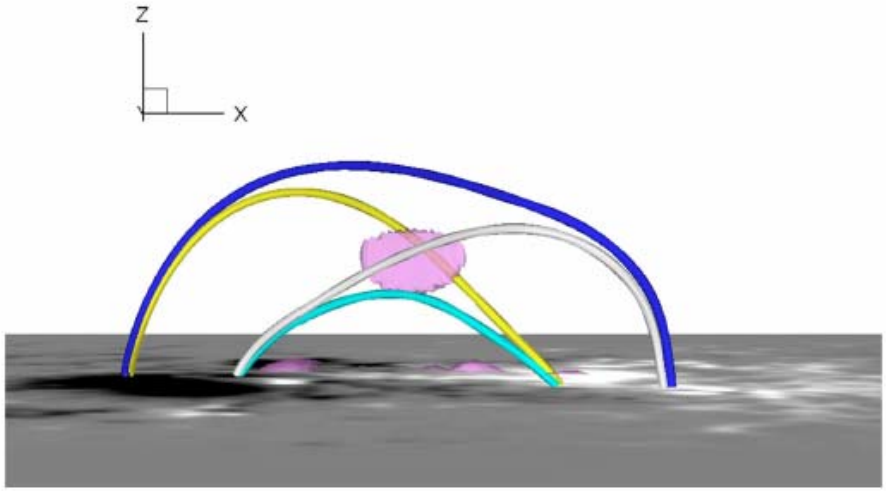

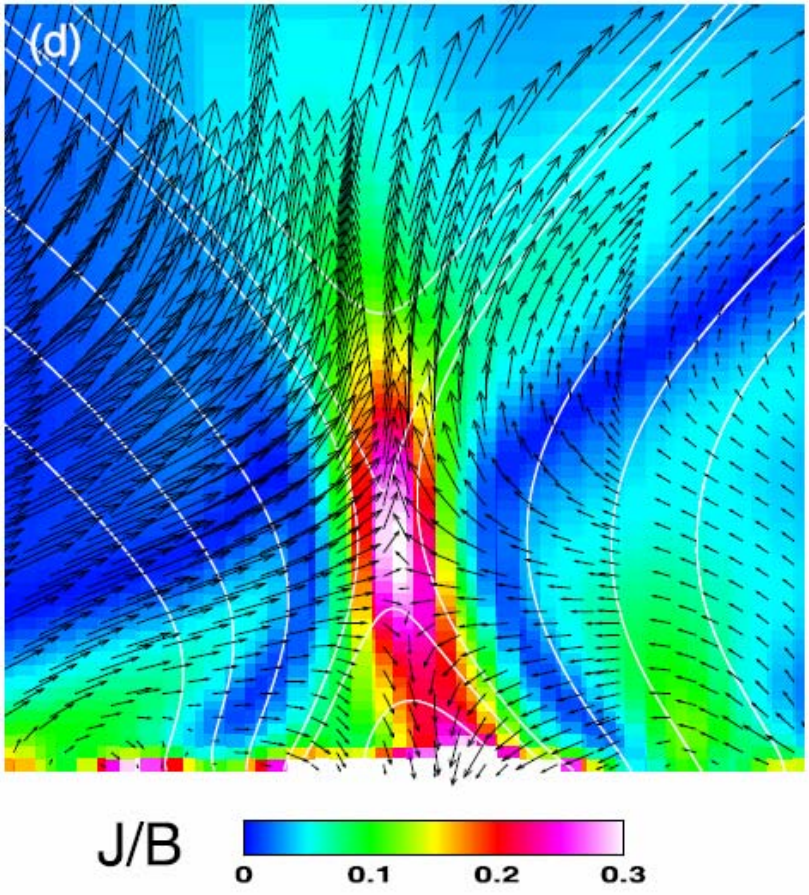

Decipher the Three-Dimensional Magnetic Topology of a Great Solar Flare February 9, 2018

Chaowei Jiang, Peng Zou, Xueshang Feng, Qiang Hu, Aiying Duan, Pingbing Zuo, Yi Wang, Fengsi Wei

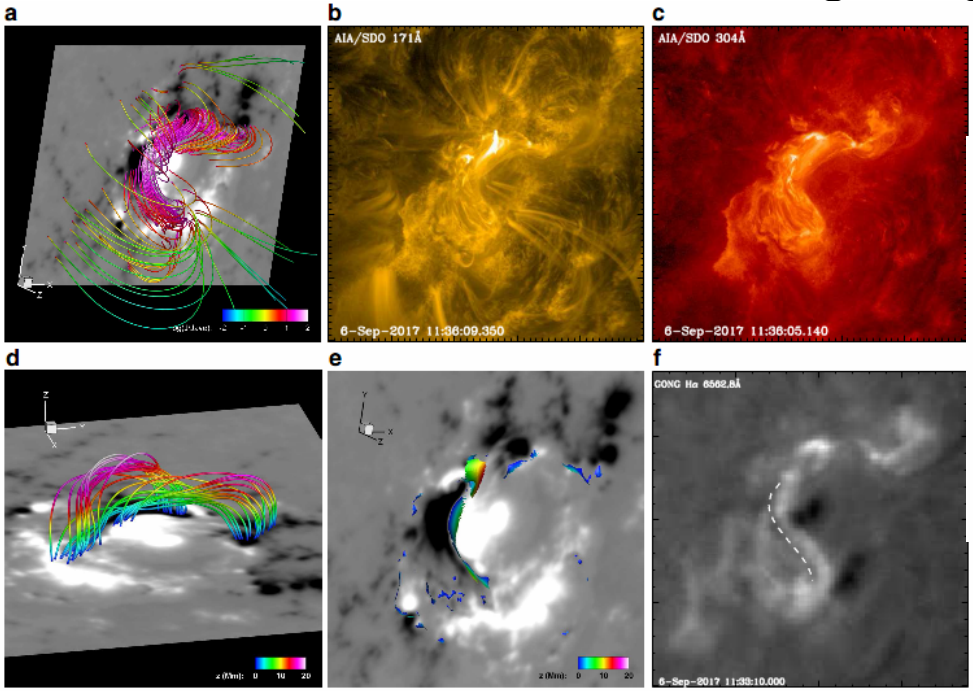

Figure 2: **Comparison of the reconstructed magnetic field with the observed features of the solar corona prior to the flare.** (a) SDO view of sampled magnetic field lines of the NLFFF reconstruction. The color of the lines represents the value of current density J (normalized by its average value $J_{\rm ave}$ in the computational volume). The background is the photospheric magnetogram. (b) and (c) SDO/AIA 171 Å and 304 Å images of the pre-flare corona. (d) The low-lying magnetic field lines in the core region. The field lines are color-coded by the value of height z. (e) Locations of dips in the magnetic field lines, and the color indicates the value of height z. (f) GONG Hα image of the AR. The dashed curve denotes the location of a long filament.

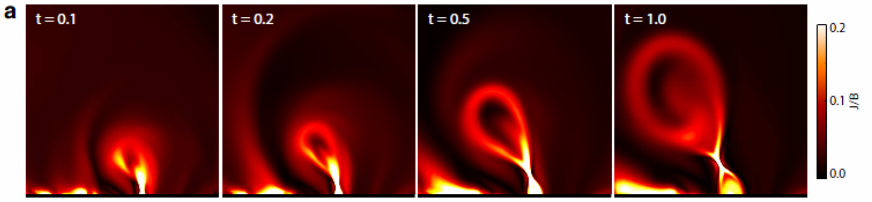

Figure 4: **Temporal evolution of the eruptive structure in 2D view.** Distribution of current density on the vertical cross section (the $y = 0$ plane). Here the current density is normalized by local magnetic field strength, which provides a high contrast of thin current layers with other volumetric currents.

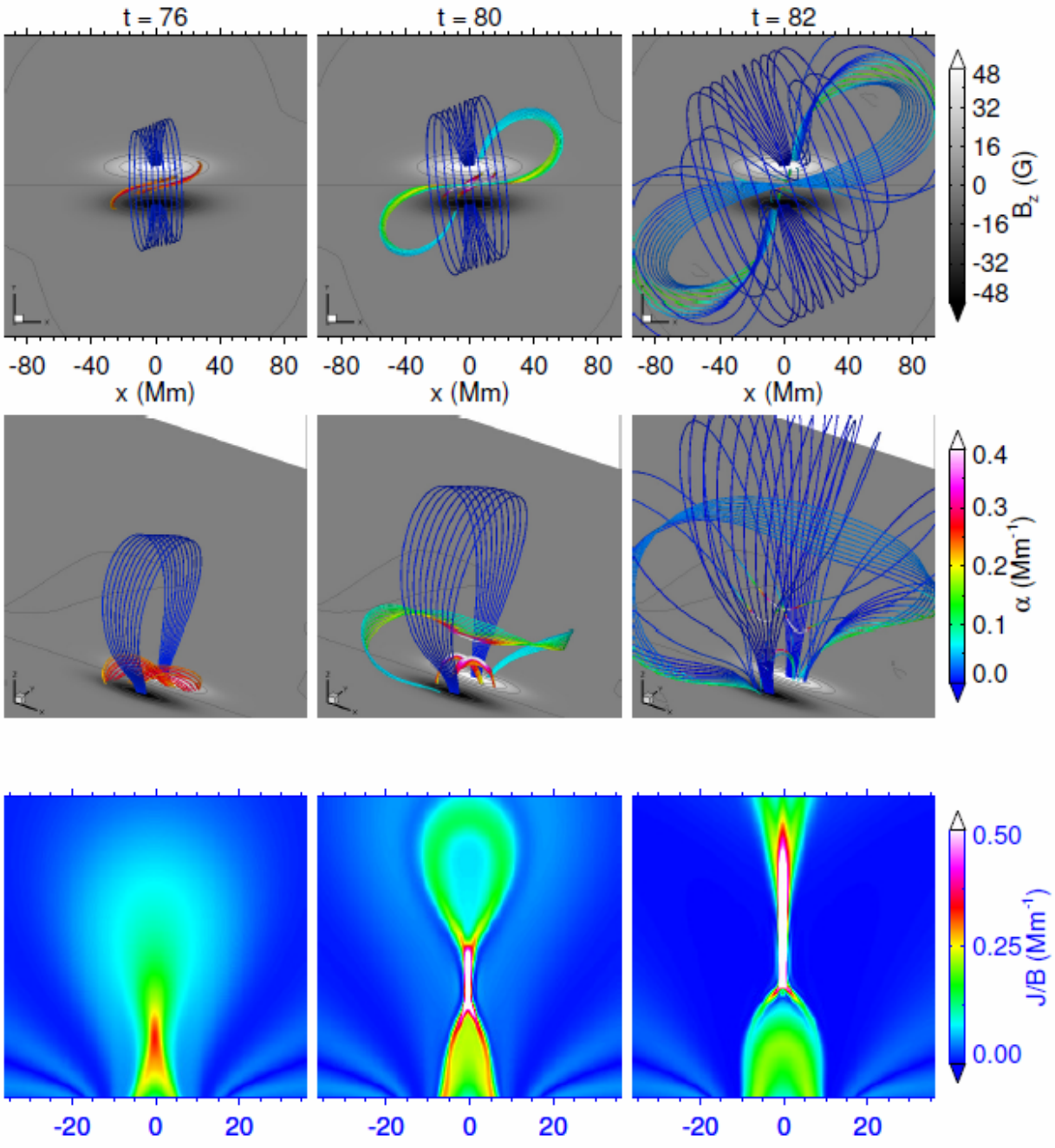

Numerical Simulation of a Fundamental Mechanism of Solar Eruption with Different Magnetic Flux Distributions

X. Bian, C. Jiang, X. Feng, P. Zuo, Yi Wang, X. Wang

2021

In the PERESVET program:

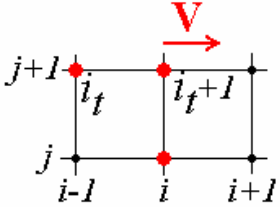

- Finite-difference scheme is upwind for diagonal terms.
- The scheme is absolutely implicit, it is solved by iteration method ($\Delta t V_w/\Delta x<1$ is not necessary).

$$\mathbf{u}_i^{(i_t+1)\,j+1} = \mathbf{u}_i^{j} - \mathbf{v}\frac{\Delta t}{\Delta x}\left(\mathbf{u}_i^{(i_t+1)\,j+1} - \mathbf{u}_{i-1}^{(i_t)\,j+1}\right)$$

- The scheme is conservative relative to magnetic flux [divB]=0

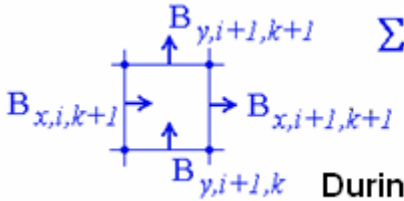

$$\sum \mathbf{B}_n \Delta S = 0$$

Equivalency of equations

$$\partial \mathbf{B}/\partial t = \mathrm{rot}(\mathbf{V}\times\mathbf{B}) + \nu_m \Delta \mathbf{B} \quad \text{and} \quad \partial \mathbf{B}/\partial t = \mathrm{rot}(\mathbf{V}\times\mathbf{B}) - \nu_m \mathrm{rot}(\mathrm{rot}\mathbf{B})$$

During dissipation relaxation of magnetic field, the current density [rot B] → 0

- Nonsymmetrical (upwind) approximation V×B.

Other methods:

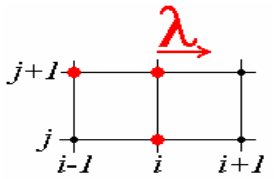

- Explicit finite-difference schemes
- Often Godunov type (Riemann waves)

$$\mathbf{w}_i^{j+1} = \mathbf{w}_i^{j} - \lambda\frac{\Delta t}{\Delta x}\left(\mathbf{w}_i^{j} - \mathbf{w}_{i-1}^{j}\right)$$

- The special methods are used to obtain high order approximation (FCT, TVD)
- Also Lagrangian schemes with further recalculation by interpolation on each step.
- Some schemes are also conservative relative to magnetic flux [divB]=0, but with symmetrical approximation V×B.

$\mathbf{V}\times\mathbf{B}$ contains $\mathbf{V}(\mathrm{B}_{y,i+1,k+1} + \mathrm{B}_{y,i,k+1})/2$

Initial potential magnetic field

$$\mathbf{B} = \nabla \varphi_m$$

$\Delta \varphi_m = 0$ is solved using finite-difference scheme in the region

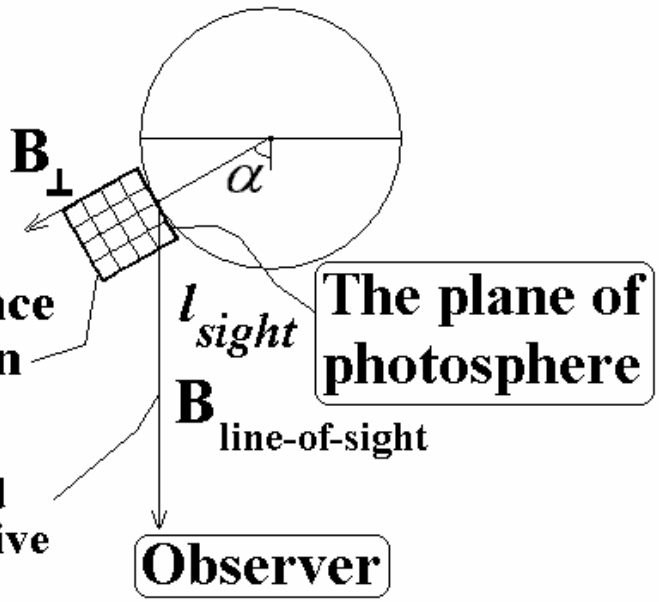

Boundary condition on the plane of photosphere:

$$\frac{\partial \varphi_m}{\partial l_{sight}} = \mathbf{B}_{line\text{-}of\text{-}sight}$$

- inclined derivative

On the net corresponded to conservative relative to magnetic flux finite-difference scheme for solving MHD equations

$$[rot]B=0 \quad [div]B=0$$

2 methods of $\Delta \varphi_m = 0$ solution :

1. $\Delta \varphi_m = 0$ directly by iterations
2. By relaxation of diffusion equation $\frac{\partial \varphi_m}{\partial t} = \Delta \varphi_m$

The stabilization of the instability at the boundary, which appears especially often at low viscosity in the region (magnetic and ordinary), requires small steps and a large number of iterations.

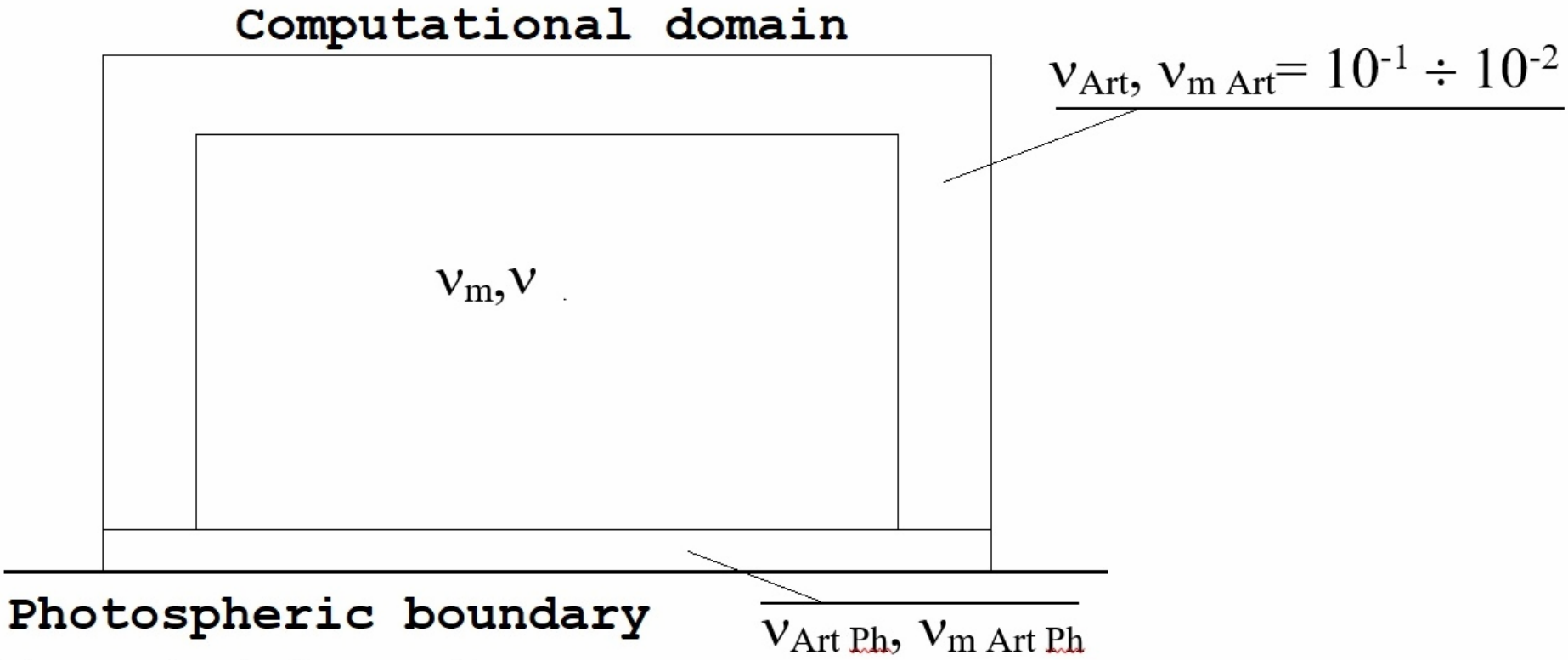

Two calculations with parameter sets:

1. $\nu_m=0.3\times10^{-5}$ ($Rm=3\times10^5$); $\nu=10^{-4}$ ($Re=10^4$); $\nu_{Art\ Ph}$, $\nu_{m\ Art\ Ph}=0.3\times10^{-2}$
2. $\nu_m=10^{-9}$ ($Rm=10^9$); $\nu=10^{-7}$ ($Re=10^7$); $\nu_{Art\ Ph}$, $\nu_{m\ Art\ Ph}= 10^{-4}$

(In the solar corona $Rm=10^{16}$, $Re=10^4$, $Re_B=10^{20}$; the grid viscosity viscosity $\nu_{grid}=h\,V_{DimLess}$; $h=0.5\times10^{-2}$; $V_{DimLess}=10^{-6} \div 10^{-3}$; $a=\nu_m/V_{in}$)

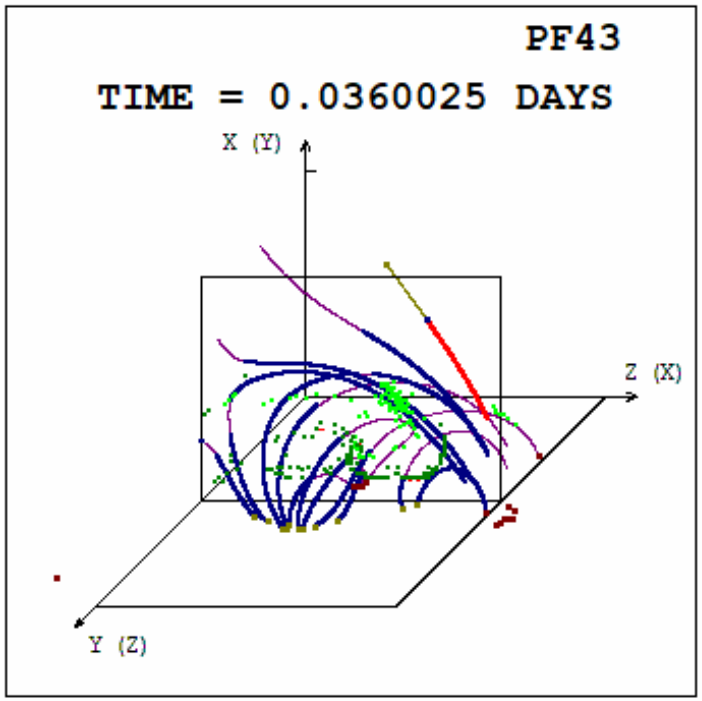
PF43
TIME = 0.0360025 DAYS
X (Y)
Z (X)
Y (Z)

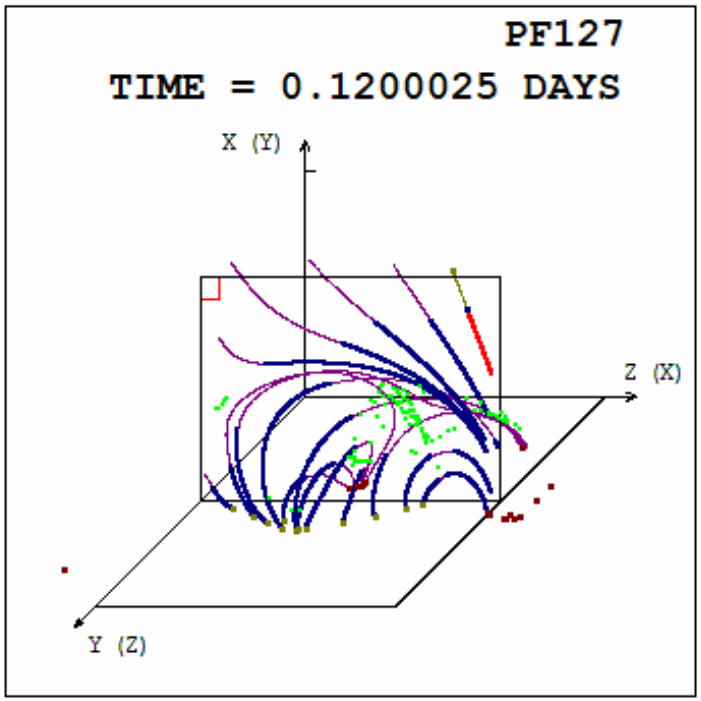
PF127
TIME = 0.1200025 DAYS
X (Y)
Z (X)
Y (Z)

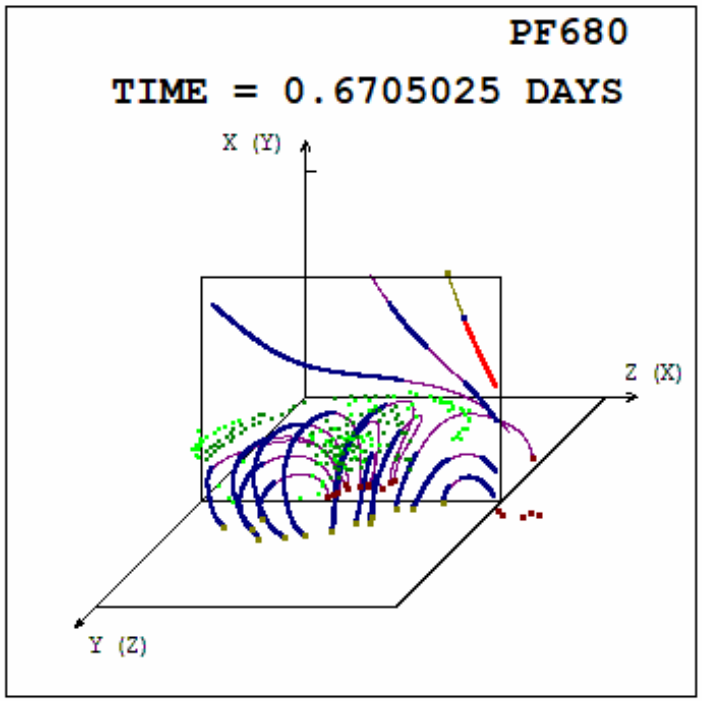
PF680
TIME = 0.6705025 DAYS
X (Y)
Z (X)
Y (Z)

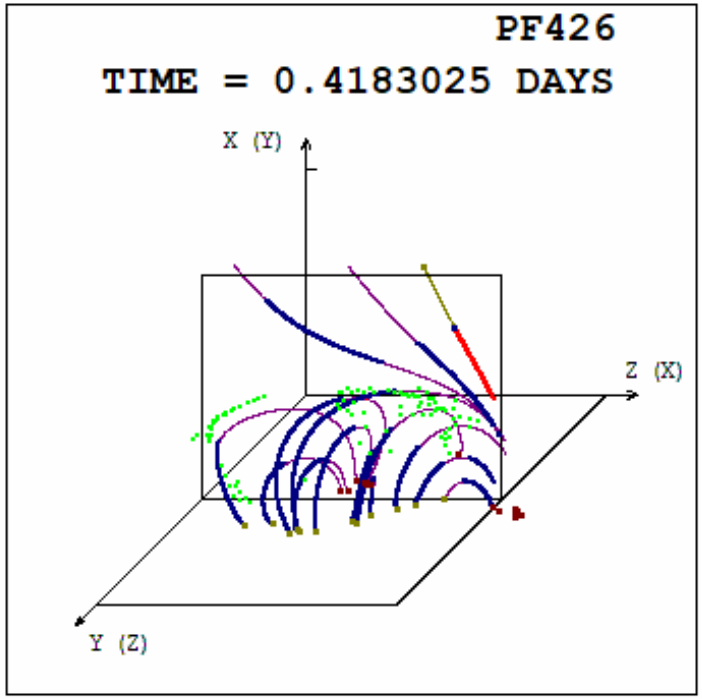
PF426
TIME = 0.4183025 DAYS
X (Y)
Z (X)
Y (Z)

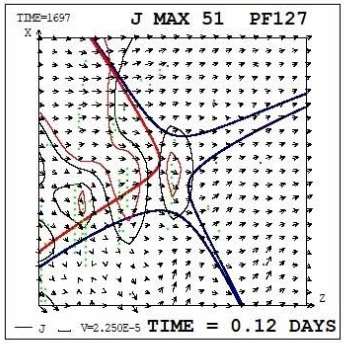
TIME=1697
J MAX 51 PF127
TIME = 0.12 DAYS

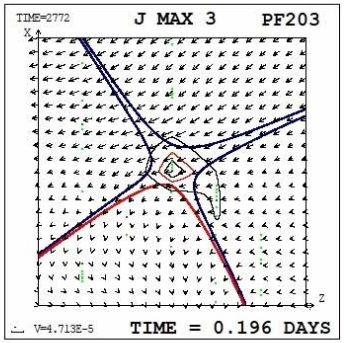
TIME=2772
J MAX 3 PF203
TIME = 0.196 DAYS

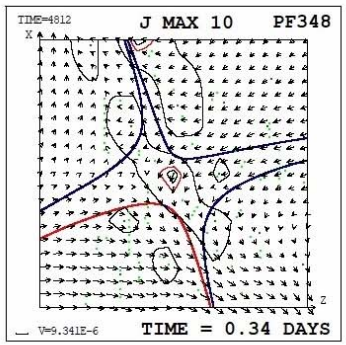
TIME=4812
J MAX 10 PF348
TIME = 0.34 DAYS

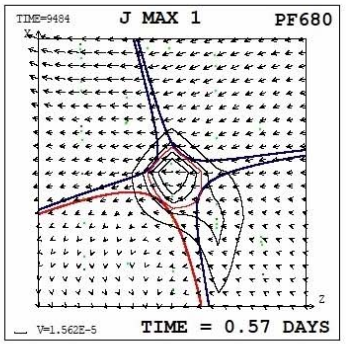
TIME=9484
J MAX 1 PF680
TIME = 0.57 DAYS

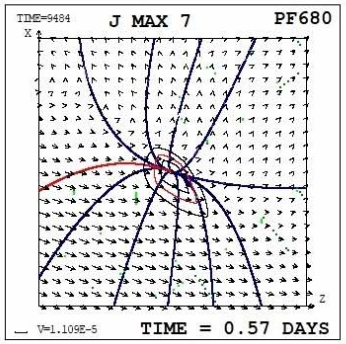
TIME=9484
J MAX 7 PF680
TIME = 0.57 DAYS

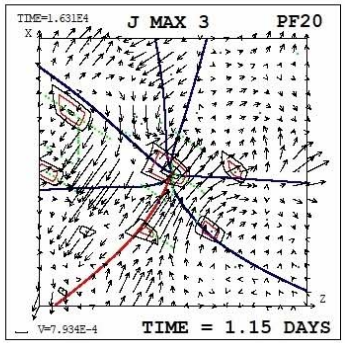
TIME=1.631E4
J MAX 3 PF20
TIME = 1.15 DAYS

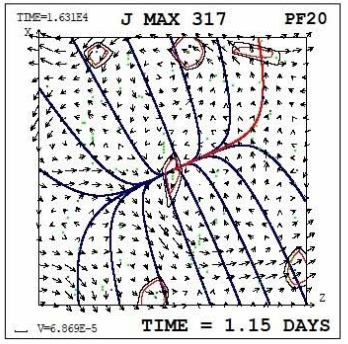
TIME=1.631E4
J MAX 317 PF20
TIME = 1.15 DAYS

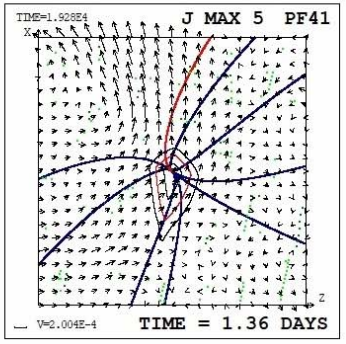
TIME=1.928E4
J MAX 5 PF41
TIME = 1.36 DAYS

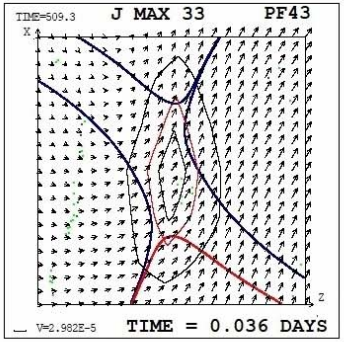
TIME=509.3
J MAX 33 PF43
TIME = 0.036 DAYS

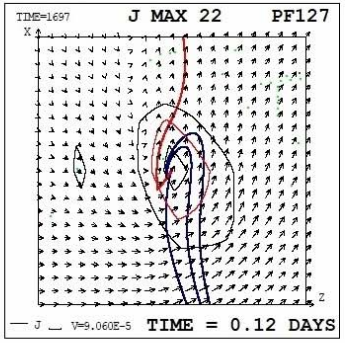
TIME=1697
J MAX 22 PF127
TIME = 0.12 DAYS

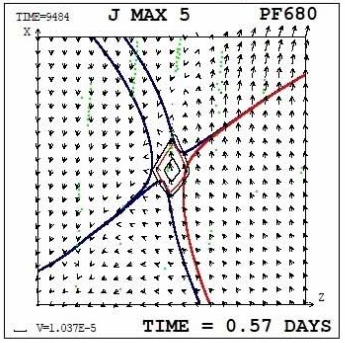
TIME=9484
J MAX 5 PF680
TIME = 0.57 DAYS

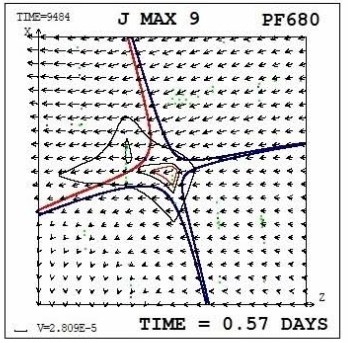
TIME=9484
J MAX 9 PF680
TIME = 0.57 DAYS

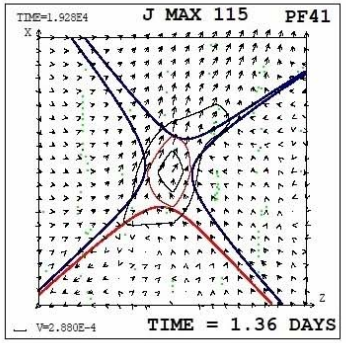
TIME=1.928E4
J MAX 115 PF41
TIME = 1.36 DAYS

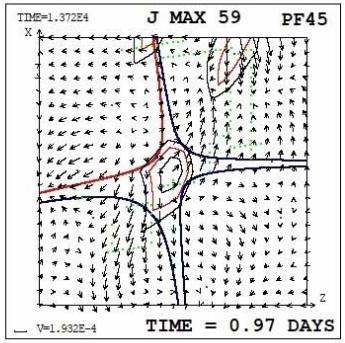
TIME=1.372E4
J MAX 59 PF45
TIME = 0.97 DAYS

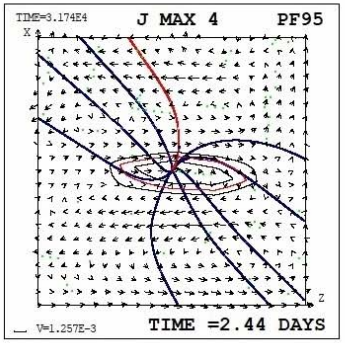
TIME=3.174E4
J MAX 4 PF95
TIME =2.44 DAYS

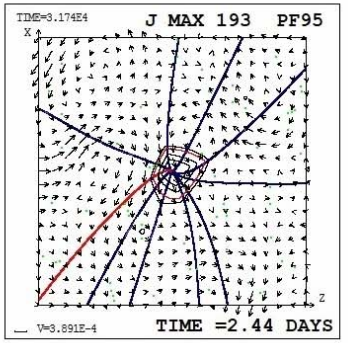
TIME=3.174E4
J MAX 193 PF95
TIME =2.44 DAYS

Radio emission at a frequency of 17 Ghz, obtained with the Nobeyama Radioheliograph

- J MAX 115
- J MAX 5

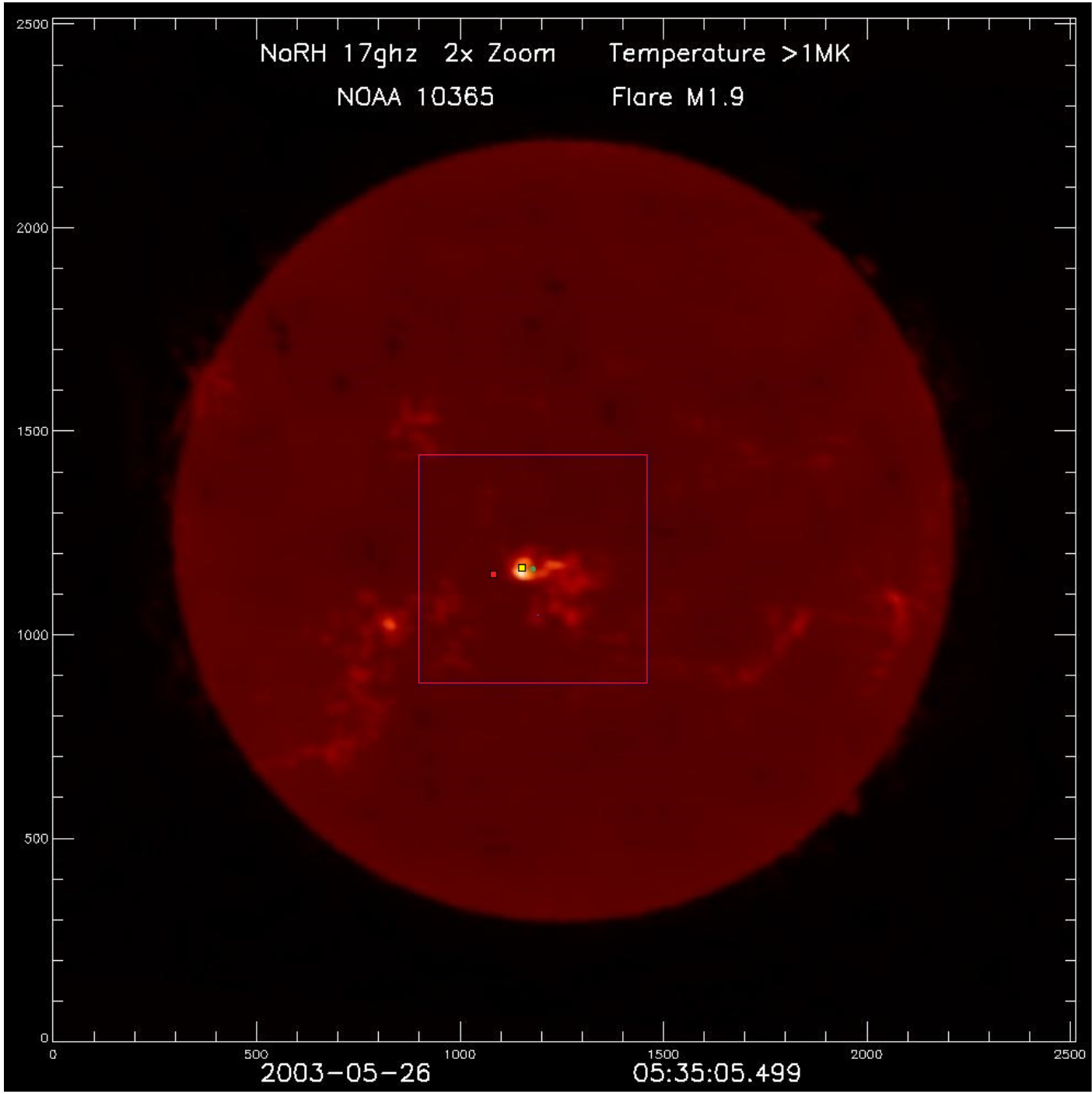

Before flare M1.9 26.05.2003 at 05:34 above AR 10365, moment 01:00

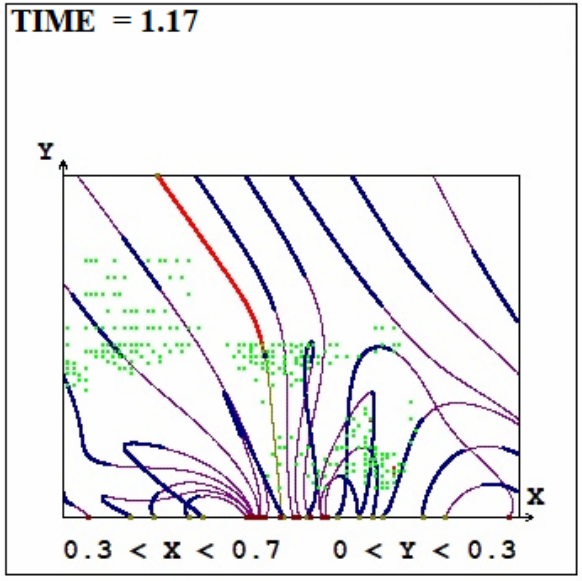

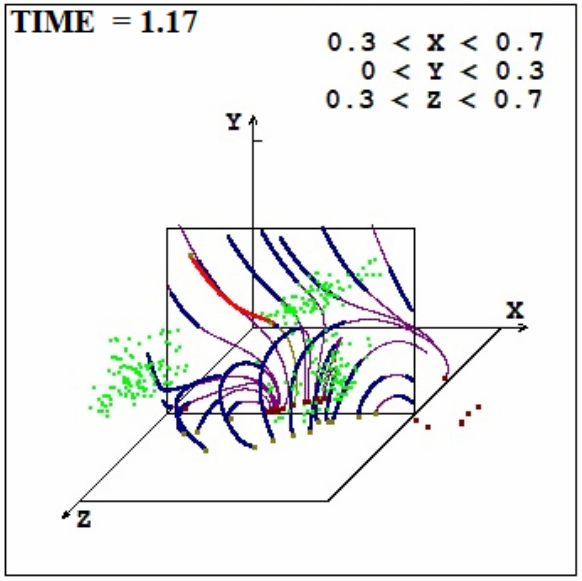

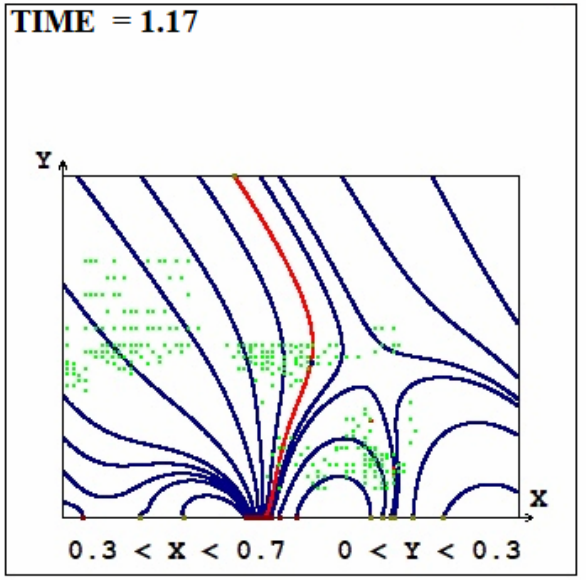

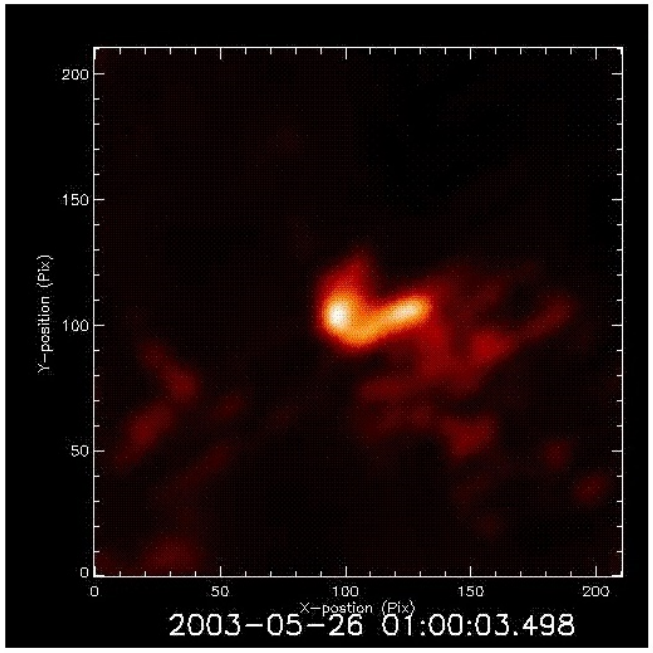

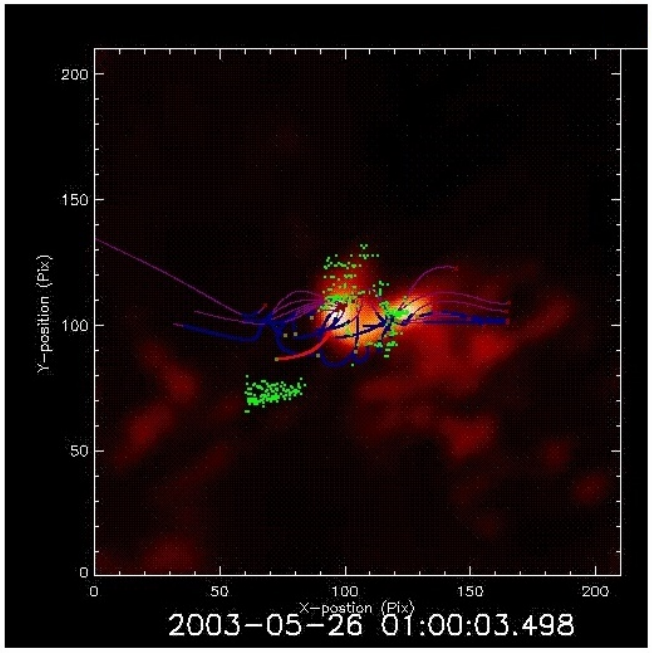

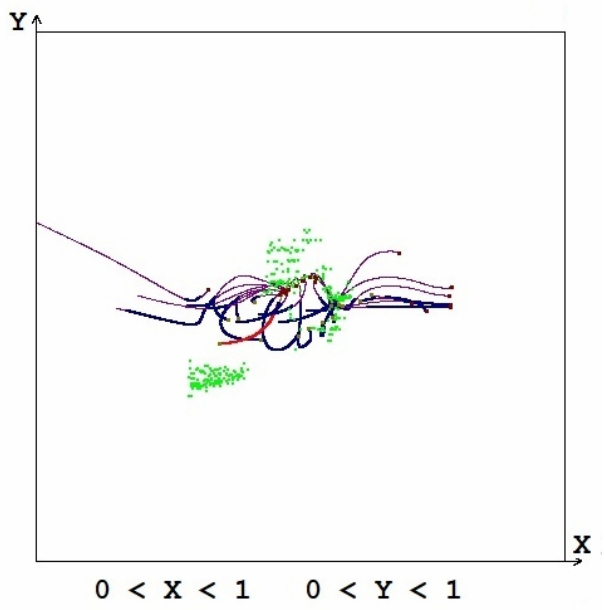

Radio emission at a frequency of 17 Ghz, obtained with the Nobeyama Radioheliograph

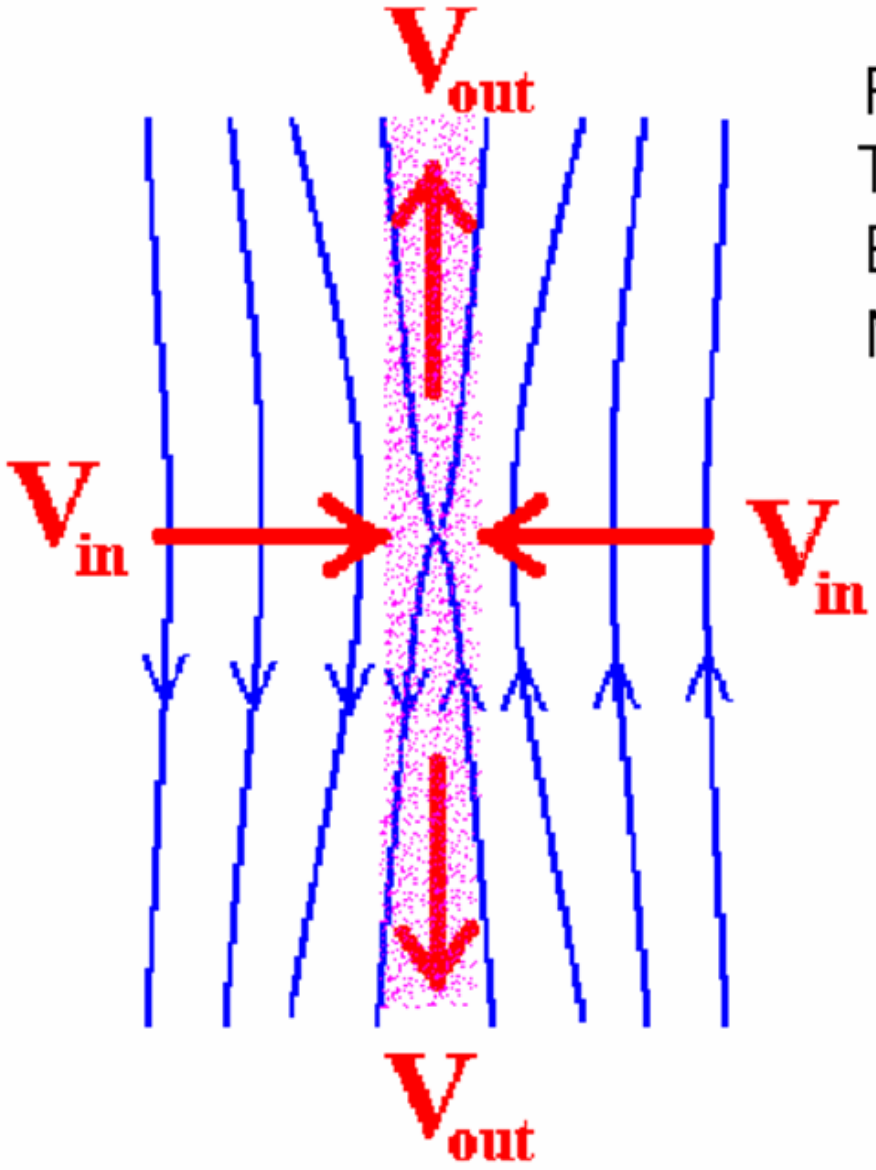

From RHESSI: $(ME)=5\cdot10^{49}\,cm^{-3}$.
$T=3.1$ keV $n=10^{11}\,cm^{-3}$.
$B^2/8\pi = nkT \rightarrow B = 110\,G$.
$M = Nm_p \sim 10^{15}\,g$ --- CME.

At $V_{in} = 2\times10^{7}$ cm/s and $L=10^{9}$ cm.

$E = V \times B/c$. $E=20$ V/cm.

$W=2\times10^{10}$ eV.

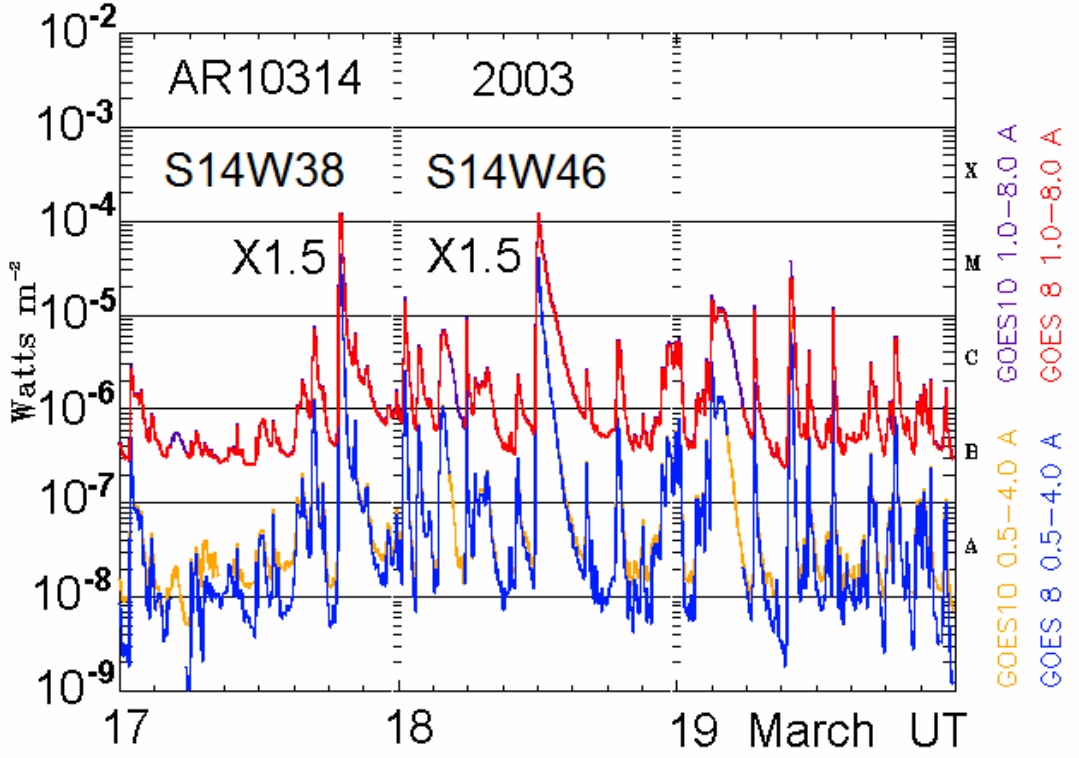
AR10314 2003
S14W38 S14W46
X1.5 X1.5
Watts m⁻²
GOES10 0.5–4.0 A
GOES10 1.0–8.0 A
GOES 8 0.5–4.0 A
GOES 8 1.0–8.0 A
X
M
C
B
A
17 18 19 March UT

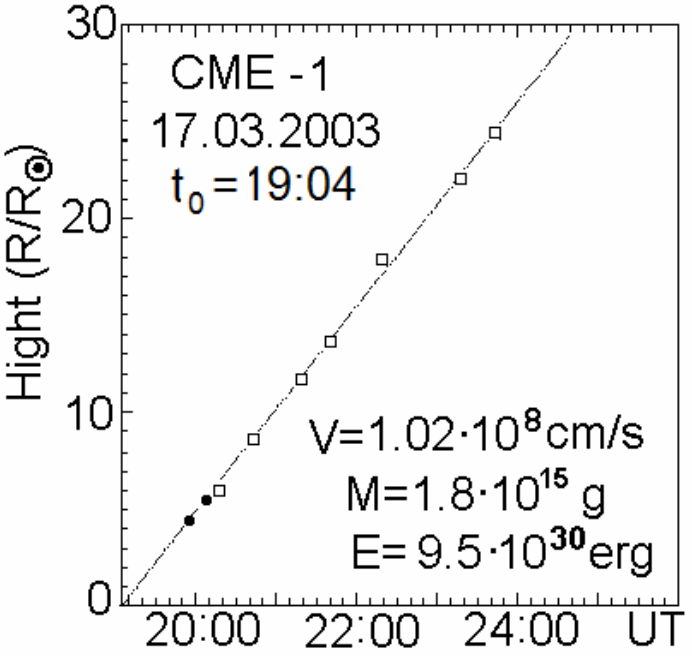
CME -1
17.03.2003
t0 = 19:04
V=1.02·10⁸cm/s
M=1.8·10¹⁵ g
E= 9.5·10³⁰erg
Hight (R/R⊙)
20:00 22:00 24:00 UT

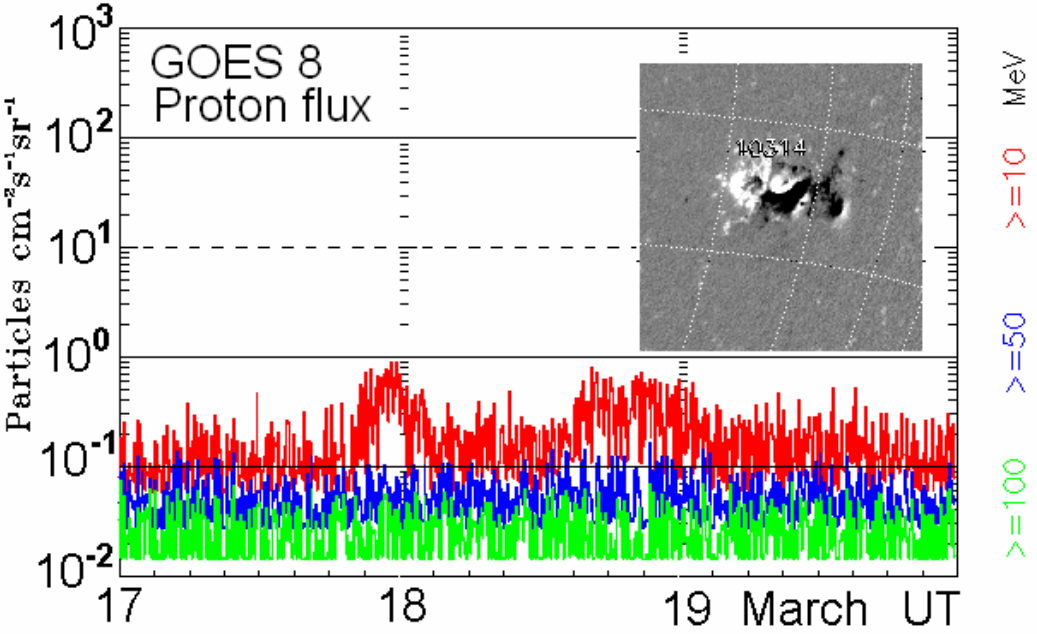
GOES 8
Proton flux
10314
Particles cm⁻²s⁻¹sr⁻¹
>=10 MeV
>=50
>=100
17 18 19 March UT

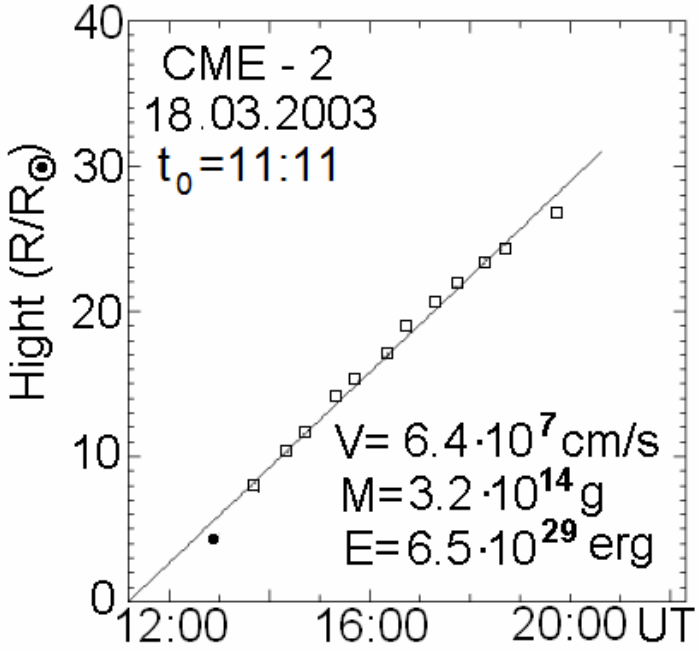
CME - 2
18.03.2003
t0 =11:11
V= 6.4·10⁷cm/s
M=3.2·10¹⁴g
E=6.5·10²⁹ erg
Hight (R/R⊙)
12:00 16:00 20:00 UT

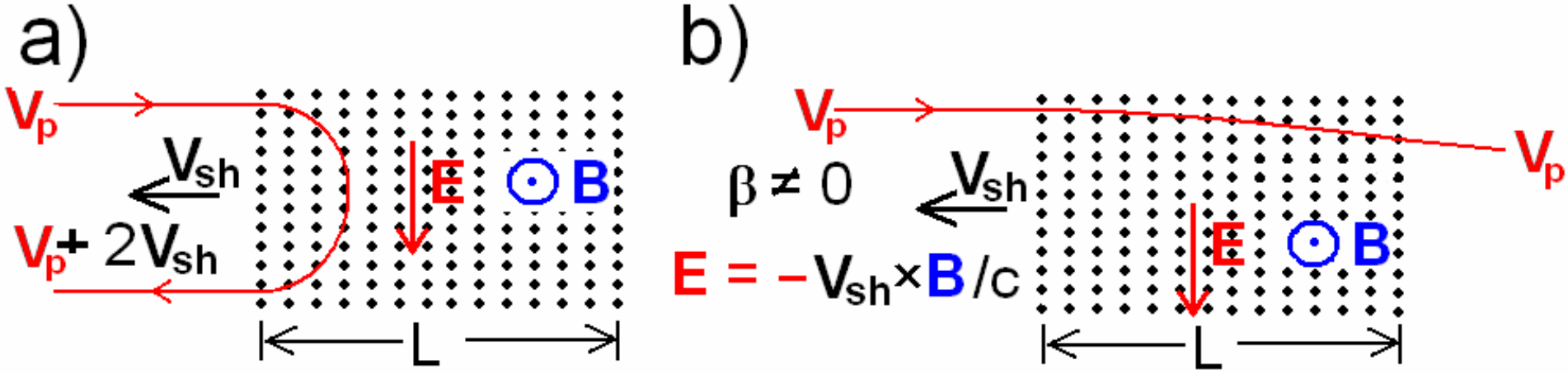

$$\delta W = 2\rho E e \qquad \rho = \frac{M V_p c}{e B} \qquad \delta W = 2 M V_p V_{sh} \qquad \delta V_p = 2 V_{sh}$$

For Fermi particle acceleration, it is necessary that the size of the magnetic cloud (thickness of the shock wave) L be larger than the Larmor radius of the particle ρ. Otherwise, the particle passes through a magnetic cloud. The maximum achievable energy corresponds to the equality of the Larmor radius $\rho \sim W/300B$ to the size of the magnetic cloud. When the magnetic field in the shock wave is $B = 5\times10^{-4}$ G, for particle acceleration to 2×10^{9} eV, it is necessary the wave front width to be larger than $\sim10^{10}$ cm. The accumulation of such inhomogeneities in the solar wind has never been observed.

Not all flares are accompanied by the appearance of solar cosmic rays. Only 30% of the most powerful flares (class X) cause SCRs. According to our ideas, charged particles always accelerate at the site of the primary flare energy release in the solar corona, but they will not always be able to get out of the magnetic field configuration above the active region.

Examples of alternative models of the solar flare

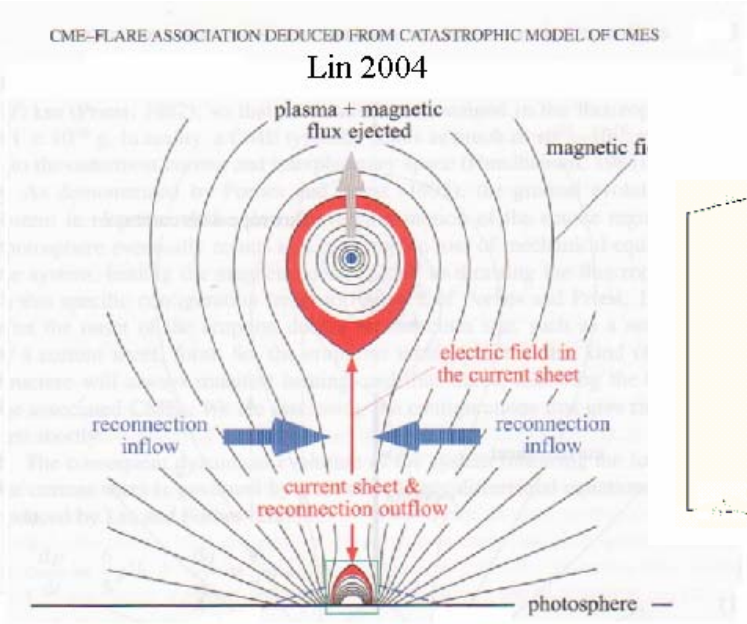

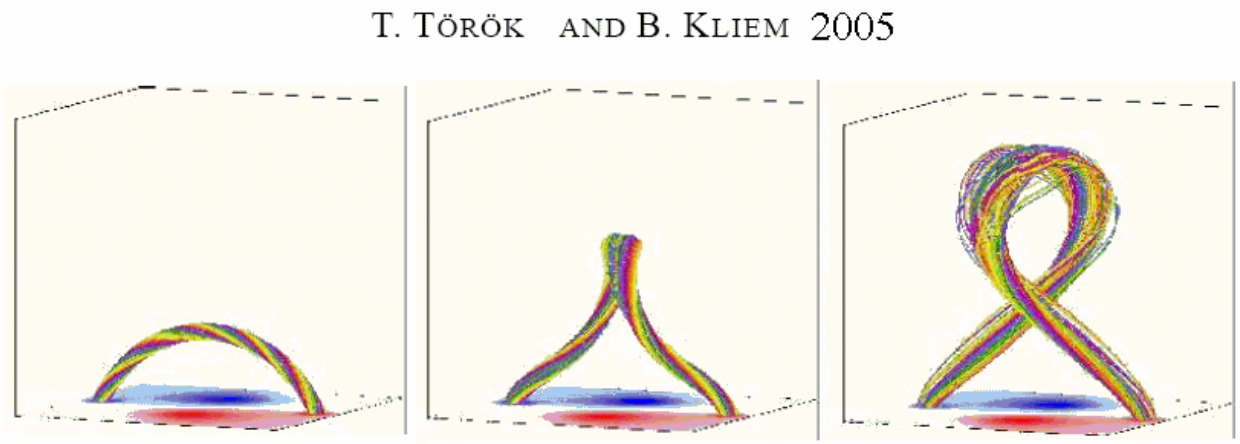

It is unclear how the rope can appear due to real disturbances on the photosphere.

In any case to verify the validity of these models it is necessary to perform presented here MHD simulations for real active region.

Zuccarello F. P., Aulanier G., Dudik J., Demoulin P., Schmieder B., Gilchrist,S. A. 2017

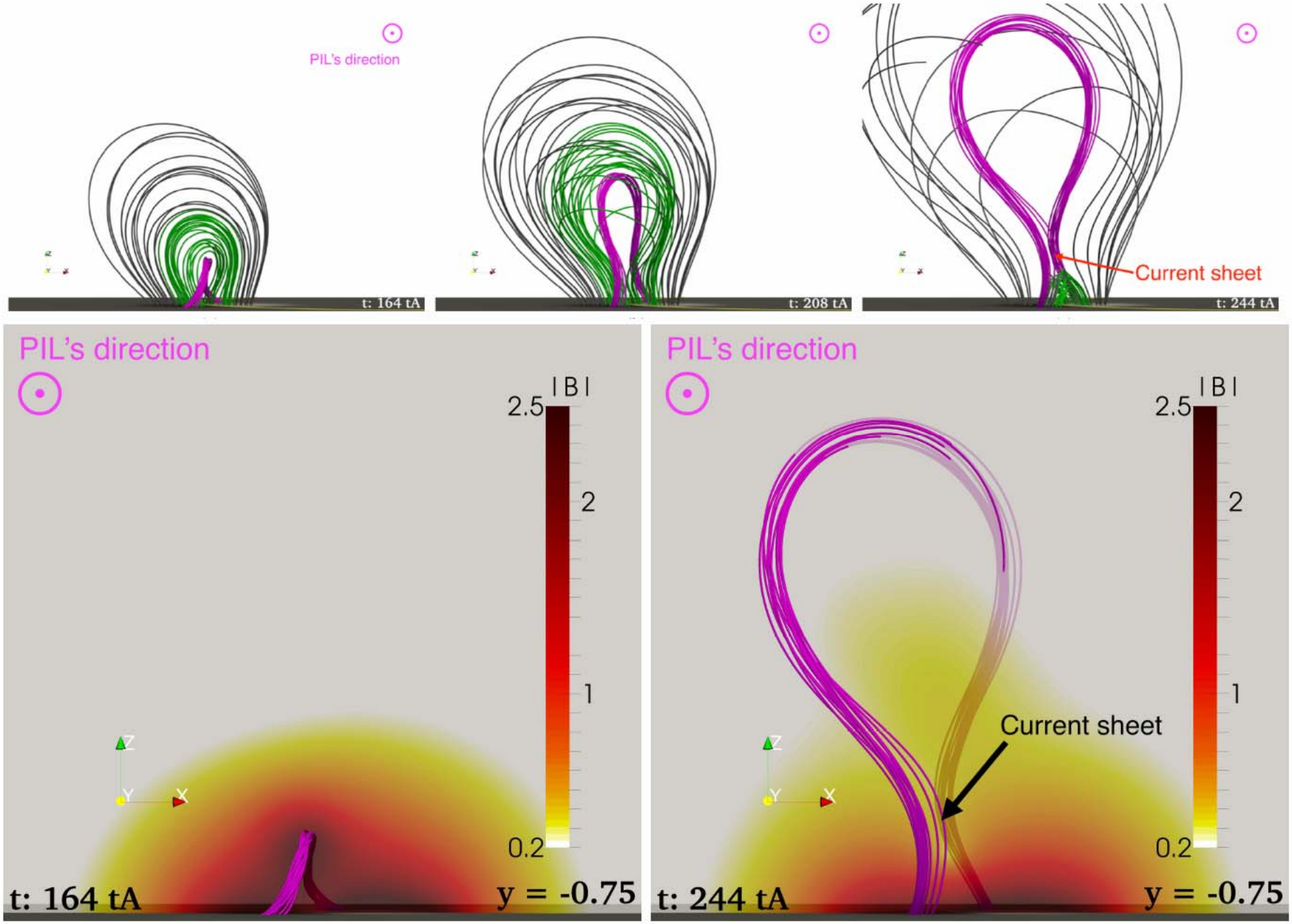

Calculation of magnetic field in **force-free** approximation (rot**B**=α**B**).

SAVCHEVA, VAN BALLEGOOIJEN, DELUCA, APJ 744:78, 2012

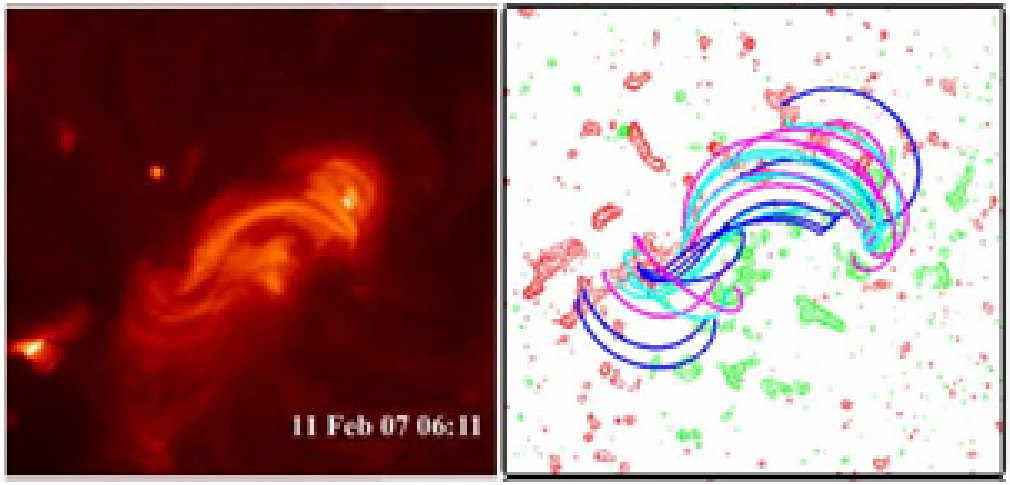

Savcheva et al. ApJ, 750:15, 2012

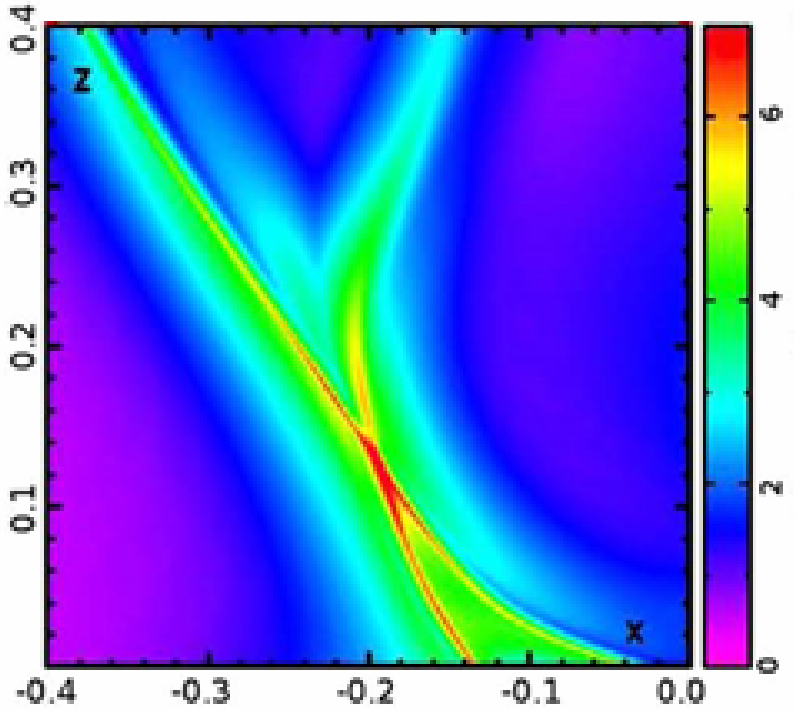

Our aim is:

To find solar flare mechanism directly by MHD simulation in real active region.

At setting the conditions of simulation, no assumptions were done about the flare mechanism. All conditions are taken from observations.

Jiang, C., Wu, S.T., Yurchyshyn, V., Wang, H., Feng, X., Hu, Q. 2016

2014 October 24 21:00 UT
AR 12192 X3.1

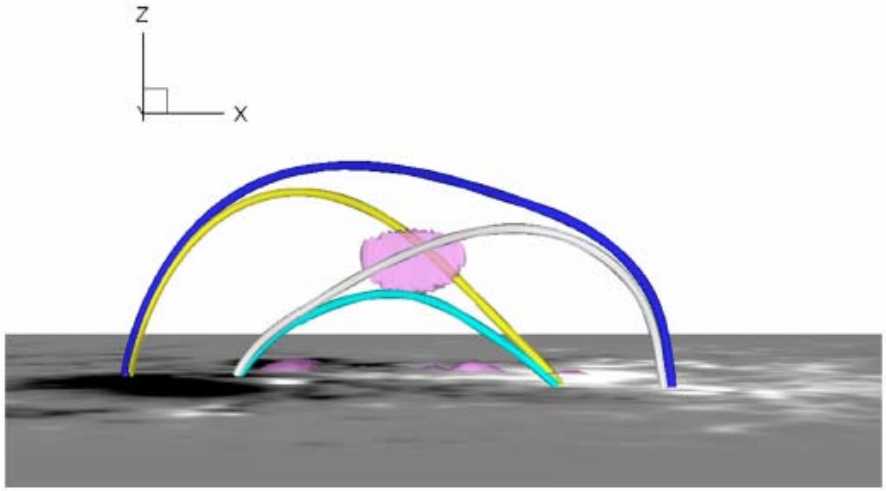

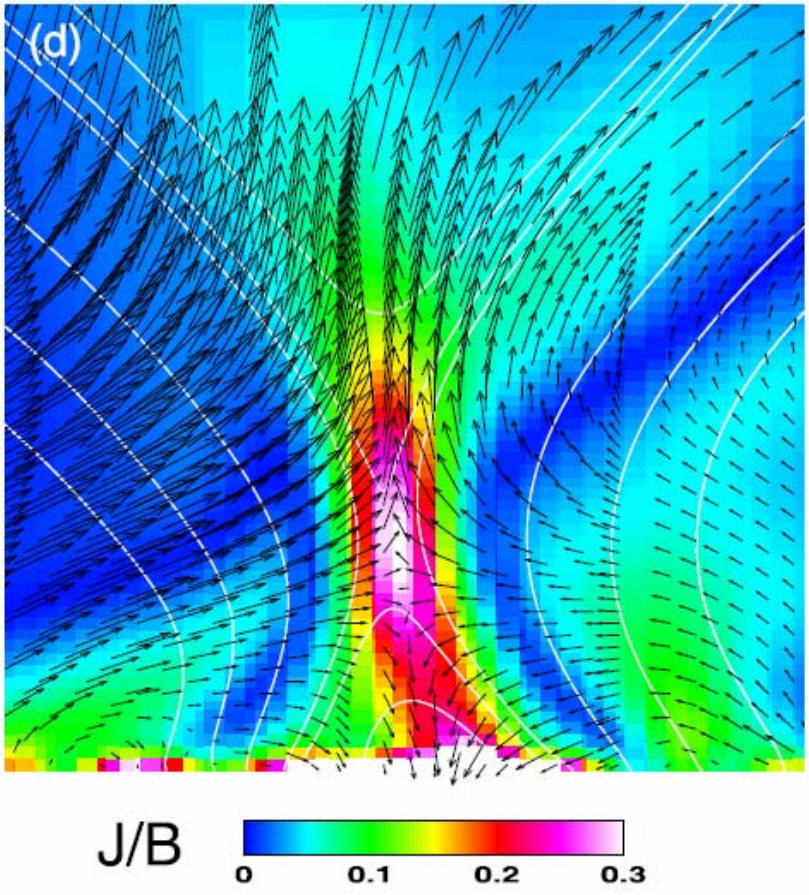

Decipher the Three-Dimensional Magnetic Topology of a Great Solar Flare February 9, 2018

Chaowei Jiang, Peng Zou, Xueshang Feng, Qiang Hu, Aiying Duan, Pingbing Zuo, Yi Wang, Fengsi Wei

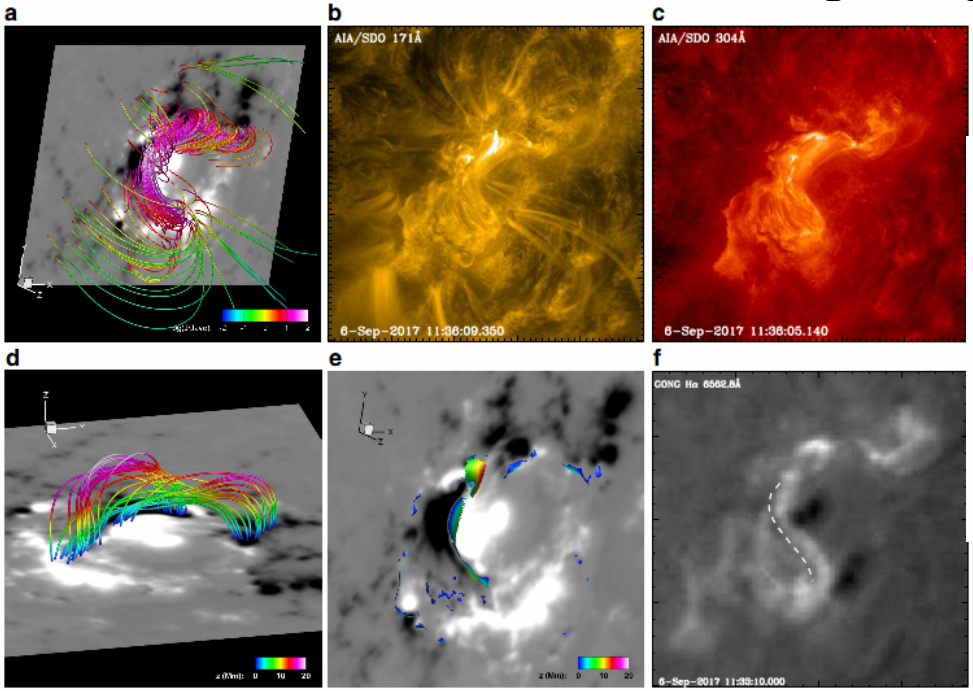

Figure 2: **Comparison of the reconstructed magnetic field with the observed features of the solar corona prior to the flare.** (a) SDO view of sampled magnetic field lines of the NLFFF reconstruction. The color of the lines represents the value of current density J (normalized by its average value $J_{\rm ave}$ in the computational volume). The background is the photospheric magnetogram. (b) and (c) SDO/AIA 171 Å and 304 Å images of the pre-flare corona. (d) The low-lying magnetic field lines in the core region. The field lines are color-coded by the value of height z. (e) Locations of dips in the magnetic field lines, and the color indicates the value of height z. (f) GONG Hα image of the AR. The dashed curve denotes the location of a long filament.

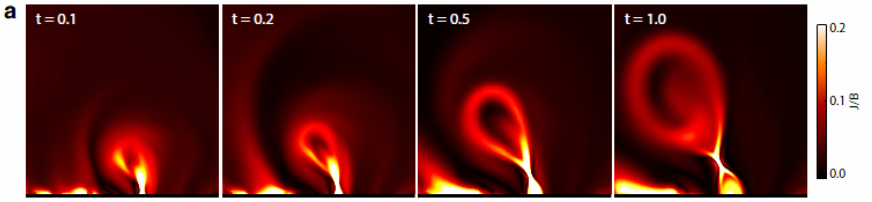

Figure 4: **Temporal evolution of the eruptive structure in 2D view.** Distribution of current density on the vertical cross section (the $y = 0$ plane). Here the current density is normalized by local magnetic field strength, which provides a high contrast of thin current layers with other volumetric currents.

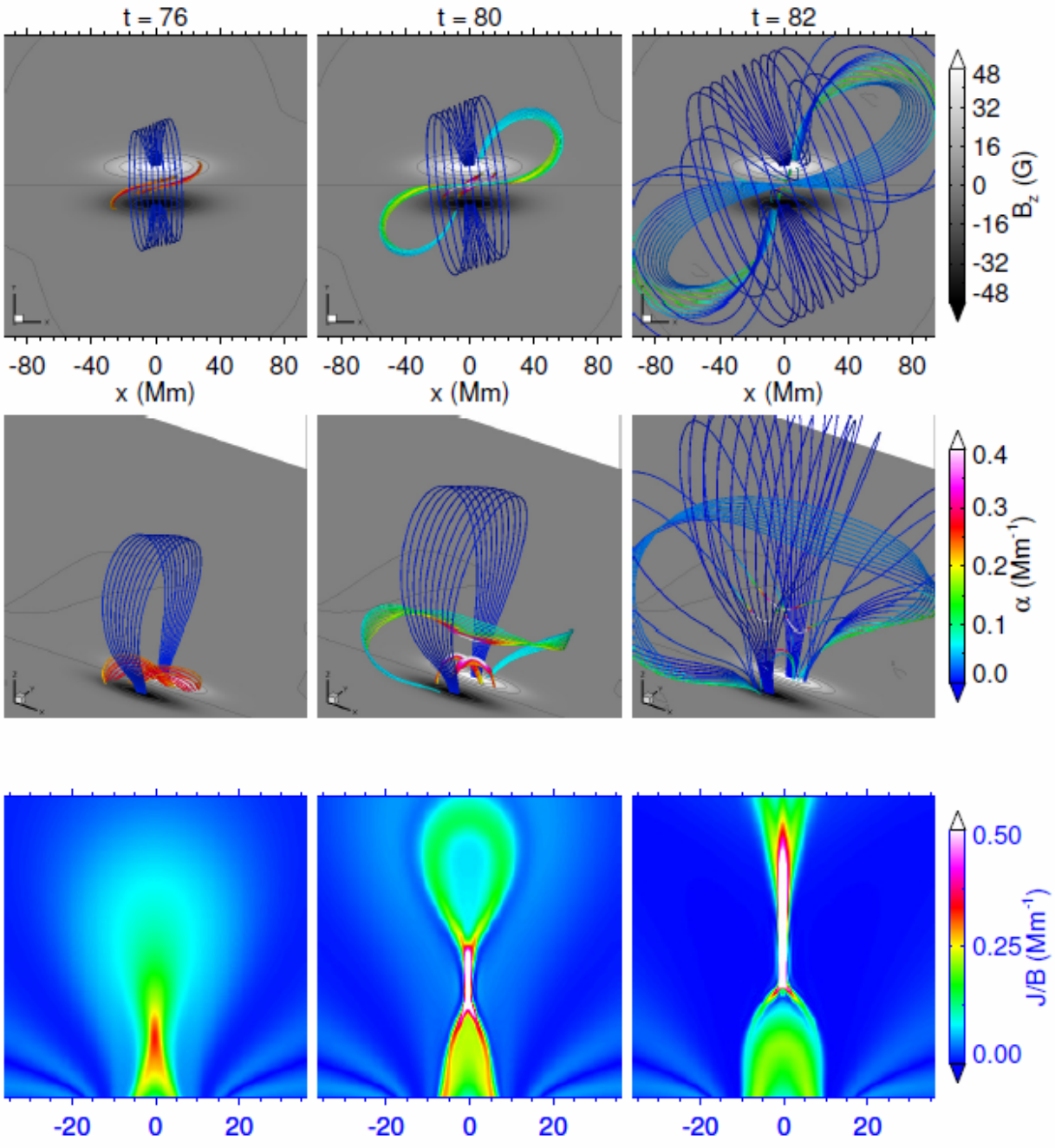

Numerical Simulation of a Fundamental Mechanism of Solar Eruption with Different Magnetic Flux Distributions

X. Bian, C. Jiang, X. Feng, P. Zuo, Yi Wang, X. Wang

2021